

12-15-2014

# The Roles of GSK-3 $\beta$ and APC in Cytoplasmic Dynein Regulation

Feng Gao

*University of South Carolina - Columbia*

Follow this and additional works at: <http://scholarcommons.sc.edu/etd>

---

## Recommended Citation

Gao, F.(2014). *The Roles of GSK-3 $\beta$  and APC in Cytoplasmic Dynein Regulation*. (Doctoral dissertation). Retrieved from <http://scholarcommons.sc.edu/etd/2947>

This Open Access Dissertation is brought to you for free and open access by Scholar Commons. It has been accepted for inclusion in Theses and Dissertations by an authorized administrator of Scholar Commons. For more information, please contact [SCHOLARC@mailbox.sc.edu](mailto:SCHOLARC@mailbox.sc.edu).

# THE ROLES OF GSK-3 $\beta$ AND APC IN CYTOPLASMIC DYNEIN REGULATION

by

Feng Gao

Bachelor of Science  
Zhejiang University, 2008

---

Submitted in Partial Fulfillment of the Requirements

For the Degree of Doctor of Philosophy in

Biological Sciences

College of Arts and Sciences

University of South Carolina

2014

Accepted by:

Deanna Smith, Major Professor

Vicki Vance, Chairman, Examining Committee

James R. Fadel, Committee Member

Michael Felder, Committee Member

Lydia Matesic, Committee Member

Lacy Ford, Vice Provost and Dean of Graduate Studies

© Copyright by Feng Gao, 2014  
All Rights Reserved.

## **DEDICATION**

I dedicate this work to my parents and my wife. I am really grateful for all your support. Thank you for the sacrifices you have made. I love you guys so much!

## **ACKNOWLEDGEMENTS**

I am very grateful that I have the opportunity to conduct research under the mentorship of Dr. Deanna Smith. Your support is meant a lot to me.

I appreciate the help and suggestions from my dissertation committee. I enjoy every minute with you in my committee meetings, which help my development in scientific area.

I enjoyed the time with all my colleagues in the Smith Lab. Dr. Sachin Hebbar, thank you for all guidance and suggestions, which means a lot to a new graduate student. Dr. Jai Pandey, thank you for helping me be familiar with the lab and the department. Dr. Liang Shi, Thank you for teaching me how to use mass spectrometry. Ms. Xu Gao, Thank you for your all suggestions. Mr. Tim Hines, Thank you for your positive energy.

I also want to say thank you to all my friends. You all make my life more exciting.

## ABSTRACT

Dynein is a microtubule minus-end directed molecular motor, participating in a broad range of cellular functions, such as organelle transport, cell migration and mitosis. Dynein dysfunction is linked to many diseases including ALS, schizophrenia, Alzheimer's disease, Parkinson's disease and cancer. The mechanism of dynein regulation is largely unknown.

We have provided evidence that glycogen synthase kinase 3 $\beta$  (GSK-3 $\beta$ ) directly regulates dynein in both neurons and non-neuronal cells. GSK-3 $\beta$  interacts with and phosphorylates dynein *in vitro*. Dynein phosphorylation by GSK-3 $\beta$  reduces its interaction with Ndel1, a regulator contributing to dynein force generation. Dynein motility is stimulated both by pharmacological GSK-3 $\beta$  inhibitors and by enhanced insulin signaling that leads to GSK-3 $\beta$  inactivation. Thus our study connects a well-characterized insulin-signaling pathway directly to dynein stimulation via GSK-3 inhibition.

There is considerable debate over whether thiazolidinediones, peroxisome proliferator-activated receptor gamma (PPAR- $\gamma$ ) agonists, are chemopreventive or carcinogenic during the development of colorectal cancer, where mutations in adenomatous polyposis coli (APC) often occur. We have demonstrated that the interplay of APC and dynein may be important for PPAR- $\gamma$  signaling to regulate cancer development. Dynein and APC physically interact with each other, which

is positively regulated by GSK-3 $\beta$ . Rosiglitazone increases dynein activity and cell migration in wild type (WT) but not in Apc (min/+) cells, and causes spindle misorientation in Apc (min/+) but not in WT cells. We provide evidence that this involves different PI3K/AKT/GSK-3 $\beta$  signaling responses to rosiglitazone between WT and Apc (min/+) cells and the disruption of the dynein-APC interaction by ApcMin mutation.

Dynein intermediate chain (IC) is essential for dynein assembly and mediates the interactions of dynein to regulators. To dissect how GSK-3 $\beta$  and APC regulate dynein, we developed a mass spectrometry (MS)-based systematic method to map phosphorylation sites on IC. We identified that T154, S88 and T89 on IC-2C are targeted by GSK-3 $\beta$  using MS and mutagenesis. S88 and T89 are conserved in all mouse IC isoforms and ICs from all other mammalian species. Furthermore, we demonstrate that S87 or T88 on IC-1B (corresponding to S88 or T89 on IC-2C) from both mouse and rat are targeted by GSK-3 $\beta$  using MS. The method has the potential to be applied to identify other *bona fide* substrates of GSK-3 $\beta$  or other kinases.

## TABLE OF CONTENTS

DEDICATION.....	iii
ACKNOWLEDGEMENTS.....	iv
ABSTRACT.....	v
LIST OF FIGURES.....	viii
LIST OF ABBREVIATIONS.....	x
GENERAL INTRODUCTION.....	1
CHAPTER 1: GSK-3 $\beta$ phosphorylates cytoplasmic dynein and inhibits dynein motility.....	6
CHAPTER 2: Adenomatous polyposis coli (APC) is a novel multifaceted dynein regulator: the concerted interplay is vital for the effect of thiazolidinediones.....	47
CHAPTER 3: A mass spectrometry-based systematic method to map GSK-3 $\beta$ phosphorylation sites on dynein intermediate chain.....	79
CONCLUSIONS.....	112
REFERENCES.....	114

## LIST OF FIGURES

Figure 1.1 Inhibition of GSK-3 $\beta$ stimulates retrograde transport in adult rat DRG neurons.....	32
Figure 1.2 Direct phosphorylation of dynein by GSK-3 $\beta$ .....	34
Figure 1.3 Dynein phosphorylation by GSK-3 $\beta$ impacts Ndel1 interaction.....	36
Figure 1.4 Pharmacological inhibition of GSK-3 $\beta$ causes dynein to accumulate at centrosomes in colon cell lines .....	37
Figure 1.5. GSK-3 $\beta$ inhibition is responsible for the dynein accumulation at centrosomes .....	38
Figure 1.6 Dynein is released from peripheral/cortical sites in response to GSK-3 $\beta$ inhibition.....	40
Figure 1.7 An insulin-sensitizing drug, rosiglitazone, causes centrosomal dynein accumulation via GSK-3 $\beta$ inactivation .....	42
Figure 1.8 Rosiglitazone induced dynein redistribution requires PPAR- $\gamma$ and new transcription, but expression of dynein and related proteins is not increased .....	43
Figure 1.9 Dynein accumulation at centrosomes in response to ROZ is due to increased motor transport activity .....	44
Figure 1.10 A model for GSK-3 $\beta$ -dependent regulation of dynein dependent retrograde organelle transport .....	46
Figure 2.1 Dynein, APC and GSK-3 $\beta$ physically interact with each other in mouse brain.....	69
Figure 2.2 GSK-3 $\beta$ positively regulates the interaction of dynein to APC .....	70
Figure 2.3 Characterize APC status and PPAR- $\gamma$ expression in YAMC and IMCE.....	71
Figure 2.4 ApcMin mutation prevents dynein activation in response to ROZ.....	72

Figure 2.5 ApcMin mutation alters spindle orientation in response to ROZ .....	73
Figure 2.6 ApcMin mutation prevents ROZ induced cell migration shown in wound healing and enterocyte motility assay.....	74
Figure 2.7 ApcMin mutation alters PI3K/AKT/GSK-3 $\beta$ signaling, which is essential for ROZ response .....	76
Figure 2.8 GSK-3 $\beta$ inhibition significantly rescues dynein activation in ApcMin mutation cells, and AKT inhibition prevents ROZ induced cell migration in WT cells.....	77
Figure 2.9 ApcMin mutation disrupts the interaction between dynein and WT APC .....	78
Figure 3.1 A systematic workflow of identifying and confirming kinase-specific phosphorylation sites based on tandem mass spectrometry and mutagenesis ..	96
Figure 3.2 GSK-3 $\beta$ phosphorylates N-terminal of IC-2C without priming phosphorylation.....	97
Figure 3.3 Identification of T154 phosphorylation on IC-2C by mass spectrometry .....	99
Figure 3.4 Identification of S88, T89 phosphorylation sites on IC-2C by mass spectrometry .....	101
Figure 3.5 Quantification of T154, S88 or T89 phosphorylation on IC-2C by mass spectrometry .....	103
Figure 3.6 Confirmation of T154, S88 or T89 phosphorylation on IC-2C by mutagenesis .....	105
Figure 3.7 Location of and conservation of T154, S88 or T89 on IC.....	107
Figure 3.8 Identification of S87 or T88 on Rat IC-1B targeted by GSK-3 $\beta$ .....	108
Figure 3.9 Identification of S87 or T88 on mouse IC-1B targeted by GSK-3 $\beta$ ...	110

## LIST OF ABBREVIATIONS

AD.....	Alzheimer's disease
AKT.....	protein kinase B
APC.....	Adenomatous Polyposis Coli
ATP.....	Adenosine triphosphate
ALS.....	amyotrophic lateral sclerosis
C-APC.....	c-fragment of APC protein
CDK5RAP2.....	CDK5 regulatory subunit-associated protein 2
CDK.....	cyclin dependent kinase
DMSO.....	dimethyl sulfoxide
DRG.....	dorsal root ganglion
ERK.....	extracellular signal-regulated kinases
FL.....	full length
GSK-3.....	glycogen synthase kinase 3
GST.....	glutathione S-transferase
EGFP.....	enhanced Green fluorescent protein
HC.....	dynein heavy chain
IRS.....	insulin receptor substrate
IC.....	dynein intermediate chain
IC-1B.....	dynein intermediate chain1B
IC-2C.....	dynein intermediate chain 2C

IP ..... immunoprecipitation  
 IPTG ..... isopropyl-d-thiogalactoside  
 ITS ..... Insulin, Transferrin, Selenium  
 LIC ..... dynein light intermediate chain  
 LiCl..... lithium chloride  
 LC ..... dynein light chain  
 LC-MS/MS ..... HPLC-tandem mass spectrometry  
 Lis1 .....platelet-activating factor acetylhydrolase IB subunit alpha  
 MBO..... membrane-bounded organelles  
 MDCK .....Madin-Darby canine kidney  
 MT..... microtubule  
 Min ..... multiple intestinal neoplasia  
 MS .....mass spectrometry  
 N106 .....N-terminal fragment of IC-2C with 106 amino acids  
 N237 .....N-terminal fragment of IC-2C with 237 amino acids  
 Nde1 .....nuclear distribution protein E  
 Ndel1 ..... nuclear distribution protein nudE-like 1  
 NOC.....nocodazole  
 P150 .....p150-glued, a Dynactin subunit 1  
 P50 ..... dynactin subunit 2  
 PBS.....phosphate buffered saline  
 PI3K .....phosphoinositide 3 kinase  
 PIP3 .....phosphatidylinositol (3, 4, 5)-trisphosphate

PLC $\gamma$  ..... phosphoinositide phospholipase C  
PPAR- $\gamma$  ..... peroxisome proliferator-activated receptor gamma  
PTM ..... post-translational modification  
ROZ ..... rosiglitazone  
RT ..... room temperature  
S/T ..... serine/threonine  
SGG ..... Shaggy, a homolog of GSK-3 in *Drosophila*  
WT ..... wild type  
YAMC ..... young adult mouse colon

## GENERAL INTRODUCTION

**Transport is essential for life:** as we all know transport is essential for our life, we transport different cargo by different transportation system and tools to different destinations in order to support our life. There is also an essential transport system happening inside us all the time, which is cellular transport. Cells need to exchange items with outside in order to support itself. It uptakes cargo, such molecules and vesicles, from outside through endocytosis (Marsh and McMahon, 1999). Endocytotic vesicles could be transported by intracellular transport system to different locations and utilized (Vale, 2003). Cell also produces cargo by its organelles such as nucleus and mitochondria. These cargo are transported by intracellular transport system to the different location inside cells, and some of them could be transported to cell periphery followed by exocytosis. Microtubule is the main system responsible for the intracellular transport (Vale, 2003). Microtubules (MT) are polymerized of alpha and beta tubulins and have a distinct polarity. The minus end of MT is anchored at the microtubule organization center (MTOC), which typically locates at the centrosome, while the plus end is continuing growing to the cell periphery (Brinkley, 1985). The polarity of microtubules is very important for intracellular transport, because there are two distinct types of molecular motors, cytoplasmic dynein and kinesin (Vale, 2003). Dynein prefers to moving cargo from the plus end of MT to the minus end of MT, while kinesin moves the cargo from the minus

end of MT to the plus end of MT. I am particularly interested in dynein dependent organelles transport, because it is a very important cellular process and dynein is not as well studied as kinesin.

**Functions and regulation of cytoplasmic dynein:** As a motor, dynein uses ATP as power source (Gibbons, 1988). Dynein is an ATPase that hydrolyzes ATP into ADP. In order to efficiently use ATP and transport cargo on the microtubules, dynein needs a sophisticated structure (Schiavo et al., 2013). Dynein heavy chain (HC) has 4626 amino acids. C-terminus of HC is the motor domain, and N-terminus is stem domain. With the help from other dynein subunits, intermediate chains (IC) and light intermediate chains (LIC), HCs form a dimer (Allan, 2011). Dynein has many functions that could be divided into two main categories: interphase and mitosis. During the interphase, dynein plays important roles in intracellular transport and cell migration; during the mitosis, dynein plays essential roles in spindle formation, spindle position, chromosome alignment and separation. Loss of both copy of *Dync1h1* is embryonic lethal (Harada et al., 1998). Dysregulation of dynein is involved in many neurodegenerative diseases such as Alzheimer's disease, Parkinson's disease, Huntington's disease and ALS, which strongly affect patient's life quality (Eschbach and Dupuis, 2011). The common feature of diseases is the accumulation of toxic aggregation-prone proteins in related neurons (Blokhuis et al., 2013; Rubinsztein, 2006; Tanzi and Bertram, 2005). Therefore, if we are able to remove these toxic proteins by transporting them into proper subcellular locations to degrade them, such as lysosome, these diseases may be cured.

Dynein may play important roles in cancer development because of regulating spindle formation and chromosome separation (Raaijmakers et al., 2013). In order to cure those diseases, we need to understand how dynein is regulated. In order to properly carry out its functions, dynein needs help from other regulators such as dynactin, Bicaudal D, Lis1, Nde1/Ndel1 and more (Kardon and Vale, 2009). Dynactin is able to increase dynein processivity on microtubules (McKenney et al., 2014). The processivity of dynein on microtubules is essential, because dynein only move 8 nm/s and axons of some neurons are over 1 m. Lis1 and Nde1/Ndel1 induces a persistent force generation by dynein (McKenney et al., 2010). The ability of dynein to generate the persistent force is also very important, because many of dynein cargo are very heavy, such as nucleus and mitochondria, and need to be transported for a long distance to reach destinations. If everything works properly, dynein is a very reliable and powerful motor. Dynein is able to move cargo at 1  $\mu\text{m/s}$ , which is 125 steps/s. We are impressed by Bolt for his 100 m world record, which he finished with 41 steps in 9.58 s. However, it is still less than 5 steps/s. Lifting capacity of dynein is even more impressive: the molecular weight of dynein is  $2.49 \times 10^{-9}$  pg and dynein is able to lift over 1 pN or 100 pg, so dynein is able to lift over  $4.01 \times 10^{10}$  times its body weight. Because dynein is so powerful, it really needs precise regulation. Signaling that controls dynein to start, pause or stop at the proper time and area is needed. The signaling passing on dynein could be post-translational modifications, and phosphorylation is the one of the most important.

Phosphorylation regulates interactions and turnover of proteins, therefore, dynein regulation by kinases can be a very important mechanism.

**The functions and regulation of glycogen synthase kinases-3 (GSK-3):** GSK-3 is a serine/threonine protein kinase. It is a fundamental enzyme involved in many cellular processes. It has over 100 substrates and many of them are very essential, such as glycogen synthase, Tau and  $\beta$ -catenin (Sutherland, 2011). In mammals there are two GSK-3 genes, GSK-3 $\alpha$  and GSK-3 $\beta$  (Woodgett, 1991), but their catalytic domains are highly conserved (Castano et al., 2010; Mukai et al., 2002; Soutar et al., 2010; Wood-Kaczmar et al., 2009). GSK-3 $\beta$  usually phosphorylates and inhibits its substrates. Dysregulation of GSK-3 $\beta$  is involved in many diseases including type-2 diabetes, neurodegenerative diseases and cancer. Therefore, GSK-3 $\beta$  activity also requires precise regulation. GSK-3 $\beta$  is highly active in resting cells because of an activating auto-phosphorylation at Tyr 216 (Cole et al., 2004). However, upstream kinases including AKT/PKB, protein kinase A, and protein kinase C phosphorylate GSK-3 $\beta$  at serine 9 (S9) and inhibit it (Cross et al., 1995; Fang et al., 2002; Fang et al., 2000). Inhibition is a main tool to regulate GSK-3 $\beta$  in the cell. Many pharmacological inhibitors of GSK-3 $\beta$  are being studied in order to treat diseases such as Alzheimer's disease and diabetes (Eldar-Finkelman and Martinez, 2011; Meijer et al., 2004).

**The functions and regulation of Adenomatous Polyposis Coli (APC):** APC is well known as a scaffolding protein in Wnt signaling, where it regulates phosphorylation, ubiquitination and turnover of  $\beta$ -catenin (Espada et al., 2009).

Besides that, APC is also known as a MT plus end-binding protein and plays important roles in cell migration, spindle assembly, cell adhesion and chromosome segregation (Hanson and Miller, 2005). The Apc (min/+) mouse, which harbors a truncating APC mutation, is a prominent animal model to study human colorectal cancer (Taketo and Edelman, 2009; Yamada and Mori, 2007). There is considerable debate over whether thiazolidinediones, peroxisome proliferator-activated receptor gamma (PPAR- $\gamma$ ) agonists, are chemopreventive or carcinogenic during the development of colorectal cancer, where mutations in APC often occur.

In chapter 1, I will provide evidence that GSK-3 $\beta$  directly phosphorylates and regulates dynein in both neurons and non-neuronal cells. In chapter 2, I will show that APC is a novel multifaceted regulator of dynein and the interplay of APC and dynein may be important for PPAR- $\gamma$  signaling to regulate development of cancer and other diseases. In chapter 3, I will demonstrate a mass spectrometry (MS)-based systematic method to map GSK-3 $\beta$  dependent phosphorylation sites on dynein intermediate chains.

## CHAPTER 1

GSK-3 $\beta$  phosphorylates cytoplasmic dynein and inhibits dynein motility<sup>1</sup>

### ABSTRACT

Glycogen synthase kinase 3 (GSK-3) has been linked to regulation of kinesin-dependent axonal transport in squid and flies, and to indirect regulation of cytoplasmic dynein. We have now found evidence for direct regulation of dynein by mammalian GSK-3 $\beta$  in neurons and in non-neuronal cells. GSK-3 $\beta$  coprecipitates with mouse brain dynein and phosphorylates purified dynein *in vitro*. Dynein phosphorylation by GSK-3 $\beta$  reduces its interaction with Ndel1, a protein that contributes to dynein force generation. Mammalian dynein motility is stimulated both by pharmacological GSK-3 $\beta$  inhibitors and by an insulin response pathway that leads to GSK-3 $\beta$  inactivation. Thus our study connects a well-characterized insulin-signaling pathway directly to dynein stimulation via GSK-3 inhibition.

### INTRODUCTION

Microtubule motors are important force-generating proteins found in all eukaryotic cells. Two types of processive motors move along microtubules in animal cells. The kinesins are mainly plus end directed, and cytoplasmic dynein is the primary motor for minus end directed transport. Both classes of motors

---

Feng J. Gao<sup>1</sup>, Sachin Hebbar<sup>2</sup>, Xu A. Gao<sup>1</sup>, Michael Alexander<sup>1</sup>, Jai P. Pandey<sup>3</sup>, Stephen J. King<sup>4</sup>, Deanna S. Smith<sup>1\*</sup>. Submitted to Traffic Journal, 10/13/2014.

carry out axonal and dendritic transport and defects in both classes have been linked to late- neurological disorders (Franker and Hoogenraad, 2013; Hirokawa et al., 2010). Defective microtubule-based transport can also contribute to other diseases, including cancer (Liu et al., 2013) and diabetes (Baptista et al., 2014). Two focus areas have dominated the study of motor proteins over the last decade – studies aimed at elucidating how ATP hydrolysis translates into processivity, and studies aimed at elucidating how motors “select” specific cargo. Structural analyses of motor components have begun to answer the first question (Gennerich and Vale, 2009), and there is a large body of work addressing cargo selectivity through interaction of accessory subunits, scaffolds, and cargo adaptors (Fu and Holzbaaur, 2014). The sheer diversity of cargos, coupled with the diversity of potential subcellular destinations, suggest that mechanisms must be in place to regulate the timing and whereabouts of motor activation by extracellular cues. There is growing evidence that movement of cargo, especially membrane-bounded organelles and vesicles, is an effort of teamwork among motors rather than individual motors functioning in isolation (Rai et al., 2013). Motors activity may be influenced by regulatory binding proteins, by changes in the cytoskeleton or cell membranes, by signaling pathways or by a combination of all of the above (Dobrowolski and De Robertis, 2012).

Our particular interest is in how cytoplasmic dynein is regulated by extracellular signals. It was recently shown that the presence of cargo adaptor components was sufficient to induce *in vitro* processivity of mammalian dynein motors (Schlager et al., 2014). Yeast dynein is processive in the absence of both

cargo or cargo adaptors, so there may be some species variability in activation mechanisms among different organisms or cell types (Huang et al., 2012). Less is known about the signals regulating dynein's association with cargo adaptors or the signals regulating its cooperation with other motors. It is thought that dynein is ferried towards microtubule plus ends by kinesin (Roberts et al., 2014; Yamada et al., 2008), where it can become attached to the membrane (Kardon and Vale, 2009; Markus et al., 2009). At this point motors are poised to become activated. In neurons a well-supported hypothesis proposes that neurotrophins acting on neurotrophin receptors in growth cones or synapses induce the transport of signaling endosomes carrying survival signals to the cell body (Wu et al., 2009). These signaling endosomes contain the neurotrophins and receptor, as well as downstream effectors including components of the Ras/ERK pathway, PI3K, and PLC $\gamma$ . In zebra fish, stimulation with a growth factor, IGF-1, caused the rapid dissociation of GSK-3 $\beta$  from signaling endosomes following the transient association of AKT with the endosomes (Schenck et al., 2008). However, there is little known about the mechanisms activating retrograde transport motors to carry the signaling endosomes.

Kinases have been directly or indirectly linked to motor regulation (Mitchell et al., 2012; Yano et al., 2001). Relevant to this study are three reports linking glycogen synthase kinase 3 (GSK-3) to axonal transport. The *Drosophila* homolog of GSK-3 (*SHAGGY*, *SGG*) was found to regulate axonal transport of a kinesin-1 cargo (amyloid precursor protein, APP) but not a kinesin-3 cargo (synaptic vesicle precursor, SVP) (Weaver et al., 2013). Because retrograde

movements of the kinesin-1 cargo were also affected, the authors speculated that dynein motors were indirectly affected by SGG regulation of kinesin-1, pointing to growing evidence that motors of one class can impact the other class (Mallik et al., 2013). Another group found that expressing a constitutively active form of SGG resulted in more kinesin, dynein, and activated SGG co-fractionating with a light membrane fraction from larval brains (Dolma et al., 2014). They observed bidirectional SGG dependent changes in speeds, run lengths, and pause frequencies of synaptobrevin vesicles and mitochondria moving in larval segmental nerves. An earlier study demonstrated that rat kinesin light chains were substrates for purified GSK-3 (Morfini et al., 2002). However, in squid axoplasm, active GSK-3 only inhibited plus end (but not minus end) transport of membrane-bounded organelles (MBOs) (Morfini et al., 2002). Taken together, these data suggest that it is not clear whether GSK-3 directly regulates dynein, which may be species and cargo dependent.

Our study now adds significantly to the understanding of how GSK-3 influences dynein-dependent axonal transport in mammalian systems. We find that direct inhibition of GSK-3 or increased insulin signaling activates dynein motility. We also show that GSK-3 can directly phosphorylate dynein, which negatively impacts its interaction with a well-characterized regulatory protein, Ndel1.

## **RESULTS**

**Inhibition of GSK-3 $\beta$  stimulates retrograde movement in neuronal cells:** To ascertain whether dynein-dependent transport is influenced by GSK-3

in mammalian axons, we examined organelle transport in axons of cultured adult dorsal root ganglion (DRG) neurons, which can extend many hundreds of microns in culture. We used LysoTracker dye to label acidic organelles. In a previous study kymographs were used to determine the percentage of organelles that moved anterogradely, retrogradely, switched directions, or remained static during the recording interval (Pandey and Smith, 2011). On average, three times more organelles moved retrogradely in control axons. Axons extended by these cells have uniformly polarized microtubules with minus ends towards the cell body (Baas and Lin, 2011), so retrogradely moving organelles are likely to be dynein-driven. Indeed, interfering with dynein or its regulators, Lis1 or Ndel1, interfered with motility in these assays.

In the current study DRG neurons were exposed to the GSK-3 inhibitors CT90221 or LiCl for 12 hr. Time-lapse movies from 100  $\mu\text{m}$  segments of 11-30 axons for each condition (and relevant controls) were used to generate kymographs. Figure 1.1 A and B shows representative kymographs from DMSO and CT99021 treated axons. The absolute number of organelles analyzed for each condition ranged from 160-429. In our system, blocking GSK-3 by both CT99021 (Figure 1.1 C, D) and LiCl (Figure 1.1 E, F) caused a shift towards more retrogradely moving organelles relative to static organelles, and had little if any effect on anterograde trafficking, possibly because of the choice of organelle that is being analyzed.

**Dynein interacts with GSK-3 $\beta$  *in vivo* and is phosphorylated by GSK-3 $\beta$  *in vitro*:** Because the number of retrogradely moving organelles was

increased by GSK-3 $\beta$  inhibition, we considered the possibility that dynein might be a target for GSK-3 $\beta$  phosphorylation. A small but reproducible amount of GSK-3 $\beta$  coprecipitated with dynein from adult mouse brain homogenates, indicating that these proteins may exist in a complex *in vivo* and supporting the idea that GSK-3 $\beta$  may be in a position to phosphorylate dynein (Figure 1.2A). Moreover, several dynein subunits (heavy chains, HC, intermediate chains, IC, and light intermediate chains, LIC) in a highly purified bovine brain dynein preparation (Bingham et al., 1998) incorporated  $\gamma$ -<sup>32</sup>P-ATP when incubated with purified human GST-GSK-3 $\beta$  in an *in vitro* kinase assay (Figure 1.2B). Unlike most kinases, GSK-3 $\beta$  is constitutively active in resting cells because of an activating auto-phosphorylation at Tyr 216 (Cole et al., 2004). This site is also known to be phosphorylated in GST-GSK-3 $\beta$ , whose size is similar to IC. There is a small amount of autophosphorylation apparent in a reaction that did not include dynein (Figure 1.2B left panels). However, to ensure IC was a target *in vitro*, we also used a smaller his-tagged GSK-3 $\beta$  (~48kDa) *in vitro* kinase assay (Figure 1.2B right panels).

For future studies we chose to focus our attention on ICs, which interact directly with several regulatory proteins including Ndel1/Nde1, dynactin, and LCs (Nyarko et al., 2012). Mammalian ICs are encoded by two genes, *DYNC111* and *DYNC112*, that share about 70% protein identity (Kuta et al., 2010). Both are highly conserved among mammalian species. We will refer to the proteins as IC-1 and IC-2. To examine whether one or both ICs can be targets of the kinase *in vitro*, we expressed EGFP-tagged proteins (rat IC-1B and mouse IC-2C) in Cos-7

cells, The ICs were immunoprecipitated from cell extracts with a GFP antibody and exposed to GSK-3 $\beta$ . Both were targeted by the kinase, but IC-1B was a better substrate (Figure 1.2C). Interestingly, bands of the size of HC's and endogenous IC's were present in the IP, and were also phosphorylated. This suggests that the EGFP-ICs could interact with the endogenous dynein subunits. A phosphorylated band that could be LIC was detected in the EGFP-IC-1B IPs, but not in the EGFP-IC-2C IPs.

Many known GSK-3 $\beta$  substrates require a priming phosphorylation at a serine or threonine residue position four amino acids C-terminal to the GSK-3 $\beta$  target residue (Sutherland, 2011). The mammalian IC sequences we compared contain between 9 and 11 potential priming consensus sites. Several sites are located in the N-terminus, a region with binding sites for regulatory proteins (McKenney et al., 2011; Wang and Zheng, 2011). To determine if existing endogenously acquired phosphates on purified brain dynein impacted phosphorylation by GSK-3 $\beta$  *in vitro*, phosphates were "stripped" from immobilized dynein by incubation with  $\lambda$ -phosphatase. After extensive washing to remove residual phosphatase, a GSK-3 $\beta$  kinase assay was performed. Less  $\gamma$ -<sup>32</sup>P-ATP was incorporated into ICs that had been stripped of phosphates suggesting that priming phosphorylation may be important (Figure 1.2D). However, residual phosphorylation suggested the possibility that other sites may not require priming, as has been shown for several proteins including tau (Doble and Woodgett, 2003; Eldar-Finkelman, 2002). This prompted us to whether GSK-3 $\beta$  could also phosphorylate bacterially expressed IC, which is unlikely to have been

subjected to priming phosphorylation. Interestingly, two bacterially expressed recombinant IC-2C proteins, FL-IC-2C and an N-terminal fragment of IC-2C (N237) (King et al., 2003), were phosphorylated by GSK-3 $\beta$  *in vitro* (Figure 1.2E, F). Future studies will be aimed at trying to identify both GSK-3 $\beta$  targeted consensus and non-consensus sites on ICs.

**IC phosphorylation by GSK-3 $\beta$  impacts Ndel1 interaction:** Lis1 and Ndel1/Nde1 are dynein-binding proteins that work together to regulate dynein. Some studies suggest that these proteins regulate force production (McKenney et al., 2010), while other studies suggest that they regulate dynein plus end trafficking (Roberts et al., 2014; Yamada et al., 2008) and directing dynein to cortical sites during mitosis (Li et al., 2005; Moon et al., 2014). We previously showed that phosphorylation of Ndel1 by cyclin dependent kinases impacted its interaction with dynein and Lis1 (Hebbar et al., 2008b). To determine if GSK-3 $\beta$ -dependent phosphorylation of dynein alters its capacity to bind to Lis1 or Ndel1, immunoprecipitated, purified dynein was incubated with GSK-3 $\beta$ . After extensive washing to remove kinase, beads were exposed to purified Lis1 and Ndel1. Ndel1, but not Lis1, was less likely to coprecipitate with dynein if it was pre-phosphorylated by GSK-3 $\beta$  (Figure 1.3A). McKenney et al (2010) reported that Nde1, a homolog of Ndel1, stabilized the interaction of LIS1 with purified dynein motors (McKenney et al., 2010). In support of this we found that purified FL-IC2C was unable to pull down Lis1 unless Ndel1 was present (Figure 1.3B). Interestingly, less Ndel1 was pulled down if FL-IC2C was first phosphorylated by GSK-3 $\beta$  (Figure 1.3C).

To determine if GSK-3 $\beta$  activity could influence the Ndel1 binding to IC in cells, we treated the WT young adult mouse colon cell line (YAMC) with the GSK-3 $\beta$  inhibitor, CT99021. More Ndel1 was pulled down by dynein in immunoprecipitation if cells had been exposed to CT99021 (Figure 1.3D). Interestingly, CT99021 also caused an increased colocalization of Ndel1 and dynein at apparent centrosomes (Figure 1.3E, F), suggesting that GSK-3 inhibition induced more dynein motors and Ndel1 translocation to the hub of microtubule minus ends.

**Direct GSK-3 $\beta$  inhibition causes accumulation of dynein at centrosomes:** To confirm that dynein was accumulating at centrosomes following GSK-3 $\beta$  inhibition, YAMC and HCT116 cells (a human cancer cell line) were treated with CT99021, then costained for ICs (74.1) and the centrosomal protein CDK5RAP2. A clear increase in dynein staining at the marked centrosomes was observed in most cells exposed to the GSK-3 $\beta$  inhibitor (Figure 1.4A-D). IC immunofluorescence intensity was measured in a circular area drawn around the CDK5RAP2 signal in treated and control cells (Figure 1.5A, B). Cells in which the intensity in the circle was at or above 60 arbitrary fluorescence units were categorized as having dynein accumulation at centrosomes. The percentage of HCT116 cells or YAMC cells with this phenotype increased dramatically after 12 hr of exposure to CT90221 (Figure 1.5C). Enrichment was also observed after 6 hr of exposure (not shown). Several other experiments provided confidence that GSK-3 $\beta$  inhibition was the relevant change. First, another known GSK-3 inhibitor, LiCl, had the same effect (Figure 1.5D). Second,

transient expression of a dominant negative GSK-3 $\beta$  construct (GSK-3 $\beta$  K85A) also caused the accumulation phenotype (Figure 1.5E). Finally, because GSK-3 activity is known to be inhibited by insulin, we also looked for and found the accumulation phenotype if starved cells were exposed to a supplement containing high levels of insulin (ITS - Figure 1.5F). Serum alone was not sufficient to induce the change, possibly because FBS has tenfold lower insulin concentration than the ITS supplement.

**GSK-3 $\beta$  inhibition causes loss of dynein from the cell periphery:**

Dynein distribution at the cell periphery appeared punctate in both control and CT90221-treated cells and was somewhat variable between cells and regionally within cells. However, the dynein puncta in CT90221 treated cells appeared less intense. To quantify this observation, 30 peripheral regions of control and CT90221 treated cells immunostained for IC (Figure 1.6A, B) were analyzed using ImageJ particle analysis software. Only interphase cells with cortical edges that were not contacting other cells were analyzed. While the lamella in both control and treated cells had on average the same overall number of dynein puncta (Figure 1.6C), the puncta in the CT90221 treated cells were on average smaller ( $0.087 \mu\text{m}^2$  compared to  $0.178 \mu\text{m}^2$  in control cells, Figure 1.6D) suggesting that dynein redistribution involves release from specific sites at the cell periphery and translocation towards microtubule minus ends at the centrosome. Because minus ends of microtubules in the radial array are anchored in centrosomes and the plus end of microtubules interact with the cell cortex (Lansbergen et al., 2006; Rodionov et al., 1999), the dynein redistribution

may represent increased minus end directed movement of a pool of dynein in response to GSK-3 inhibition.

**The insulin-sensitizing drug rosiglitazone also causes centrosomal dynein accumulation via GSK-3 $\beta$  inhibition:** To further explore the role of insulin in dynein activation, we utilized rosiglitazone (ROZ), a drug that is used to treat type-2 diabetes by acting as an insulin sensitizer. This compound is sold under the trade name Avandia (Hernandez et al., 2003). Interestingly, ROZ caused dynein to accumulate at centrosomes in both YAMC and HCT116 cells suggesting that the drug might be inhibiting GSK-3 (Figure 1.7A). Although ROZ clearly sensitizes cells to insulin, the exact mechanism is not precisely understood and may be cell and context dependent. The drug is known to be a PPAR- $\gamma$  agonist, mimicking the effect of endogenous ligands like fatty acids and eicosanoids. PPAR- $\gamma$  was expressed in our colon cell lines (Figure 1.8A), and dynein redistribution was prevented by transient expression of a dominant negative PPAR- $\gamma$  mutant, demonstrating that the effect is very likely to be a PPAR- $\gamma$ -dependent effect (Figure 1.8B). A transcription inhibitor also blocked ROZ-induced dynein accumulation at centrosomes (Figure 1.8C). IC expression was not changed, nor was several known dynein regulators (Figure 1.8D). Therefore, the relevant transcriptional changes may be related to increased insulin sensitivity rather than a change in the expression of dynein regulators. In support of this, the presence of either insulin or FBS, along with ROZ was required for dynein accumulation at the centrosome (Figure 1.7B). Thus, while

there was insufficient insulin in FBS to stimulate dynein accumulation in the absence of ROZ, ROZ was able to sensitize cells to this amount of insulin.

**PI3K/AKT signaling is involved in the dynein response to ROZ:** An early response to insulin signaling is activation of PI3K (phosphoinositide 3 kinase) (Saltiel and Pessin, 2002). Auto-phosphorylation of insulin receptors promotes binding and phosphorylation of IRS (insulin receptor substrate family). This leads to activation of PI3K and production of PIP3 (phosphatidylinositol (3, 4, 5)-trisphosphate) on the cytoplasmic side of the plasma membrane. PIP3 recruits AKT/PKB (protein kinase B), which is then stimulated by other kinases at the plasma membrane, where it phosphorylates and inactivates GSK-3 $\beta$  on serine 9 (S9). This pathway is likely involved in the response to rosiglitazone because pharmacological inhibition of PI3K by either LY294002 or Wortmannin blocked dynein redistribution (Figure 1.7C). Also, phospho-AKT (Thr308) became prominently localized at the plasma membrane in starved cells exposed to ROZ in the presence of insulin and FBS (Figure 1.7D). The percentage of cells with this staining pattern increased from ~10% to over 30% by 12 hr (*Mean +/- 95% CI; \*\*\*P<0.0001, t-test*). Total phospho-AKT levels had increased in cells by 6 hr after ROZ exposure, but were reduced by 12 hr (Figure 1.7E). ROZ also induced S9 phosphorylation to the same extent as LiCl, further supporting the involvement of this well-known signaling pathway (Figure 1.7F). Moreover, centrosome accumulation of dynein was blocked by overexpression of a constitutively active GSK-3 $\beta$  isoform (GSK-3 $\beta$  S9A), demonstrating that the rosiglitazone response involves inactivation of GSK-3 $\beta$  (Figure 1.7G).

Interestingly, the baseline of dynein accumulation in control cells was also significantly reduced by expression of this construct.

**Dynein redistribution in response to ROZ requires its motor activity:**

Because dynein normally accumulates at centrosomes as cells enter the S/G2 phase in cycling cells (Quintyne and Schroer, 2002), we were interested in determining whether drug treatments were causing a S/G2 arrest. However, we did not observe that rosiglitazone exposure increased the number of cells with nuclear CENPF (not shown), which becomes detectable in late S/G2 and is degraded after mitosis (Landberg et al., 1996; Liao et al., 1995). Also, most of the cells with enriched centrosomal dynein were not CENPF positive (Figure 1.9A), so S/G2 arrest was unlikely to be the underlying cause of dynein accumulation at centrosomes. Rather, changes in dynein motility seem to be involved, as two different manipulations known to reduce dynein-dependent transport, Lis1 RNAi or dynactin p50 overexpression, prevented dynein accumulation (Figure 1.9B, C) (Lam et al., 2010; McKenney et al., 2010; Mesngon et al., 2006; Smith et al., 2000). Dynactin subunits also became enriched at the centrosome in response to the insulin sensitizer suggesting that the dynein that moved towards centrosomes was coupled with dynactin (Figure 1.9D, E). In support of increased dynein motility, acidic organelles labeled with LysoTracker (late endosomes and lysosomes) moved more rapidly inward and clustered near the nucleus (Figure 1.9F-H). Finally, ROZ increased retrograde transport of LysoTracker-labeled organelles in adult rat DRG axons (Figure 1.9I, J).

## DISCUSSION

### **A novel and direct link between GSK-3 activity and dynein motors:**

This study is, to our knowledge, the first showing a direct interaction between cytoplasmic dynein and GSK-3. We show that brain dynein and GSK-3 can exist in a complex, and that the purified kinase can phosphorylate multiple dynein subunits *in vitro*. We also demonstrate that phosphorylation impacts the interaction of dynein with Ndel1, and show that GSK-3 activity alters dynein and Ndel1 distribution in cells as well as retrograde transport of acidic organelles in axons and in non-neuronal cells.

Our work adds significantly to previous studies of effects of GSK-3 on transport. The study of squid axoplasm only reported an impact on speeds of anterograde MBOs (Morfini et al., 2002). We used a different organelle pool (acidic organelles) and saw primarily an impact on retrograde, presumably dynein-driven, transport. One of the *Drosophila* studies did observe changes in both retrograde and anterograde movement of a kinesin-1 cargo (APP-associated vesicles) in larval segmental nerves but only found a small change in anterograde movements of a kinesin-3 cargo, SVPs (Weaver et al., 2013). The study also showed that GSK-3 influences the number of active kinesin motors per vesicle, not the total number of motors. The authors speculated that the change in retrograde movements of APP vesicles was caused indirectly through kinesin-1 regulation of dynein, as has been suggested by many studies (Mallik et al., 2013). The second study in *Drosophila* found that SHAGGY alterations influenced bidirectional transport of other cargos and that expression of active

SHAGGY increased binding of both dynein and kinesin to light membranes (Dolma et al., 2014). However, neither study determined which motor protein subunits or regulatory factors were being targeted by the kinase. Thus, our finding that GSK-3 $\beta$  directly phosphorylates dynein represents a significant advance in our understanding of how this kinase could influence axon transport. It is likely that kinesin was also being affected in our manipulations in neurons and non-neuronal cell lines. This could contribute to the changes in dynein distribution, but is less likely to be responsible for the changes we observed in long-distance retrograde transport of acidic organelles in axons.

### **GSK-3 $\beta$ phosphorylation of dynein reduces its interaction with**

**Ndel1:** In mammals there are two GSK-3 genes, GSK-3 $\alpha$  and GSK-3 $\beta$ . Many of our studies used GSK-3 $\beta$  specific tools. However, it is possible that GSK-3 $\alpha$  also interacts with dynein motors – this remains to be determined. Nonetheless, when dynein intermediate chains are phosphorylated by GSK-3 $\beta$  they are less able to interact with Ndel1, an important dynein regulator. We have reported that Ndel1 and its partner protein, Lis1, are critical for dynein dependent axon transport of acidic organelles (Hebbar et al., 2008b; Pandey and Smith, 2011). Moreover, a homolog of Ndel1, Nde1, modulates dynein force production based on single molecule studies *in vitro* (McKenney et al., 2010). In a different study, Lis1 was found to be important for maintaining processive movement of dynein along microtubules (Moughamian et al., 2013). However, other studies indicate that Lis1 and Ndel1/Nde1 are important for plus end directed transport of dynein motors by kinesin and recruitment of dynein to plus ends (Lansbergen et al.,

2006; Markus et al., 2009; Moughamian et al., 2013; Roberts et al., 2014; Yamada et al., 2008; Zhang et al.). Our current finding supports an activating role of Ndel1 with respect to dynein, but does not rule out other functions. Moreover, phosphorylation of Ndel1 itself is likely to contribute to distinct modes of motor regulation (Bradshaw et al., 2013).

**Mapping target sites in ICs:** Both IC-1 and IC-2 can be phosphorylated by GSK-3 $\beta$ . The majority of known or suspected GSK-3 $\beta$  substrates share a consensus target sequence, S/TXXXSp/Tp, in which priming phosphorylation of the downstream serine or threonine dramatically increases the capacity for phosphorylation by GSK-3 $\beta$  at an S/T four residues upstream of the priming site (Doble and Woodgett, 2003; Sutherland, 2011). There are multiple GSK-3 $\beta$  consensus sequences in both ICs (9-11, depending on the isoform and the species). Based on kinase assays, we suspect that one or more of these are targeted by GSK-3 $\beta$ . Mass spectrometry of purified bovine brain ICs and ICs precipitated from mouse brain extracts supports this, as phosphates were detected at both priming and GSK-3 $\beta$  target sites in both IC isoforms (not shown). Analysis of an *in vitro* phosphorylated N-terminal fragment of IC-2 expressed in bacteria suggests that a non-consensus residue may also be targeted by the kinase. Studies are under way to determine which of these candidate sites is *bona fide* and biologically relevant.

**Insulin and insulin sensitizing drugs stimulate dynein:** Another novel aspect of our study is that it directly links a known insulin-signaling pathway to dynein regulation. Insulin is a hormone that acts through insulin receptors and

insulin-like receptors in many tissues. In adipocytes, rosiglitazone stimulates trafficking of a glucose transporter, GLUT4 (Velebit et al., 2011). Interestingly, dynein-driven translocation of GLUT4 to perinuclear membranes appears to be required for optimal GLUT 4 regulation by insulin (Huang et al., 2001). It will be interesting to determine if GSK-3 inhibition contributes to trafficking of this transmembrane protein, and if insulin regulates trafficking of other receptor types. Although there are many remaining questions, our data allow us to advance a model in which GSK-3 inhibition serves as an activating switch for dynein motors in response to extracellular cues (Figure 1.10). In an unstimulated cell, constitutively active GSK-3 $\beta$  phosphorylates dynein motors, helping to maintain a steady-state equilibrium between phosphorylated and unphosphorylated dynein. The phosphorylated pool of dynein is prevented from interacting with Ndel1, and remains paused on microtubules or docked at the cell cortex (Figure 1.10A). When the cell is stimulated by insulin, PI3K/AKT signaling shuts down GSK-3 $\beta$  at the plasma membrane. This shifts the equilibrium between phosphorylated and dephosphorylated dynein, so that Ndel1/Lis1 can "jump start" this pool of dynein motors (Figure 9B). When cells are treated with GSK-3 $\beta$  inhibitors such as CT99021 or LiCl, it is likely that GSK-3 is inhibited throughout the cell, and the equilibrium shifts more towards active dynein motors (Figure 1.10C). This latter may explain why we observed a greater increase in retrograde transport in axons when GSK-3 was inhibited directly (compare Figure 1.1 to Figure 1.9I, J).

**Insulin, GSK-3, dynein and human neurological diseases:** There is increasing evidence that type 2 Diabetes causes age-related dementia, and this

has in some cases been linked to alterations in insulin signaling (Sato and Morishita, 2014). In fact, neurodegenerative diseases have frequently been associated with the onset of insulin resistance – and many of these are also associated with altered dynein-dependent transport (Eschbach and Dupuis, 2011). Our finding that the insulin sensitizing drug rosiglitazone stimulates retrograde axonal transport in adult neurons may provide a framework from which to understand how insulin resistance might negatively impact neuronal function. It will be interesting to determine if dynein-dependent alterations in receptor trafficking are also triggered in neurons by increased insulin sensitivity. The GSK-3 $\beta$  inhibitor LiCl has been widely used to treat mood disorders, but whether this involves alterations in dynein remains to be determined (Marmol, 2008). PPAR- $\gamma$  agonists like rosiglitazone are being considered for therapeutic treatments in AD primarily because of their known anti-inflammatory characteristics (Landreth et al., 2008). Our findings concerning the impact of this class of drugs on dynein dependent trafficking will be of interest for those and similar studies.

**GSK-3 regulation of dynein in other cell types:** Organization of the microtubule network within specific cells could play a role in where and when cells use this GSK-3 $\beta$  regulatory mechanism to control cargo trafficking. In our cultured colon cell lines microtubule plus ends tend to be positioned near the cell periphery so that dynein activation results cargo being transported towards minus ends near the nucleus. Other cell types may have different microtubule arrays and cargo could be transported to other cellular locations by dynein. Also, dynein

functions in mitotic events that require force generation including nuclear envelope breakdown, spindle orientation, and chromosome segregation (Barton and Goldstein, 1996; Hebbbar et al., 2008b; Kotak and Gonczy, 2013; Raaijmakers and Medema, 2014). GSK-3 activity has been linked to many of the same processes (Acevedo et al., 2007; Bobinnec et al., 2006; Fumoto et al., 2008; Harwood et al., 2013; Izumi et al., 2008; Tighe et al., 2007; Wakefield et al., 2003; Wojcik, 2008), and it remains to be determined whether GSK-3 regulation of dynein is relevant in these events. Cells in the mammalian colon express PPAR- $\gamma$  protein, so our studies indicate that rosiglitazone (and insulin) have the potential to regulate dynein in the colon (Lefebvre et al., 1998; Su et al., 2007). Moreover, rosiglitazone and similar drugs have been reported to be both chemopreventive and carcinogenic in rodent models, which has garnered substantial interest in these compounds (Lefebvre et al., 1998; Su et al., 2007). Interestingly, there is a higher incidence of colorectal cancer among diabetics (Larsson et al., 2005). Our studies should guide experiments that examine the effect of these drugs on mitotic regulation and will be useful in interpreting outcomes of pre-clinical and clinical trials in non-nervous tissues.

**How are dynein regulatory mechanisms coordinated?** Our studies have begun to define a mechanism that can regulate dynein motors in response to an increase in insulin signaling. They also raise a new set of questions. For example, we also detected phosphate incorporation in HC and LIC subunits – how are these events coordinated? Do phosphatases play a role in dynein regulation? Do other post-translational modifications of dynein and its interacting

proteins function coordinately with GSK-3 $\beta$ , or are they utilized in different cellular processes that require distinct modes of dynein regulation? Phosphorylation of dynein by other kinases has been identified (Mitchell et al., 2012; Pullikuth et al., 2013) and Ndel1/Nde1 phosphorylation by multiple kinases has been reported (Bradshaw et al., 2013). For example, we found that phosphorylation of Ndel1 by both CDK5 and CDK1, but not either alone, inhibited Ndel1 binding to dynein and increased its interaction with Lis1 (Hebbar et al., 2008b). How are all of these events coordinated in the cell? Finally, can other ligands known to induce GSK-3 inhibition also stimulate dynein? How does dynein regulation alter kinesin behavior and vice versa? Future studies from our group and others should be able to resolve these interesting questions and shed light on the complex regulatory mechanisms controlling these vital motor proteins.

## **MATERIALS AND METHODS**

**Cells:** Adult rat DRG neurons were prepared as described in (Pandey and Smith, 2011) and maintained in Hamm's F12 medium supplemented with 10% horse serum. The human colon cancer cell line, HCT-116, was maintained in DMEM supplemented with glutamine (2mM), 10% FBS, penicillin (100 U/ml) and streptomycin (100  $\mu$ g/ml). The murine YAMC epithelial cell line was derived from the colonic mucosa of a transgenic mouse generated by the introduction of a temperature sensitive, interferon inducible, SV40 T Ag, tsA58, the Immortomouse (Whitehead et al., 1993). YAMC cells were maintained at the permissive temperature (33°C) in RPMI 1640 media supplemented with glutamine (2mM),

10% FBS, penicillin (100 U/ml), streptomycin (100 µg/ml), murine gamma interferon (5 U/ml), and 1% ITS.

**Pharmaceutical reagents:** The following pharmaceutical reagents were used: GSK-3 inhibitors CT99021 (3µM, Selleck) and LiCl (10mM, Sigma-Aldrich), The PPAR-γ agonist and insulin sensitizer, rosiglitazone (10µM, Biomol), the transcription inhibitor, 5, 6-dichloro-1-β-D-ribofuranosylbenzimidazole DRB (80µM, Fisher, Inc.), and the PI3K inhibitors LY294002 (10µM, Cell Signaling) and Wortmannin (0.5µM, Biomol). Cultures exposed to vehicle alone (DMSO or H<sub>2</sub>O) served as controls. For drug treatments, YAMC or HCT116 cells were serum starved for 12 hr prior to exposure to drugs in full medium for an additional 12 hr (or as indicated). The starvation was designed to increase insulin receptor trafficking to the cell surface and/or to lower exposure to natural ligands of PPAR-γ to increase sensitivity to rosiglitazone. DRG neurons did not undergo serum starvation, but were maintained in culture for 24 hr with 10% horse serum prior to addition of drugs.

**Expression Vectors:** EGFP-C2 IC2C, PRSET-A IC2C and PRSET-A N237 expression vectors were described previously (King et al., 2003). The EGFP-IC1B vector was provided by K.Pfister (Univ. VA). HA-GSK-3β K85A and HA-GSK-3β S9A expression vectors were from Addgene (plasmid ID 14755 and 14754). The p50-EGFP plasmid was provided by T.A. Schroer (Johns Hopkins). Complementary hairpin sequences for *Lis1* (1,062–1,080 bp; GAGTTGTGC-TGATGACAAG) were synthesized and cloned into pSilencer under the control of the U6 promoter (version 2.0; Ambion) (Pandey and Smith, 2011). The flag-

tagged, dominant-negative human PPAR- $\gamma$  expression vector (dnPPAR- $\gamma$ ) was provided by V.K. Chatterjee (Oxford Univ). This mutant retains ligand and DNA binding, but exhibits markedly reduced transactivation and impaired corepressor interaction, which is thought to produce the dominant negative effect (Gurnell et al., 2000). Cells were transfected using Lipofectamine 2000 reagent (Invitrogen).

**Protein purification:** Bovine brain cytoplasmic dynein was purified as described previously (Bingham et al., 1998; Culver-Hanlon et al., 2006). Recombinant dynein and NdeI1 proteins were expressed in BL-21 cells. Cells were grown at 37°C to an OD600 of 0.4, and then 0.1 mM isopropyl-d-thiogalactoside (IPTG) was added to induce protein expression. Bacteria were lysed in his-tagged protein purification binding buffer (Invitrogen) with protease inhibitors. The cells were sonicated and pelleted by centrifugation at 10,000 g at 4°C for 30 min. Ni-NTA beads (Invitrogen) were added into the cell supernatant and incubated at 4°C for 1 hr. The protein was washed three times and then eluted from beads. His-tagged recombinant Lis1 was expressed in Sf9 insect cells using a baculovirus kindly provided by A. Musacchio. His-tagged Lis1 was purified using Ni-NTA beads.

**Cell and brain extract preparation:** For preparation of cell extract, cells at 90% confluency were lysed in buffer containing 50 mM Tris (pH 7.5), 0.1% NP-40, 100mM NaCl, 1 mM MgCl<sub>2</sub>, 5 mM EDTA, protease inhibitor cocktail (Fisher) and Halt phosphatase inhibitor cocktail (Fisher) on ice for 30 minutes. Cell lysates were sonicated for 10 pulses at level 1 with 10% output 3 times. The lysates were incubated on ice for another 10 min and then centrifuged at 17,000

g for 20 minutes at 4°C. For preparation of mouse brain extract, brains were quickly dissected and dounce-homogenized in the above lysis buffer. The lysates were incubated on ice for 30 min and then centrifuged at 17,000 g for 30 minutes at 4°C. Concentrations of extracts were determined by a BCA protein assay (Pierce).

**Protein kinase assays:** The GST-GSK-3 $\beta$  Kinase Enzyme System and SignalChem GST-GSK-3 $\beta$  or His-GSK-3 $\beta$  purified kinases (Promega) were used for all kinase assays. Lambda protein phosphatase was purchased from New England BioLabs. For some assays, purified dynein was first immobilized on 74.1 mouse monoclonal IC antibody conjugated agarose (Santa Cruz Biotechnology, Inc). Potential substrates were incubated with 50ng GSK-3 $\beta$  and 0.03  $\mu$ Ci/ $\mu$ l  $\gamma$  <sup>32</sup>P-ATP for 30 minutes at 37 °C. The reaction was stopped by the addition of sample buffer. In one experiment brain dynein was pre-incubated with Lambda protein phosphatase (1000 U) to remove preexisting phosphates. Some reactions also included 3 $\mu$ M of the GSK-3 inhibitor CT99021. Proteins were separated by SDS-PAGE and the wet min-gel was sealed in saran wrap and exposed to X-ray film overnight at -80°C. After exposure gels were stained with Coomassie brilliant blue to visualize proteins.

**Immunoprecipitation and Western blot:** For IPs from cell or brain extracts, 1  $\mu$ g 74.1 IC antibodies were first incubated with 30  $\mu$ l Protein-A dynabeads (Invitrogen) for 2 hr at room temperature and washed with lysis buffer twice. The antibody conjugated dynabeads were incubated with 1 mg extracts at 4°C overnight. Dynabeads were subject to two washes of lysis buffer and then

two washes of PBS-T (phosphate buffered saline with 0.1% Tween 20) at 4°C. For IPs from purified bovine brain dynein or IC2C, proteins were first incubated with 74.1 mouse monoclonal IC antibody conjugated agarose (Santa Cruz Biotechnology, Inc) in PBS-T with protease and phosphatase inhibitors overnight. Beads were spun down and washed with PBS-T twice and then PHM-T buffer (60 mM PIPES, 25 mM HEPES, 4 mM MgSO<sub>4</sub>, 0.1% Tween 20, pH 6.9). Beads then were incubated with Lis1 or Ndel1 or both in PHM-T buffer with protease and phosphatase inhibitors for 1 hr at RT. Beads were washed 3 times with PHM-T buffer and eluted in 60 µl PBS plus 20 µl 6X sample buffer and boiled for 3 min before samples were loaded onto SDS-PAGE gels. For western blots, samples were transferred to PVDF or nitrocellulose membranes and subjected to standard protocols to identify proteins.

**Antibodies:** The 74.1 dynein IC mouse mAb, H100 PPAR-γ1 rabbit polyclonal Ab, H-3 His-probe rabbit polyclonal Ab, and IRβ mouse mAb were from Santa Cruz Biotechnology. The 3D10 GSK-3β mouse mAb, 5B3 S9 Phospho-GSK-3β rabbit mAb, 11E7 AKT rabbit mAb, D25E6 T308 pAKT rabbit mAb and D9E S473 p-AKT rabbit mAb were from Cell Signaling, Inc. The EB1, p150, p50, and β-catenin mouse mAbs were from BD Biosciences. The CDK5RAP2 rabbit polyclonal Ab was from Millipore. The α-tubulin mouse mAb was from Sigma-Aldrich. The rabbit polyclonal CENPF Ab was from Novus Biologicals. Lis1 and Ndel1 rabbit polyclonal antibodies were described previously (Hebbar et al., 2008b; Pandey and Smith, 2011).

**Immunofluorescence:** For IC or pericentrin, cells were fixed in 100% ice-cold methanol for 2 min. For p50, p150glued and pAKT immunofluorescence, cells were fixed in 3% paraformaldehyde followed by permeabilization with 0.2% Triton X-100 for 10 minutes. Nuclei were visualized using Hoechst dye (33258; Sigma-Aldrich). Coverslips were mounted on glass slides using ProLong Gold Antifade (Invitrogen). Cells were visualized with an Axiovert 200 inverted microscope (Carl Zeiss, Inc.) using Plan-Neo 100×/1.30 or Plan-Apo 63×/1.40 oil-immersion objectives (Immersionol 518F; Carl Zeiss, Inc.). Optical sections were deconvolved using AxioVision's combined iterative algorithm to obtain confocal images if necessary. The accumulation of dynein at centrosomes was determined by measuring the mean pixel intensity of immunofluorescence (arbitrary fluorescence units – afu) in a fixed circular area (0.008 inches<sup>2</sup>) encompassing the centrosome visualized by CDK5Rap2. Intensities were determined using ImageJ software. For most experiments, dynein enrichment was considered positive if it was greater than or equal to 60 afu (this was typically 3 times higher than randomly selected regions of the cell). The analysis of dynein puncta at cell periphery is described in the legend for Figure 1.6.

**Analysis of acidic organelle movement in living cells:** Cells were incubated with 100 nmol LysoTracker Red (Invitrogen) for 30 min prior to imaging. Coverslips were transferred into fresh medium containing 25 mM HEPES, pH 7.4 and OxyFluor (Oxyrase Inc.) in a water-heated custom-built microscope stage warmed to 37°C. Cells expressing a relatively low level of LysoTracker Red were selected for imaging. Fluorescent images were acquired every 2s for 4 min

(YAMC) or 2 min (DRG axons) using a Plan-Apo 63×/1.2 W/0.17 water objective. *YAMC cells*: Velocities and run lengths of retrograde, minus end-directed organelle movement (towards the nucleus) were measured using the “particle tracking” plugin for ImageJ software. *DRG axons*: kymographs were generated from time-lapse movies using NIH ImageJ software. Images were acquired in 2s intervals for 2 minutes. The kymographs were generated such that the direction toward the cell body was always to the right, so lines that sloped toward the right at any point with a net displacement of >5 μm were categorized as retrograde organelles. Lines that sloped toward the left >5 μm at any time during the recording interval were considered anterograde organelles. Lines that zigzagged were categorized as bidirectional, and lines that showed <5 μm lateral displacement in any direction during the recording interval were categorized as static.

**Statistics:** All analyses were carried out using GraphPad prism. In all figures, error bars represent +/-95% CI (confidence interval). One-way ANOVA with Tukey’s multiple comparison test or an unpaired, two-tailed student’s t-test was used and described in each figure legend

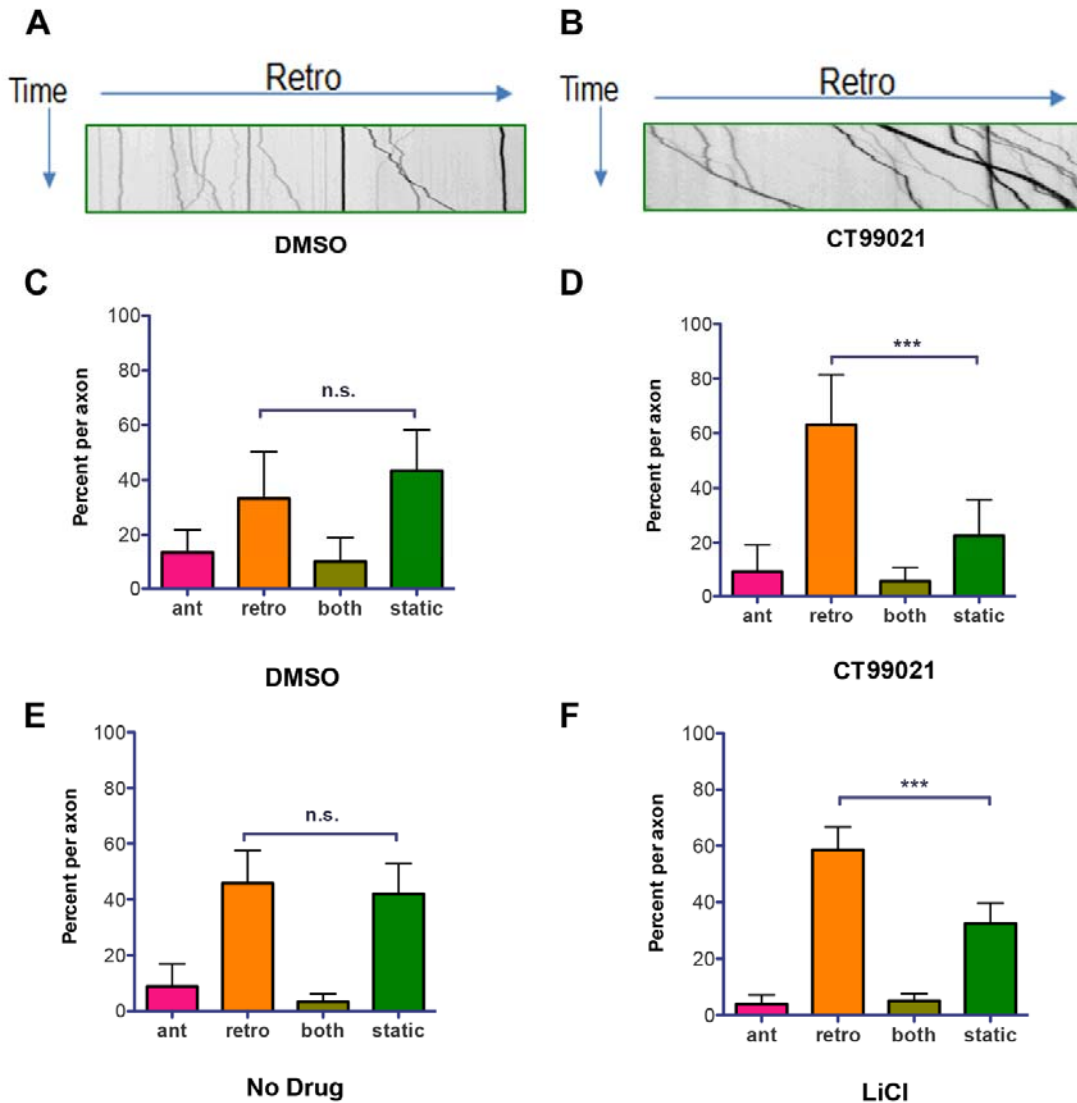


**Figure 1.1 Inhibition of GSK-3 $\beta$  stimulates retrograde transport in adult rat DRG neurons**

Time-lapse movies of Lysotracker-labeled organelles moving in living DRG axons exposed to GSK-3 inhibitors were converted to kymographs using NIH Image J software. **(A, B)** Representative kymographs for axons exposed to DMSO (A), or CT99021 (B) for 12 hr are shown. The horizontal arrow indicates the retrograde direction (towards the cell body for the 100 $\mu$ m axon segment). The vertical arrow indicates time (2 minutes total recording time). **(C, D)** Organelle movement was categorized as anterograde (ant), retrograde (retro), both, or static and the percentage of organelles per axon in each category determined. There were significantly more retrograde organelles than static organelles following CT99021 exposure (D) but not following exposure to DMSO alone (C). 16 axons in cultures from 2 different rats were analyzed for each condition. *Mean +/- 95% CI; N.S.,*

$P > 0.05$ , \*\*\*  $P < 0.0001$ , one-way ANOVA). **(E, F)** Similar results were obtained with LiCl (Mean  $\pm$  95% CI; N.S.,  $P > 0.05$ , \*\*\*  $P < 0.0001$ , one-way ANOVA). (Xu Gao performed the experiments in figure 1.1 for the manuscript.)

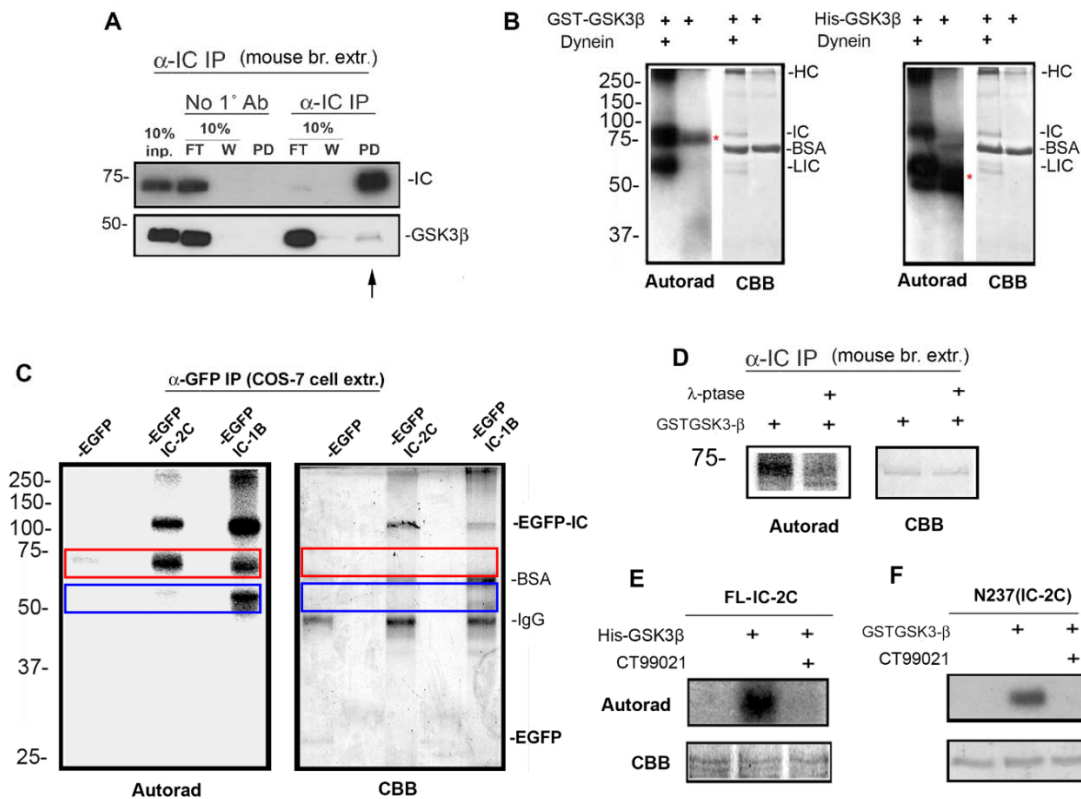


## Figure 1.2 Direct phosphorylation of dynein by GSK-3 $\beta$

**A)** The 74.1 IC antibody was used to immunoprecipitate dynein motors from whole mouse brain extract (IC-IP). The control was brain extract incubated with protein A beads but no 74.1 (No 1° Ab). FT = 10% of flow through, W = 10% of first wash, PD = pull down. GSK-3 $\beta$  was pulled down only if dynein was pulled down (arrow). **B)** Purified bovine dynein was incubated with (+) or without GST-GSK-3 $\beta$  (left panel) or His-GSK-3 $\beta$  (right panel) in a kinase assay. The SDS-PAGE gel was exposed to X-ray film (Autorad) and then stained to visualize proteins (CBB). A band the size of IC's appeared robustly phosphorylated. Heavy chains (HC) and light intermediate chains (LIC) were also phosphorylated. Auto-phosphorylated GST-GSK-3 $\beta$  (~73 kDa) and His-GSK-3 $\beta$  (~48kDa) were also detected (red asterisk). **C)** EGFP-tagged IC-2C or IC-1B were transiently expressed in Cos-7 cells. EGFP alone served as a control. An anti-GFP antibody was used to isolate the proteins, then beads were exposed to GST-GSK-3 $\beta$ . The autoradiograph shows phosphate incorporation into both EGFP-IC-2C and EGFP-IC-1B (the bands were cut and confirmed by mass spectrometry analysis), but not in EGFP alone. The phosphorylated bands in the red box are likely endogenous ICs in the complex. Bands in the blue box may be endogenous LIC chains interacting with IC-1B. **D)** ICs pulled down from mouse brain extract were incubated with or without lambda phosphatase to remove endogenous phosphates. After extensive washing of beads to remove residual phosphatase,

immobilized dynein was subjected to the GST-GSK-3 $\beta$  kinase assay (Autorad). “Stripped” dynein incorporated less phosphate suggesting priming may be important. **E)** Full length his-tagged IC-2C (FL-IC-2C) and an N-terminal fragment (N237 IC-2C) were expressed and purified from bacteria. Both proteins were phosphorylated by GSK-3 $\beta$  *in vitro* and phosphorylation was blocked by the specific GSK-3 $\beta$  inhibitor, CT90221, suggesting that some sites may not require priming phosphorylation.

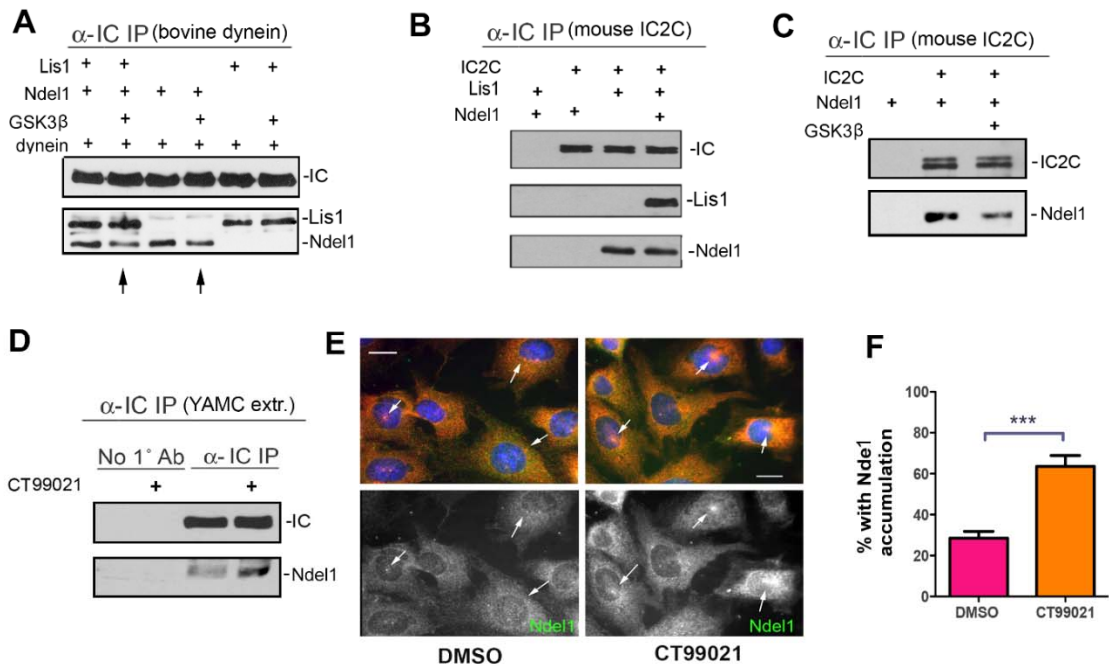


**Figure 1.3 Dynein phosphorylation by GSK-3 $\beta$  impacts Ndel1 interaction**  
**A)** Purified recombinant Lis1 and Ndel1 co-precipitated with purified bovine brain dynein complexes. However, if the dynein was previously exposed to GSK-3 $\beta$ , less Ndel1 was found in the precipitates (arrows). On the other hand, phosphorylation of dynein by GSK-3 $\beta$  seemed not to change its interaction with Lis1. **B)** Purified recombinant FL-IC2C was immunoprecipitated by IC-beads (IC-IP) and then incubated with Lis1 or Ndel1 or both. Lis1 was pulled down by FL-IC2C only when Ndel1 was present. **C)** IC-IP of purified recombinant FL-IC2C was treated with or without GSK-3 $\beta$  kinase. Less purified Ndel1 was pulled down where IC2C were pretreated with GSK-3 $\beta$ . **D)** IC-IP from YAMC cells were treated with or without CT99021. More Ndel1 was pulled down in CT99021 treated cell than control. **E)** YAMC cells were serum starved for 12 hr, then exposed to DMSO (left) or CT99021 (right) in medium with FBS and ITS for additional 12 hr. Dynein and Ndel1 distribution were evaluated by IC (red) and Ndel1 (green) antibodies. The representative figures for each treatment were shown. **F)** Quantification of percentage of cells with Ndel1 accumulation at the centrosome. Similar to dynein, cells treated with CT99021 have significantly more Ndel1 accumulation at centrosome than control cells (*Mean +/- 95% CI; \*\*\* P<0.0001 by t-test*).

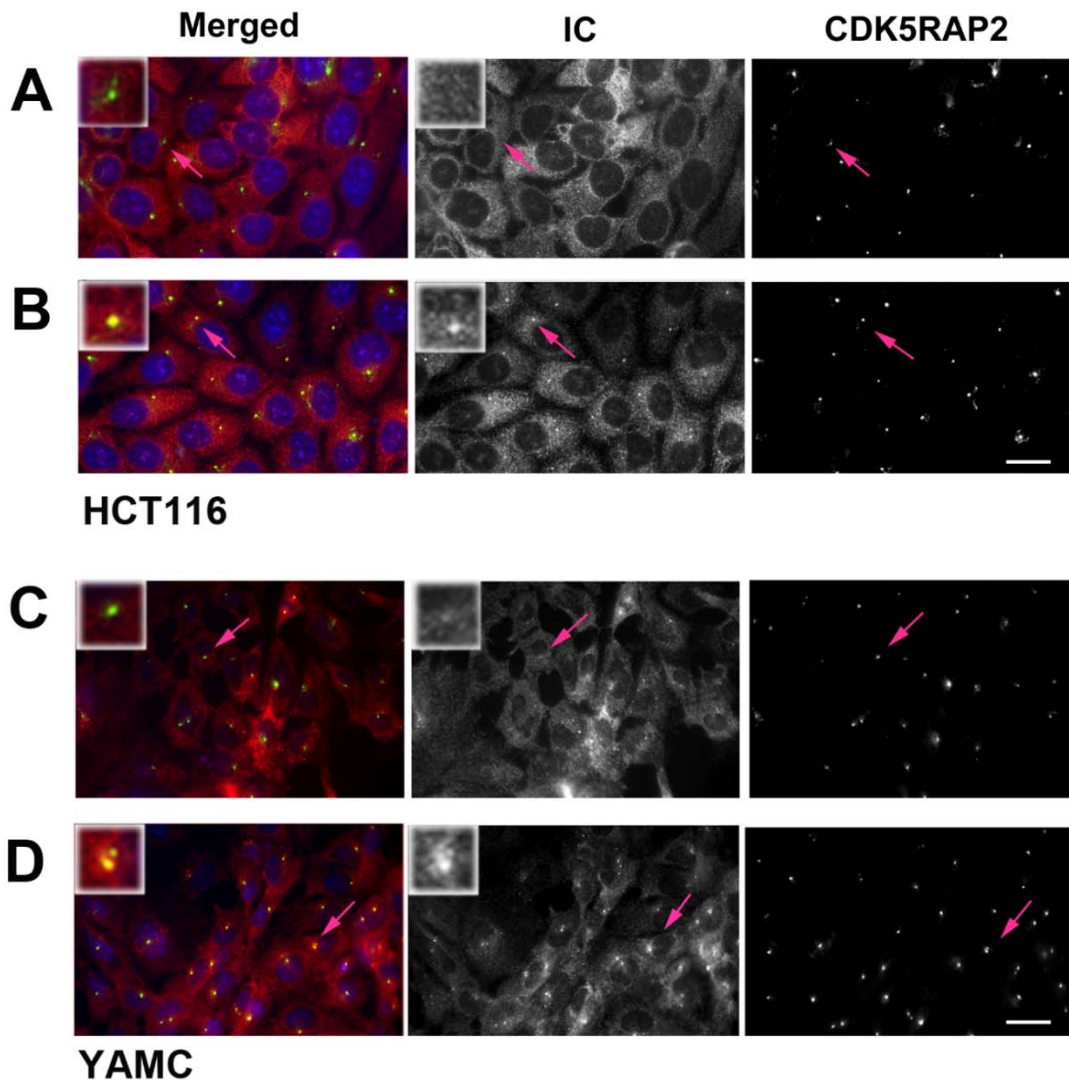


**Figure 1.4 Pharmacological inhibition of GSK-3 $\beta$  causes dynein to accumulate at centrosomes in colon cell lines**

(A, B) HCT116 human colon cancer cells were serum starved for 12 hr, then exposed to FBS and ITS (A) or CT99021 (B) in medium with FBS and ITS for an additional 12 hr. Dynein distribution was assessed by IC immunofluorescence (red, and middle panels). Centrosomes were labeled with a CDK5RAP2 antibody (green, and right panels). Nuclei are stained with Hoechst dye (blue). Insets show digitally enlarged images of centrosomes indicated by the pink arrows. (C, D) The same response was observed in YAMC cells derived from adult mouse colon.

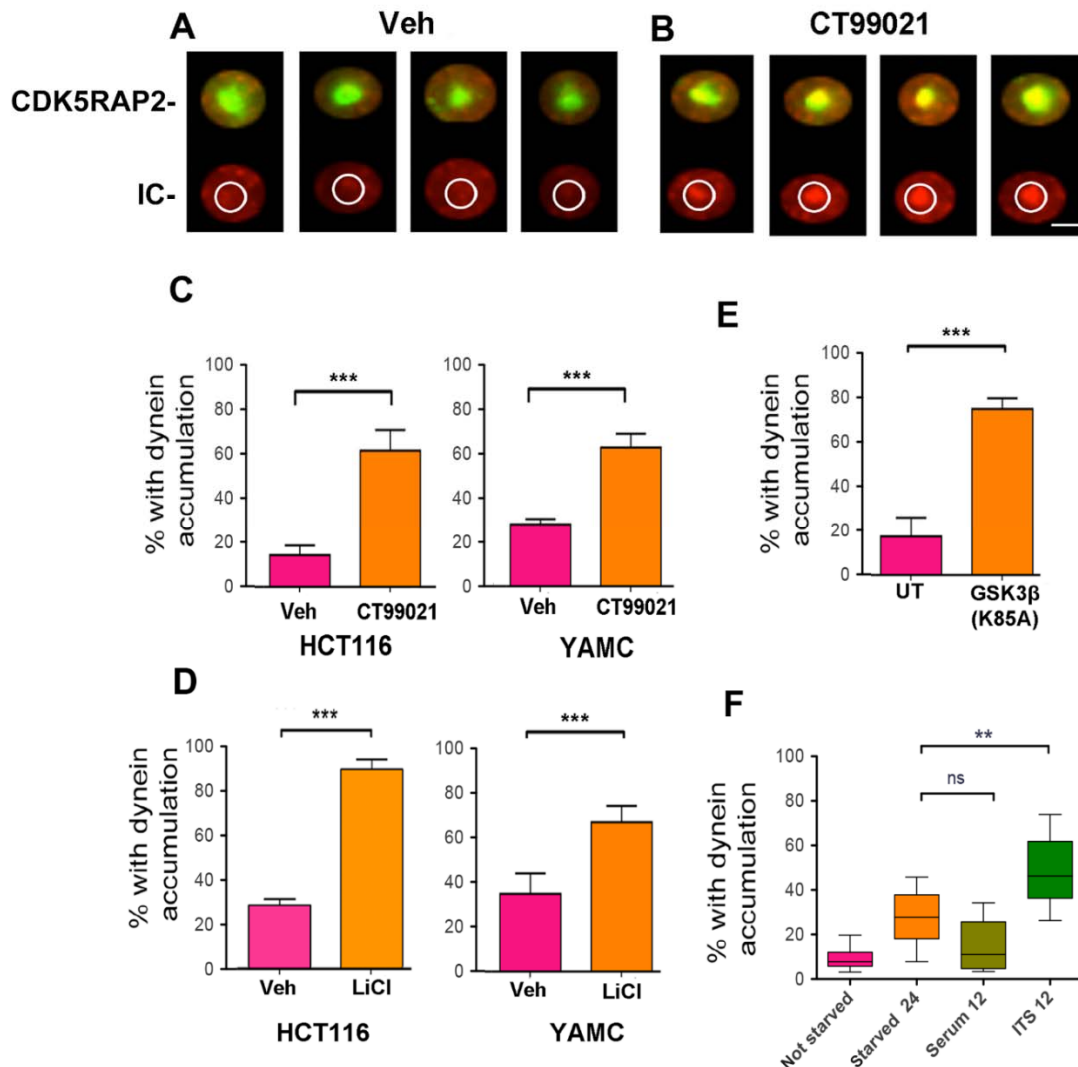


**Figure 1.5. GSK-3 $\beta$  inhibition is responsible for the dynein accumulation at centrosomes**

(A, B) IC intensity (red) was determined within a circle drawn around the centrosome (green). Cells with IC intensity equal to or greater than 60 arbitrary fluorescence units (afu) were considered to have dynein accumulation. (C) CT99021 exposure for 12 hr caused a significant increase in the percentage of HCT116 or YAMC cells with dynein accumulation compared to the DMSO vehicle control (Veh). N=400 cells measured for each condition, *Mean +/- 95% CI*; \*\*\*,  $p < 0.0001$ , *t-test*. (D) Another GSK-3 inhibitor, LiCl, produced a similar result in both cell types (N=400 cells measured for each condition, *Mean +/- 95% CI*; \*\*\*,  $p < 0.0001$ , *t-test*). (E) Overexpression of the kinase dead HA-GSK-3 $\beta$  (K85A) also caused dynein accumulation (N=217 cells). UT = HA negative cells in the same cultures (N=223 cells). *Mean +/- 95% CI*; \*\*\*,  $p < 0.0001$ , *t-test*. (F) Simply adding insulin (INS) in the absence of FBS (Serum) to starved cells was sufficient to produce an increase in the percentage of cells with dynein accumulation at the

centrosome. FBS alone did not induce accumulation. (N=100 cells measured for each condition \*\*,  $p < 0.001$ , t-test).  
*(Xu Gao performed the experiments in figure 1.5F for the manuscript.)*

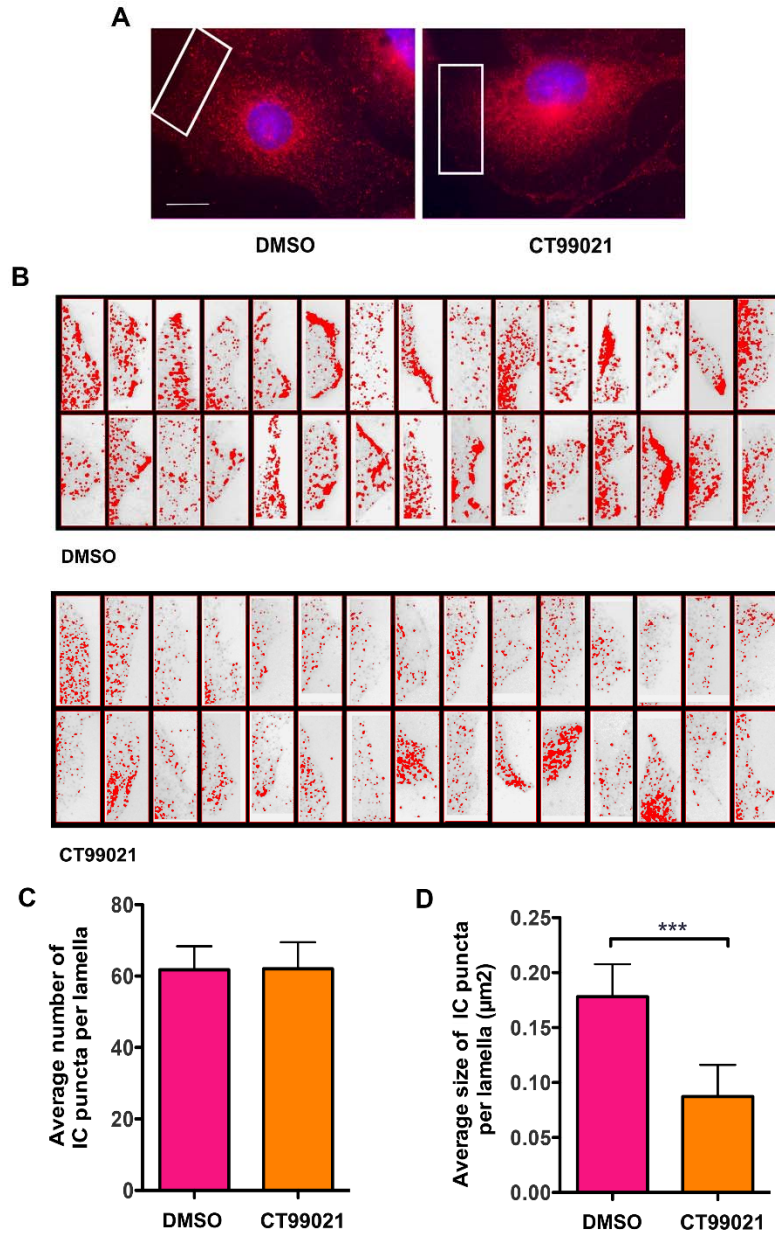


**Figure 1.6 Dynein is released from peripheral/cortical sites in response to GSK-3 $\beta$  inhibition**

**A)** YAMC cells were treated with or without CT99021 for 12 hr after serum starvation. Cells were fixed and immunostained with IC antibodies (Red) and Hoechst dye to label nuclei. **B)** 30 images of lamella of DMSO control and CT99021 treated interphase cells were acquired for each condition using the same exposure times. All of the images were adjusted together in image J using the image J threshold controls to select pixels between 150 and 200 afu, a good fit for the data. Image J was used to quantify the number and size of dynein

puncta. **C)** The average number of dynein puncta did not change (~60 per lamella). **D)** The average size of dynein puncta in CT99021 treated cells was significantly reduced compared to control cells (*Mean +/- 95% CI*; \*\*\*,  $P < 0.0001$ , t-test). A total of 1852 puncta were measured in the control images and 1861 puncta in the CT99021 treated images.

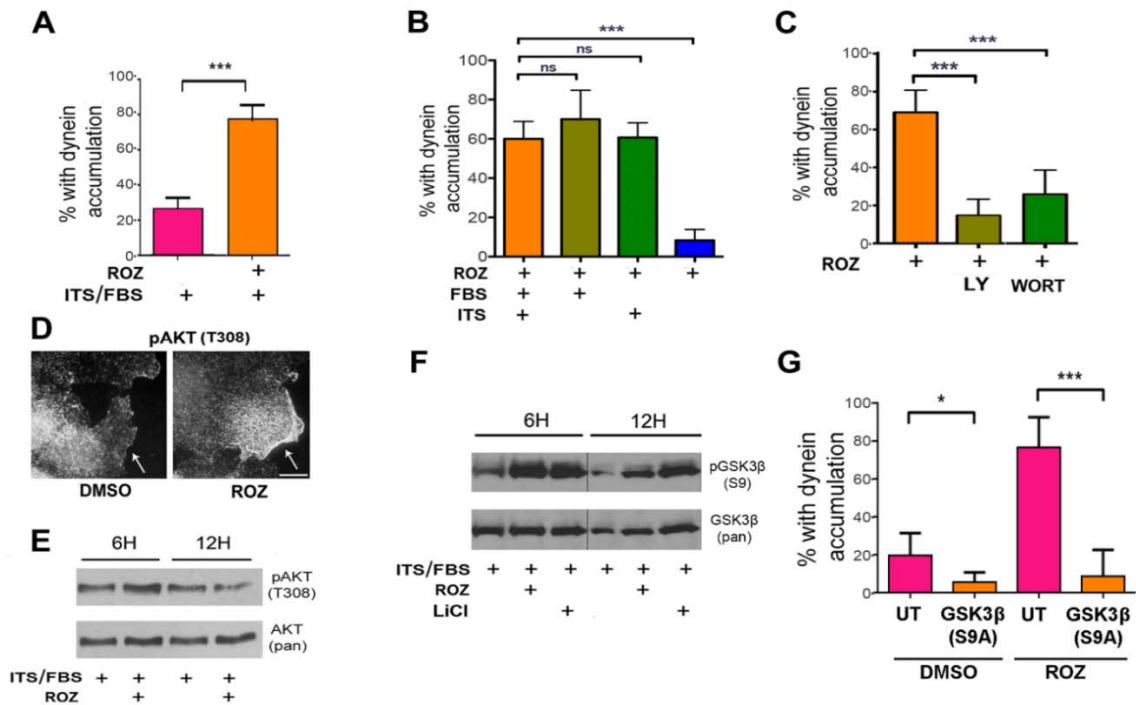


**Figure 1.7 An insulin-sensitizing drug, rosiglitazone, causes centrosomal dynein accumulation via GSK-3 $\beta$  inactivation**

**A)** 12 hr of ROZ exposure resulted in dynein accumulation at centrosomes after 12 hr of serum starvation in YAMC cells (N=150 cells for each treatment, *Mean* +/- 95% CI; \*\*\**P*<0.0001, *t*-test). **B)** Starved YAMC cells were exposed to ROZ in the presence or absence of FBS and/or ITS. The absence of FBS and ITS prevented the dynein response to ROZ, while ITS or FBS alone was sufficient to permit the response (N=150 cells for each treatment, *Mean* +/- 95% CI; \*\*\**P*<0.0001, by one way ANOVA). **C)** YAMC cells were co-treated with ROZ and the PI3K inhibitor, LY294002 (LY) or wortmannin (Wort). Both inhibitors blocked dynein accumulation at centrosomes (N=150 for cells for each treatment, *Mean* +/- 95% CI; \*\*\**P*<0.0001 by one way ANOVA). **D)** Immunostaining of YAMC cells after exposure to DMSO or ROZ with pAKT (T308) antibodies. pAKT appeared enriched at the plasma membrane with ROZ treatment. *Scale bar* 10  $\mu$ m. **E)** Western blot of YAMC cells after exposure to ROZ were probed with pAKT (T308) and pan-AKT antibodies. ROZ increased pAKT levels by 6 hr. **F)** Exposure of starved YAMC cells to ROZ or LiCl for 6 or 12 hr increased S9 phosphorylation of GSK-3 $\beta$  (pGSK-3 $\beta$ (S9)) levels relative to total kinase levels (GSK-3 $\beta$  (pan)). **G)** Transient expression of a constitutively active GSK-3 $\beta$  construct, HA-GSK-3 $\beta$  (S9A) prevented dynein accumulation in response to ROZ. HA-negative cells in the same cultures were considered un-transfected (UT). (N=100 cells for each condition, *Mean* +/- 95% CI; \**P*<0.05, \*\*\* *p*<0.0001 by one way ANOVA). (Sachin Hebbar performed the experiments in figure 1.7 B and C and Jai Pandey did the experiments in figure 1.7F for the manuscript.)

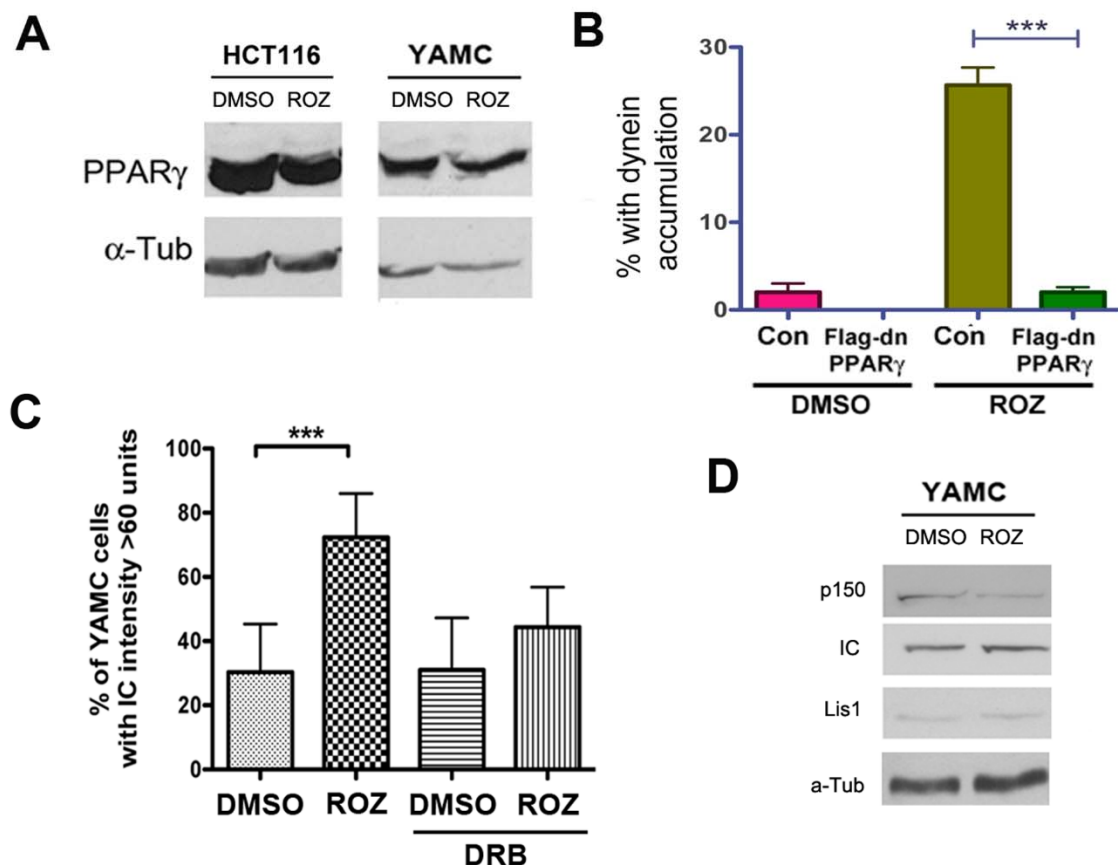


**Figure 1.8 Rosiglitazone-induced dynein redistribution requires PPAR- $\gamma$  and new transcription, but expression of dynein and its regulators is not increased.**

**A)** Western blots of both HCT116 and YAMC cell extracts show they express PPAR- $\gamma$  and ROZ treatment for 12 h does not change PPAR- $\gamma$  expression. **B)** Expression of dominant negative, flag-tagged PPAR- $\gamma$  construct significantly reduces ROZ-induced accumulation of IC at the centrosome in HCT116 cells. **C)** YAMC cells were co-incubated with 500  $\mu$ M DRB (a potent transcription inhibitor) and ROZ and stained for IC. ROZ-induced IC accumulation only happened when DRB was not present, which indicated that dynein accumulation at centrosomes requires new transcription. **D)** Treatment with 10  $\mu$ M ROZ for 12h did not alter protein expression of IC, p150, Lis1. (Sachin Hebbar performed the experiments in figure 1.8 B-D for the manuscript.)

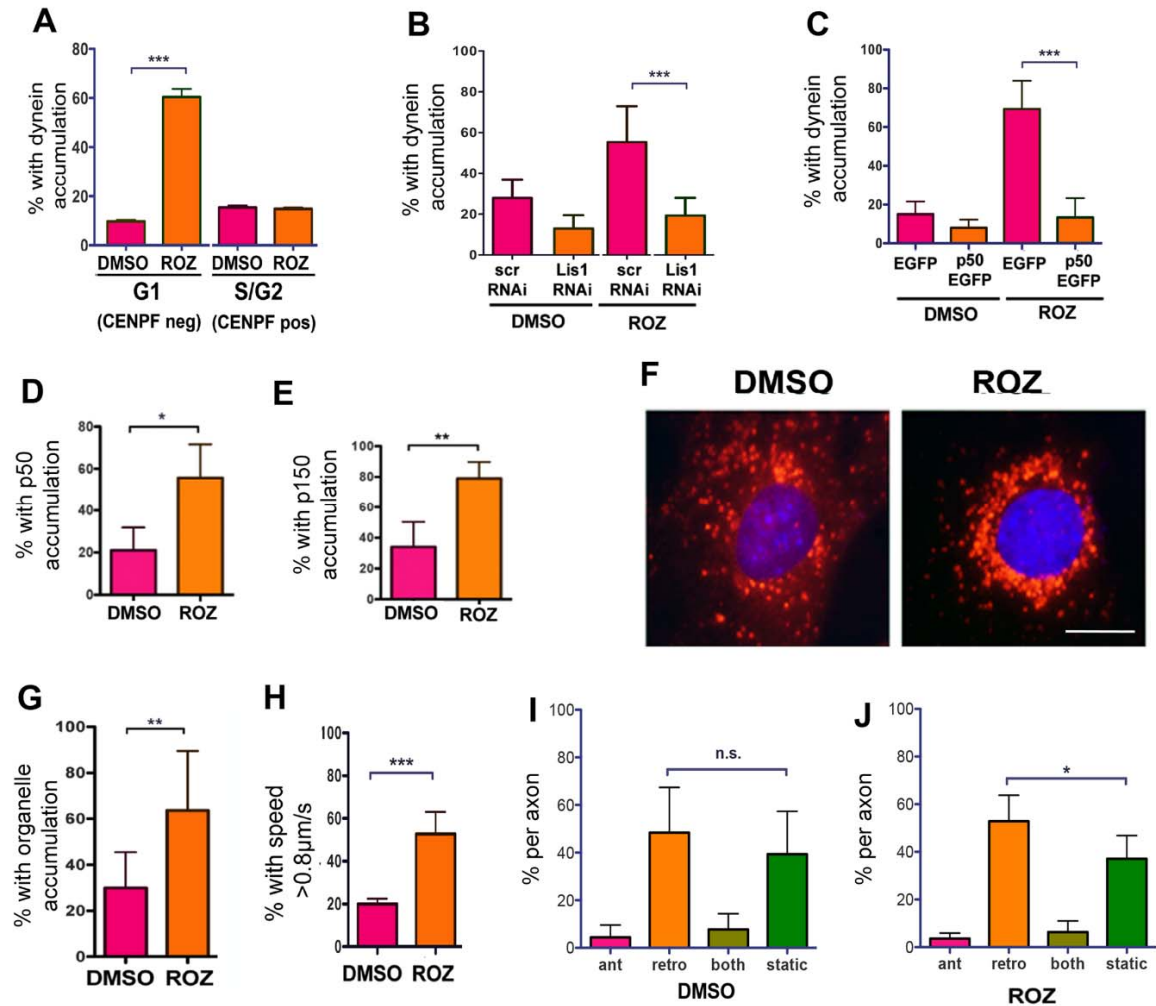


### Figure 1.9 Dynein accumulation at centrosomes in response to ROZ is due to increased motor transport activity

**A)** YAMC cells were costained for the late-S/G2 marker, CENPF, and IC after 12 hr of ROZ exposure to determine if cells were arresting at S/G2. Accumulation does not correlate with entry into S/G2 (*Mean +/- 95% CI; \*\*\* P<0.0001, one-way ANOVA*). **B)** A Lis1 shRNA construct (Lis1 RNAi), but not a scrambled sequence (scr), prevented ROZ-induced dynein accumulation at the centrosome (*Mean +/- 95% CI; \* P<0.05, \*\*\* P<0.0001 by one way ANOVA*). **C)** Overexpression of the GFP-p50 also blocked the accumulation of dynein at the centrosome (*Mean +/- 95% CI; \*\*\* P<0.0001 by one-way ANOVA*). **(D, E)** ROZ induces accumulation of the dynein subunits p50 and p150glued (p150) in HCT-116 cells. (*Mean +/- 95% CI; \* P<0.05; \*\* P<0.0029 by t-test*). **(F, G)** ROZ exposure resulted in perinuclear accumulation of LysoTracker-labeled organelles in YAMC cells (*Mean +/- 95% CI; \*\* P<0.0021 by t-test, of Scale bar 10 μm.*). **(H)** The percent of organelles with average speeds over 0.8 μm/s was higher in cells treated with ROZ in YAMC cells (*Mean +/- 95% CI; \*\*\* P<0.0001 by t-test*). **(I, J)** ROZ increased the percentage of organelles moving retrogradely in living adult DRG

axons. The neurons were not serum starved prior to drug exposure (*Mean +/- 95% CI; N.S., P>0.05, \* P<0.05 , one-way ANOVA*).*(Sachin Hebbar performed the experiments in figure 1.9 B-E, Jai Pandey performed the experiments in figure 1.9 F-H, and Xu Gao performed experiments in figure 1.9 A,I, and J for the manuscript.)*

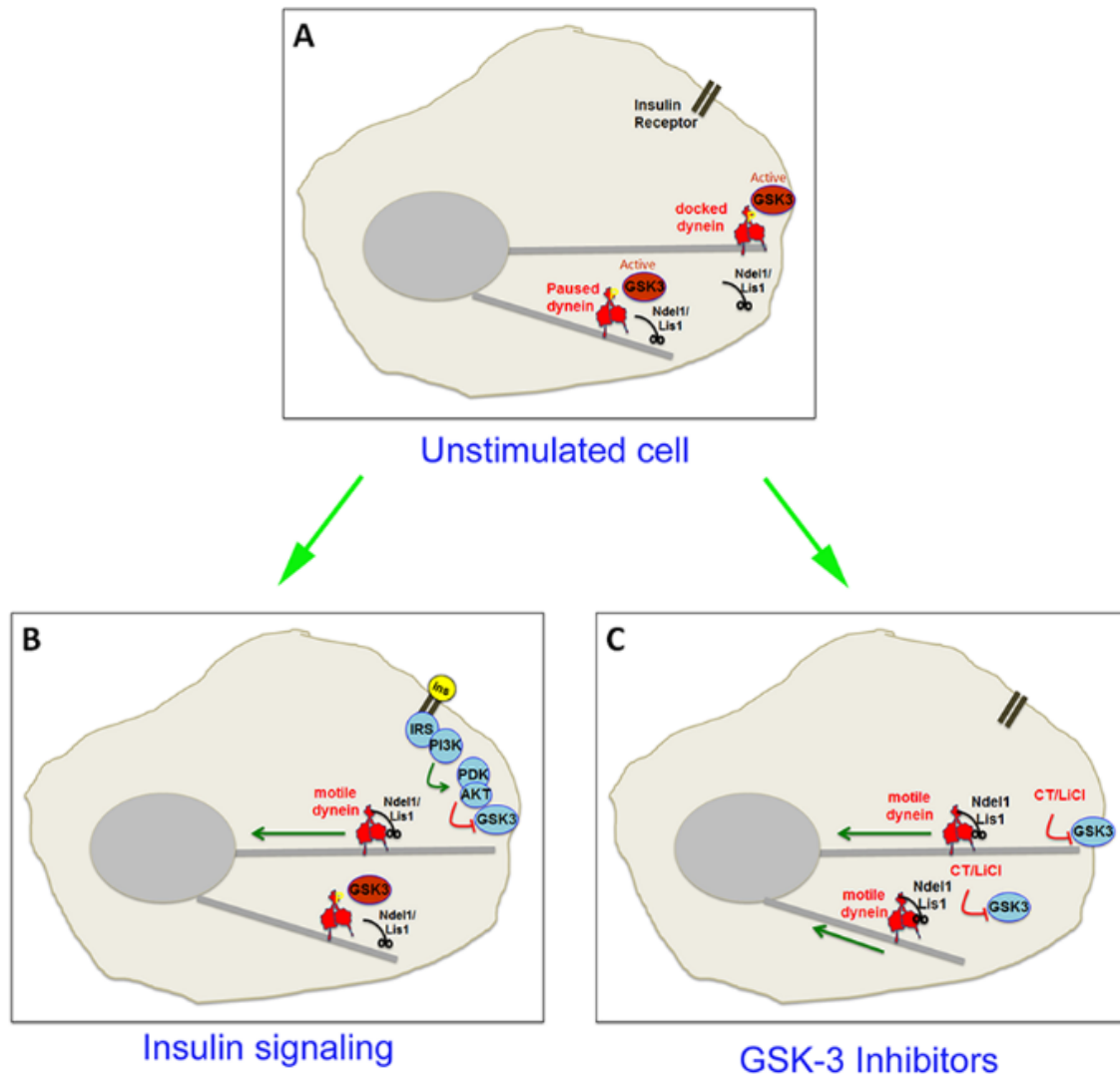


**Figure 1.10 A model for GSK-3 $\beta$ - dependent regulation of dynein dependent retrograde organelle transport**

**A)** In an unstimulated "resting" cell, GSK-3 $\beta$  is active and phosphorylates dynein. Phosphorylated dynein is not motile, and remains at microtubule plus ends and/or the cell cortex. **B)** When the cell is stimulated by insulin, PI3K/AKT signaling is initiated and GSK-3 $\beta$  is shut off. As cortical dynein loses phosphate at GSK-3 sites, or is replaced with unphosphorylated dynein, it interacts more efficiently with Ndel1/Lis1. Ndel1/Lis1 can then "jump start" dynein, leading to increased retrograde transport of cargo. **C)** Inhibition of GSK-3 $\beta$  by pharmacological inhibitors such as CT99021 (CT) or LiCl stimulates dynein-dependent retrograde organelle transport, bypassing the need for the signal transduction pathway.

## CHAPTER 2

Adenomatous polyposis coli (APC) is a novel multifaceted dynein regulator: the concerted interplay is vital for the effect of thiazolidinediones

### ABSTRACT

There is considerable debate over whether thiazolidinediones, PPAR- $\gamma$  agonists, are chemopreventive or carcinogenic during the development of colorectal cancer, where mutations in adenomatous polyposis coli (*APC*) often occur. We find that dynein and APC physically interact with each other by reciprocal co-immunoprecipitation assays. The interaction is positively regulated by GSK-3 $\beta$ , which can be inhibited by rosiglitazone through activation of PI3K/AKT pathway as shown in the chapter 1. In both cell lines and mouse models, we demonstrate that rosiglitazone increases dynein activity and cell migration in wild type (WT) cells but not in *Apc* (min/+) cells, and that rosiglitazone induces spindle misorientation in *Apc* (min/+) cells but not in WT cells. We provide evidence that this involves different PI3K/AKT/GSK-3 $\beta$  signaling responses to rosiglitazone between WT and *Apc* (min/+) cells, and that *Apc*Min mutation negatively regulates the interaction of dynein to WT APC. Our discovery of the interplay of APC and dynein provides a new insight into how PPAR- $\gamma$  signaling regulates cancer development and other cellular events.<sup>2</sup>

---

Feng J. Gao<sup>1</sup>, Sachin Hebbar<sup>2</sup>, Deanna S. Smith<sup>1\*</sup>. To be submitted to Journal of Cell Biology (Feng J Gao and Sachin Hebbar are co-first authors)

## INTRODUCTION

Adenomatous Polyposis Coli (APC) is well known for playing a central role in Wnt signaling, where a “destruction complex” including APC, Axin, GSK-3 $\beta$ , and casein kinase 1 (CK1) and the E3-ubiquitin ligase  $\beta$ -TrCP is formed (Polakis, 2002; Stamos and Weis, 2013). The complex carries out the phosphorylation and ubiquitination on  $\beta$ -catenin, which is subsequently degraded by the proteasome. Loss function of APC via mutation and aberrant Wnt signaling result in the deregulation of  $\beta$ -catenin (Kongkanuntn et al., 1999; Phelps et al., 2009; Sansom et al., 2004), which is the critical event in carcinogenesis (Espada et al., 2009). Although there is increasing evidence supporting APC as a tumor suppressor, the mechanism is still incomplete. Moreover, a large body of research implicates non-traditional roles of APC including cell migration, spindle assembly, cell adhesion, chromosome segregation, and neuronal differentiation (Hanson and Miller, 2005).

The *Apc* (*min/+*) mouse, which harbors a truncating APC mutation, is a prominent animal model to study human colorectal cancer (Taketo and Edelmann, 2009; Yamada and Mori, 2007). Many studies indicate that rosiglitazone, a peroxisome proliferator-activated receptor gamma (PPAR- $\gamma$ ) agonist, prevents colon carcinogenesis (Burgermeister et al., 2003; Chang et al., 2012; Friedrich et al., 2013; Marin et al., 2006). However, several reports indicate that the drug is carcinogenic in *Apc* (*min/+*) mice (Lefebvre et al., 1998; Peters et al., 2012; Saez et al., 1998). It is not clear how PPAR- $\gamma$  signaling affects carcinogenesis in the presence of truncating APC mutations, and most studies

have focused on its role in  $\beta$ -catenin regulation. However, an interesting relationship between APC and the microtubule (MT) cytoskeleton has been emerging over the last decade (Etienne-Manneville, 2010). Our early report showed a link between APC and Lis1, a dynein regulator (Hebbar et al., 2008a). More recently, we demonstrated that rosiglitazone induced dynein activity through the activation of PI3K/AKT/GSK-3 $\beta$  as shown in the chapter 1. Both dynein and APC are substrates of GSK-3 $\beta$  (Ferrarese et al., 2007) and well known for participating in fundamental cellular processes including cell migration, mitosis, and differentiation. Here, we characterized the interaction of dynein with APC and how the PPAR- $\gamma$  signaling regulates the interaction in both WT and Apc (min/+) cells.

Spindle orientation is important in normal intestinal turnover as stem cells dividing in intestinal crypts replenish enterocytes that migrate to the tips of villi before being shed into the intestinal lumen (Reya and Clevers, 2005). The Apc<sup>Min</sup> mutation causes a modest defect in spindle orientation in mouse intestinal stem cells, which is further exacerbated in the tumors that developed in these mice (Fleming et al., 2009). Defective spindle orientation was also reported in precancerous tissue heterozygous for Apc in mice (Quyn et al., 2010). Dynein and its regulators also have a profound impact on spindle orientation (Dujardin and Vallee, 2002; Yingling et al., 2008). It has been reported that the interactions of “MT plus end proteins” including APC, dynein and their associate proteins may be important to stabilize spindle orientation (Mimori-Kiyosue and Tsukita, 2003). Therefore, if rosiglitazone alters these interactions, different spindle orientation

responses could occur between WT and Apc (min/+) cells, which could lead to different cell fate decisions.

Cell migration is a complicated and highly integrated process that participates in many biological functions including embryogenesis, immune responses, wound healing and cancer development (Lauffenburger and Horwitz, 1996; Ridley et al., 2003). A change in the movement of cells away from crypts could affect cell fate decisions and increase or reduce the time that enterocytes are exposed to mutagenic substances in the gut (Nathke, 2004). Precise regulation of signaling events and protein-protein interactions is required for cell migration. The PI3K/AKT pathway is essential for cell migration (Seo et al., 2014). APC/MT/EB1 interactions has been linked to cell migration in a range of cell types (Etienne-Manneville, 2009). Dynein and its regulators are critical for cell migration, controlling nucleokinesis and the interaction between the nucleus and the MT-organizing center (MTOC) (Ayala et al., 2007; Tsai et al., 2007; Tsai and Gleeson, 2005). Here, we tested if the effect of rosiglitazone on cell migration in both WT and Apc (min/+) cells.

Our findings provide, for the first time, evidence that APC is a novel multifaceted dynein regulator. Specifically, we discovered that dynein, APC and GSK3 $\beta$  physically interact with each other, and the interaction of dynein to APC is positively regulated by GSK3 $\beta$ ; we also demonstrated that rosiglitazone impacts dynein activity, spindle orientation, and cell migration in an APC dependent manner; we report that ApcMin mutation affect PI3K/AKT/GSK3 $\beta$

signaling in response to rosiglitazone and negatively regulates the interaction between dynein and WT APC.

## RESULTS

**Dynein, APC and GSK-3 $\beta$  physically interact with each other:** we recently showed that GSK-3 $\beta$  directly phosphorylated and regulated dynein activity (chapter 1). APC is a known substrate of GSK-3 $\beta$  and forms complex with GSK-3 $\beta$  (Ikeda et al., 2000). In order to study the potential interplay of dynein and APC, we first tested if dynein, APC and GSK-3 $\beta$  physically interacted with each other. APC is a large protein with 2843 amino acids (aa) (Figure 2.1A). ApcMin, a truncation mutant, is due to an early termination at amino acid 850 of Apc (Su et al., 1992). A large disordered c-terminal region of APC (over 2000 aa) which is not stable and carries many missense mutations, is responsible for the interaction with many other proteins (Minde et al., 2011). We used APC-M2 pAb raised against the region of 15-aa repeats on APC to detect full length APC protein (FL-APC) (Wang et al., 2009). The antibody recognized FL-APC in both WT and Apc (min/+) mouse brain extracts. The level of FL-APC detected in WT brain was approximately two-fold greater than that in Apc (min/+) brain, while dynein intermediate chain (IC) expression was about the same in both (Figure 2.1B). Immunoprecipitation (IP) from WT mouse brain extract by an IC antibody showed that both FL-APC and GSK-3 $\beta$  were pulled down by dynein (Figure 2.1C). Reciprocal IP using anti-APC antibody corroborated these findings with both dynein and GSK-3 $\beta$  pulling down with APC (Figure 2.1D). Taken together,

these results support the hypothesis that APC, dynein and GSK-3 $\beta$  may be part of the same complex in mouse brain.

**GSK-3 $\beta$  positively regulates the interaction of dynein and APC:** APC is transported along MT by kinesin and accumulates at plus end of MT, and c-terminal of APC is important for this event (Jimbo et al., 2002; Mimori-Kiyosue et al., 2000; Mogensen et al., 2002). The Intracellular distribution of APC and dynein are important for their proper functions including MT-dependent organelle transport, spindle orientation and cell migration. Therefore, the regulation of the interaction between dynein and APC could be essential. We found that phosphorylation of purified dynein by GSK-3 $\beta$  increased the interaction of dynein with bacterial expressed c-fragment of APC protein *in vitro* (Figure 2.2A). YAMC cells were derived from WT mice and IMCE cells were derived from Apc (min/+) mice with the same genetic background (Whitehead and Joseph, 1994; Whitehead et al., 1993). Only IMCE cells carry the ApcMin mutation (Figure 2.3A). Similar to what we had observed in tissues, the APC-M2 pAb detected FL-APC protein in both YAMC and IMCE cells (Figure 2.2B). YAMC cells treated with CT99021, a potent GSK-3 $\beta$  inhibitor, showed reduced interaction between dynein and FL-APC by co-IP compared to DMSO (Figure 2.2C). Inhibition of GSK-3 $\beta$  by CT99021 also significantly decreased the colocalization of dynein and APC at the cell periphery by immunostaining (Figure 2.2D, E). These findings suggest that GSK-3 $\beta$  could regulate APC and dynein functions by regulating their interactions with one another.

**The ApcMin mutation prevents dynein activation in response to rosiglitazone:** Our recent study showed that rosiglitazone induced dynein activity through activation of PI3K/AKT/GSK-3 $\beta$  signaling. In order to study the interplay of PPAR- $\gamma$  signaling and the dynein/APC complex, we first examined dynein activity in response to rosiglitazone in both WT and Apc (min/+) cells, since both YAMC and IMCE cells express PPAR- $\gamma$  receptors (Figure 2.3B). Interestingly, unlike the effect on dynein distribution in YAMC cells, rosiglitazone was not able induce dynein accumulation at the centrosome in IMCE cells (Figure 2.4A, B). Moreover, transient expression of a truncated N-terminal APC fragment (APCN746) completely blocked the dynein response to rosiglitazone in HCT116 cells, indicating that the truncated isoform can act in a dominant negative capacity (Figure 2.4C). MT minus-ends are enriched at the apical surface of intestinal epithelial cells (Sansom et al., 2004). If dynein motility towards minus ends was stimulated by rosiglitazone, one might expect to see dynein accumulation in this region. This was in fact observed in sections from WT mice, and the phenotype was most pronounced in intestinal crypts (Figure 2.4D). This change in dynein distribution was not observed in sections from Apc (min/+) mice (Figure 2.4D). Together, the findings suggest that acute exposure to rosiglitazone exerts similar effects on dynein activity in both cultured cells and mouse intestine, and that APC status plays an important role in how the dynein responds to the drug.

**The ApcMin mutation alters spindle orientation in response to rosiglitazone:** To further characterize how PPAR- $\gamma$  signaling may regulate the

APC-dynein complex, we examined the effect of rosiglitazone on spindle orientation in both WT and Apc (min/+) cells. To examine spindle formation, YAMC and IMCE cells were exposed to rosiglitazone and immunostained with an  $\alpha$ -tubulin antibody. In control YAMC and IMCE cells, the majority of spindles were oriented parallel to the coverslip, with a small percentage oriented in a non-parallel fashion that only allowed a single spindle pole to be observed in a given focal plane. Examples of parallel and nonparallel spindles are shown in Figure 2.5A. In YAMC cells the percentage of parallel spindles was not significantly altered by rosiglitazone treatment (Figure 2.5B). However, rosiglitazone significantly increased the percentage of non-parallel spindles in IMCE cells (Figure 2.5B).

We next determined whether rosiglitazone also has a similar effect on the spindle orientation of intestinal crypt stem cells in Apc (min/+) mice. Specifically, WT and Apc (min/+) mice were administered rosiglitazone or DMSO via oral gavage for six days. Spindles in individual crypt sections were positioned with varying angles with respect to the apical surface (Figure 2.5C). Spindle angles were determined as shown in Figure 2.5D. Only spindles in which both spindle poles were visible were analyzed for spindle angle (the percentage with only one spindle pole visible was not significantly different between the WT and Apc (min/+) mice, and was not significantly altered by drug exposure). In WT crypts, the spindle was often nearly parallel to the apical surface. In WT crypts, fewer than 15% were categorized as near perpendicular (Figure 2.5E). Apc (min/+) crypts had significantly more near perpendicular spindles. Exposure to

rosiglitazone essentially randomized spindle orientation so that ~50% were categorized as “near perpendicular”. This is consistent with our cell culture data, suggesting that inappropriate PPAR- $\gamma$  signaling in the presence of the ApcMin mutation causes defects in spindle dynamics.

**The ApcMin mutation prevents rosiglitazone-induced cell migration:**

We next examined to see if the impact of rosiglitazone on cell migration is APC dependent. Changes in the migratory capacity of YAMC and IMCE cells treated with rosiglitazone were evaluated by wound-healing assay. Confluent cells were exposed to the drug for 12 hr prior to wounding. The average distance cells migrated into the wound was determined 24 hr later (Figure 2.6A). Treatment of YAMC cells with rosiglitazone significantly increased the distance migrated compared to controls (Figure 2.6B). In contrast, rosiglitazone did not stimulate migration of IMCE cells.

The movement of enterocytes towards the intestinal lumen is a form of sheet migration that causes complete turnover of the intestinal epithelium in a matter of days (Reya and Clevers, 2005). We examined enterocyte migration by monitoring the position of BrdU positive cells 24 hr after BrdU injection in WT and Apc (min/+) mice (Figure 2.6C-F). Rosiglitazone induced a significant shift in the position of BrdU positive cells towards the intestinal lumen in WT animals (Figure 2.6E). However, this was not the case for Apc (min/+) animals (Figure 2.6F), which is consistent with the wound healing assay in cell lines.

Together these data indicate that stimulating PPAR- $\gamma$  by rosiglitazone promotes migration of WT cells, which is prevented by the ApcMin mutation.

**The ApcMin mutation alters PI3K/AKT/GSK-3 $\beta$  signaling, which is essential for the rosiglitazone response:** In order to determine why rosiglitazone impacts dynein activity, spindle orientation, and cell migration in an APC-dependent manner, we examined the effect of the drug on PI3K/AKT/GSK-3 $\beta$  signaling in both WT and APC (min/+) cells. GSK-3 $\beta$  activity is important for the regulation of both APC and dynein. As we showed previously, treatment of YAMC cells for 12 hr with rosiglitazone significantly inhibited GSK-3 $\beta$  as reflected by increased S9 phosphorylation (Figure 2.7A, B). Surprisingly, rosiglitazone did not increase S9 phosphorylation of GSK-3 $\beta$  in IMCE cells. We further tested activities of upstream kinases in response to rosiglitazone. YAMC and IMCE cells were exposed to rosiglitazone for 0, 0.5, 2, 6 or 12 hr after serum starvation. There were significant differences in PI3K/AKT/GSK-3 $\beta$  signaling between the two cell lines when cells were treated with rosiglitazone for 6 and 12 hr (Figure 2.7C, D). Rosiglitazone did not affect P110 $\alpha$  expression in YAMC, but significantly reduced P110 $\alpha$  in IMCE at 6 and 12 hr. YAMC but not IMCE cells continued keeping high level of AKT phosphorylation after the serum return for 6 or 12 hr. Rosiglitazone increased pAKT (T308) in YAMC at 6 hr, while it reduced pAKT (T308) in IMCE at 6 hr. Rosiglitazone significantly increased S9 phosphorylation of GSK-3 $\beta$  in YAMC and slightly reduced that in IMCE at 6 or 12 hr.

**GSK-3 $\beta$  inhibition significantly rescues dynein activation in ApcMin mutation, and AKT inhibition prevents rosiglitazone-induced cell migration:** To test if the failure of signal transduction from rosiglitazone to PI3K/AKT/ GSK-

3 $\beta$  is the reason for different dynein and cell migration responses to rosiglitazone in cells with ApcMin mutation, we first examined if direct inhibition of GSK-3 $\beta$  increased dynein accumulation at the centrosome in IMCE. Unlike rosiglitazone, CT99021 significantly increased dynein accumulation at the centrosomes in both YAMC and IMCE (Figure 2.8A, B). We previously showed that the inhibition of PI3K prevented dynein activation in response to rosiglitazone in YAMC. Here, we tested if PI3K inhibition also prevented rosiglitazone-induced cell migration in YAMC. YAMC and IMCE cells were exposed to both ROZ and an LY294004, a potent AKT inhibitor. Cell migration was analyzed by wound healing assay. The rosiglitazone-induced cell migration was totally vanished by LY294004 in YAMC (Figure 2.8C). Moreover, the direct inhibition of PI3K reduced cell migration in both cell types (Figure 2.8C, D).

**The ApcMin mutation disrupts the interaction between dynein and WT APC:** When cells are treated with CT99021, almost all of GSK-3 $\beta$  are inhibited. However, IMCE still have less dynein accumulation at the centrosome than YAMC in the treatment of CT99021 (Figure 2.8B). Therefore, other than changing PI3K/ AKT/ GSK-3 $\beta$  signaling, there could be other ways by which ApcMin mutation affects dynein activity. One of them could be through changing the interaction of dynein and WT APC as GSK-3 $\beta$  does in Figure 2.2. Co-IP experiments showed that much less FL-APC was pulled down by dynein in IMCE cells than that in YAMC (Figure 2.9A). Similarly, less FL-APC and dynein were pulled down by each other in APC (min/+) than that in WT mouse brain shown in co-IP (Figure 2.9B). One obvious explanation is that there are less FL-APC in

Apc (Min/+) cells than that in WT cells (Figure 2.2B). However, ApcMin may also have a dominant negative effect on the interaction of dynein with WT APC. To test the hypothesis, we quantified the FL-APC pulled down ratio of WT to Apc (min/+) from mouse brain extract using IC-IP (Figure 2.9C, D). The mean of the ratio was 7, while FL-APC in WT brain is only about 2 times higher than that in min/+ brain as shown in figure 2.1B.

## DISCUSSION

**The dynein and APC interaction:** we report here for the first time that dynein and APC physically interact with each other as accessed by co-IP. We also demonstrate the interaction is positively regulated by GSK-3 $\beta$  and negatively affected by the ApcMin mutation. First, this interaction could be very important for the intracellular distribution of APC and dynein. Their special functions make their distribution even more important. As a molecular motor, dynein could transport APC to different cellular locations, while APC, as a MT associate protein, may act as an anchor for dynein controlling its motility on MT. Second, the interaction may be important for the post-translational modifications of dynein and APC. Dynein is able to transport retrograde signaling (Heerssen et al., 2004; Zweifel et al., 2005), which may induce APC post-translational modifications (PTMs). On the other hand, APC may act as a scaffold protein to recruit other signaling molecules capable of modifying dynein subunits and its regulators such as dynactin, Lis1 or Ndel1. The discovery of the role of GSK-3 $\beta$  in the regulation of the dynein and APC interaction is a good example of these events. In the future, we will study if dynein is able to change the intracellular distribution of APC, and

if the interaction of dynein with APC could affect their PTMs both in *vitro* and *in vivo*. The result that the ApcMin mutation disrupts the dynein-APC interaction provides a new angle to study the mechanism of carcinogenesis. It will be interesting to map the dynein and APC interaction in tissues from different stages of colon cancer.

**The dance of rosiglitazone with the APC/dynein complex in cellular events:** here, we also report that rosiglitazone impacts dynein activity, spindle orientation, and cell migration in an APC-dependent manner. Our previous study showed that rosiglitazone induced dynein activity, and one of the phenotypes was that it increased dynein accumulation at the centrosome. Here, we find that acute exposure to rosiglitazone induces a significant increase in the percentage of cells with dynein accumulation at the centrosome in both cultured cells and mouse intestine, and that the ApcMin mutation blocks dynein response to the drug.

The effect of rosiglitazone on dynein activity is likely to be important for the increased rate of migration observed in both cultured cells and intestinal enterocytes in response to the drug. Dynein has been implicated in cell migration in developing nervous system and in many cultured cell lines (Schmoranzler et al., 2009; Vallee et al., 2009). Intriguingly, the presence of truncated APC prevents rosiglitazone-induced cell migration rates in both cultured cells and the intestine. Another interesting finding is that rosiglitazone influences the spindle orientation in cultured cells and in the mouse intestine only when the ApcMin is present. Even in the absence of the drug, Apc (min/+) cells have more

abnormally oriented spindles. Both cell migration and spindle orientation play essential roles in cell-fate decision. The underlying molecular explanation for this is not clear, but our studies open up the possibility that the proper interaction between APC and dynein is necessary for maintaining the proper dynein activity, cell migration and spindle formation in response to signaling events.

**Different rosiglitazone signaling in WT and Apc (min/+) cells:** We previously reported that rosiglitazone-induced dynein activation requires the intact PI3K/AKT/GSK-3 $\beta$  signaling. To answer the question of why rosiglitazone affects dynein activity, spindle orientation, and cell migration in an APC status dependent manner, we compared PI3K/AKT/GSK-3 $\beta$  signaling in WT and Apc (min/+) cells. There are significant differences in PI3K/AKT/GSK-3 $\beta$  signaling between the two cell lines in response to rosiglitazone.

In PI3K/AKT pathway, rosiglitazone has no visible effect on PI3K expression in YAMC cells, but significantly reduces PI3K in IMCE cells after 6 hr. IMCE cells also display significantly lower levels of phospho-AKT as compared to YAMC cells after 6 hr return of serum, and rosiglitazone increases pAKT levels in YAMC cells but not in IMCE cells at 6 hr. As active AKT promotes cell migration (Kim et al., 2001), which may explain why we found that rosiglitazone does not induce cell migration in Apc (min/+) cells. We further support this by showing that the inhibition of PI3K prevented rosiglitazone-induced cell migration in WT cells. PI3K/AKT is enhanced in many human cancer types and regarded as an attractive therapeutic target (Carnero and Paramio, 2014; Pal and Mandal, 2012). Our report that rosiglitazone reduces PI3K/AKT activity in IMCE supports the

theory that it may act as a chemopreventive drug in patients with truncating APC mutations, though this will require further evaluation.

We also found that rosiglitazone only inhibits GSK-3 $\beta$  in YAMC and not in IMCE cells as accessed by western blot. As the inhibition of GSK-3 $\beta$  increased dynein dependent transport and accumulation at the centrosome, the failure of rosiglitazone-induced GSK-3 $\beta$  inhibition could be a reason why the ApcMin mutation prevents dynein activation by rosiglitazone. We further support this by showing that CT99021, a potent GSK-3 $\beta$  inhibitor, significantly rescued dynein activation in IMCE cells. Our study shows that the PI3K/AKT/GSK-3 $\beta$  response to rosiglitazone is a key difference between WT cells and cells with ApcMin mutation, and also provides a linkage of dynein activation to cell migration. Future study is needed to determine if rosiglitazone has a similar effect on PI3K/AKT/GSK-3 $\beta$  in other APC mutation models.

**Thiazolidinediones: chemopreventive or carcinogenic?** This question cannot have a simple answer. Our study shows that rosiglitazone misorients the spindle in Apc (min/+) cells, which is generally regarded as carcinogenic property. However, we also demonstrate that rosiglitazone reduces PI3K/AKT activity in Apc (min/+) cells, which can be viewed as chemopreventive. Therefore, we think that whether it is chemopreventive or carcinogenic in cells with ApcMin mutation is cell type dependent. For those cell types undergoing mitosis and differentiation, rosiglitazone may be carcinogenic by changing their fates. For undivided or undifferentiated cells, the rosiglitazone may be chemopreventive by inhibiting PI3K/AKT pathway. Even for the same type of cells, in different stages

of development rosiglitazone may have different effects, depending on who has a dominant effect, spindle orientation or PI3K/AKT signaling. In the future, it will be interesting to characterize the effect of rosiglitazone in other *Apc* (*min/+*) cell types.

## **MATERIALS AND METHODS**

**Cell lines:** The murine YAMC epithelial cell line was derived from the colonic mucosa of a transgenic mouse generated by the introduction of a temperature sensitive, interferon inducible, SV40 T Ag, tsA58 (Immortomouse) (Whitehead et al., 1993). The murine IMCE colon epithelial cell line was derived from the progeny of a cross between the Immortomouse strain and the *Apc* (*min/+*) mouse strain (Whitehead and Joseph, 1994). YAMC and IMCE cells were maintained at the permissive temperature (33°C) in RPMI 1640 media supplemented with glutamine (2mM), 10% FBS, penicillin (0.5 U/ml) and streptomycin (100 µg/ml), murine gamma interferon (5 U/ml), and 1% ITS (insulin, transferrin and selenium; Cellgro, Inc). The human colon cancer cell line, HCT-116, and Cos-7 cells were maintained in DMEM supplemented with glutamine (2mM), 10% FBS, penicillin (0.5U/ml) and streptomycin (100 µg/ml).

**Animals and genotyping:** C57BL6/J *Apc* (*min/+*) mice, obtained from Jackson Labs, were maintained in the Mouse Core Facility of the Center for Colon Cancer Research at the University of South Carolina. These mice carry a mutation at codon 850 in one allele of the *Apc* gene that encodes a truncated version of APC (Pellman, 2001). *Apc* (*min/+*) males were bred with C57BL6/J

wild type females and heterozygous progeny were genotyped by PCR analysis of tail genomic DNA using allele specific primers (Murphy et al., 2004).

**Pharmacological treatments:** Cultured cells: Cells were serum starved for 12h prior to treatment with 10  $\mu$ M rosiglitazone (Biomol) for 12 hr (or another specified period of time as indicated) in full media. In some experiments cells were coincubated with 10 $\mu$ m of the PI3K inhibitor, LY294009 (Biomol). In other experiments, cells were arrested in mitotic phase by incubating with nocodazole (2 $\mu$ M) for 16h. To study the effect of the direct GSK-3 inhibition in IMCE and YAMC cells, the starved cells were treated with 3  $\mu$ M CT99021 for 12hr.

Mice: 4 week old male WT and Apc (min/+) mice were used in the experiment. Three WT and Apc (min/+) mice were orally gavaged daily for 6 days with rosiglitazone at a dose of 10mg/kg body weight, while three other mice received an equal volume of vehicle (DMSO).

**Constructs and transfection:** Cells were transfected using Lipofectamine 2000 reagent (Invitrogen) according to the manufacturer's directions. Transfected cells were detected by immunofluorescence or by cotransfecting with a GFP vector. The full-length APC mammalian expression vector FL-APC EGFP originally described by Dr. J. Victor-Small (Langford et al., 2006) was provided by M. Bienz. APC N-746 was generated by cloning a *BspEI* and *HindIII* fragment of FL-APC EGFP into a pEGFP C1 vector. A 747-base-pair fragment of the 3'-end of APC (cAPC) was generated by PCR amplification from a full-length human APC construct and cloned into a pET 30 EK/LIC vector (Novagen) for expression in *E coli*.

**Antibodies:** APC-M2 pAb raised against the region of 15 aa repeats on APC was described previously (Wang et al., 2009). The Lis1 antibody has been described previously (Smith et al., 2000). The following antibodies were from Santa Cruz Biotechnology: Anti-IC mouse mAb (74.1), His-probe (H-3) and rabbit polyclonal anti-PPAR- $\gamma$ 1 (H100). GSK-3 $\beta$  (3D10) Mouse mAb, Phospho-GSK-3 $\beta$  (Ser9) (5B3) Rabbit mAb, AKT (pan) (11E7) Rabbit mAb, Phospho- AKT (Thr308) (D25E6) Rabbit mAb and Phospho- AKT (Ser473) (D9E) Rabbit mAb, PI3 Kinase p110 $\alpha$  (C73F8) Rabbit mAb and anti-BrdU mouse mAb (Bu20a) were from Cell signaling Inc. Anti- $\alpha$ -tubulin monoclonal mouse Ab was from Sigma-Aldrich. Anti-CDK5RAP2 rabbit polyclonal Antibody was purchased from Millipore.

**Imaging of fixed cells:** Cells were plated onto 12-mm glass coverslips in 24-well plates prior to drug treatment or transfection. For IC immunofluorescence, cells were fixed in 100% ice cold methanol for 2 min. For other immunofluorescence, cells were fixed in 3% paraformaldehyde followed by permeabilization with 0.2% Triton X-100 for 10 minutes. Cells were processed for immunofluorescence according to routine staining methods. Nuclei were visualized using Hoechst dye (33258; Sigma-Aldrich). Coverslips were mounted on glass slides using ProLong Gold Antifade (Invitrogen). Cells were visualized with an Axiovert 200 inverted microscope (Carl Zeiss, Inc.) using Plan-Neo 100 $\times$ /1.30 or Plan-Apo 63 $\times$ /1.40 oil-immersion objectives (Immersionol 518F; Carl Zeiss, Inc.). Some animal sections were visualized with Zeiss AxioImager M2 using EC Plan-Neofluor 40X/1.30 oil-immersion objectives. Digital images were

acquired with a CCD camera linked to AxioVision software (Carl Zeiss, Inc.). In some cases, optical sections were deconvolved using AxioVision's combined iterative algorithm to obtain confocal images. The accumulation of dynein at the centrosome was determined by measuring the mean pixel intensity of dynein immunofluorescence in a fixed area using ImageJ software.

**Cell and brain extract preparation:** For preparation of cell extract, cells at 90% confluency were lysed in buffer containing 50 mM Tris (pH 7.5), 0.1% NP-40, 100 mM NaCl, 1 mM MgCl<sub>2</sub>, 5 mM EDTA, protease inhibitor cocktail (Fisher) and Halt phosphatase inhibitor cocktail (Fisher) on ice for 30 minutes. Cell lysates were sonicated for 10 pulses at level 1 with 10% output 3 times. The lysates were incubated on ice for another 10 min and then centrifuged at 17,000 g for 20 minutes at 4°C. For preparation of mouse brain extract, brains were dissected with clean tools as quickly as possible to prevent degradation. Tissues were dounce-homogenized in lysis buffer as above. The lysates were incubated on ice for 30 min and then centrifuged at 17,000 g for 30 minutes at 4°C. Concentration of extracts was determined by BCA protein assay (Pierce).

**Expression and purification of proteins:** His-tagged c-APC: Bacteria were transformed with the relevant constructs, then exposed to isopropyl-D-thiogalactopyranoside for 3 h and lysed in B-PER buffer (Pierce) containing lysozyme and a protease inhibitor cocktail. The extract was used in dynein co-IPs. Cytoplasmic dynein was purified from bovine brain as described previously (Bingham et al., 1998). The dynein contains all subunits in the motor

holoenzyme, and the prep contains no detectable Lis1, p150glued, Ndel1, EB1 or tubulin (Mesngon et al., 2006).

**Immunoprecipitation and Western blot:** For IPs from cell or brain extracts, 1  $\mu\text{g}$  74.1 IC or APC-M2 antibodies were first incubated with 30  $\mu\text{l}$  Protein-A dynabeads (Invitrogen) for 2 hr at room temperature and washed with lysis buffer twice. The antibody conjugated dynabeads were incubated with 1 mg of extracts at 4°C overnight. Dynabeads were subject to two washes of lysis buffer and then two washes of PBS-T (phosphate buffered saline with 0.1% Tween 20) at 4°C, followed by resuspension in 60  $\mu\text{l}$  PBS plus 20  $\mu\text{l}$  6X sample buffer. The mixtures were boiled and supernatants were analyzed by western blot.

For IPs from purified proteins, purified bovine brain dynein was first incubated with 74.1 mouse monoclonal IC antibody conjugated agarose beads (IC-Beads, Santa Cruz Biotechnology, Inc) in PBS-T with protease and phosphatase inhibitors overnight. Beads were washed twice with PBS-T and once with 1X kinase buffer. Beads were incubated in kinase assay reaction with or without GSK-3 $\beta$  at 37°C for 1 hr. Beads were spun down and washed with PBS-T twice and then PHM-T buffer (60 mM PIPES, 25 mM HEPES, 4 mM MgSO<sub>4</sub>, 0.1% Tween 20, pH 6.9). Beads then were incubated with 500  $\mu\text{l}$  of the c-APC lysate. Beads were washed 3 times with PHM-T buffer and eluted in 60  $\mu\text{l}$  PBS plus 20  $\mu\text{l}$  6X sample buffer.

For western blot, lysate or IP elution were separated by SDS-PAGE and transferred to PVDF or Nitrocellulose membranes. Blots were incubated with

primary antibodies for 1 hr. at RT or overnight at 4°C, and then exposed to the appropriate HRP-conjugated secondary antibodies. Labeled proteins were detected using a Western Lightning ECL reagent (Millipore). The blots were exposed to autoradiography films (Denville) for a proper time to observe and minimize the saturation of bands.

***In vivo* bromodeoxyuridine (BrdU) enterocyte migration analysis:**

Intraperitoneal injection (i.p.) was used in animals with 30 mg/kg BrdU to label proliferating cells. After 24 hr, animals were euthanized and the intestinal tracts were excised from the duodenum to the caecum, flushed with cold PBS and divided into three equal sections, duodenum (proximal), jejunum (intermediate) and ileum/colon (distal), and opened longitudinally. The duodenal segments were fixed in 70% ethanol for the BrdU migration analysis, because the villi are the longest in the region of the intestine. Jejunal sections were fixed in 3% paraformaldehyde to stain for microtubules. Tissues were “jelly-rolled”, dehydrated, embedded in paraffin and sectioned to obtain 5 µm thick sections. Sections were deparaffinized in xylene and rehydrated through an alcohol series. Endogenous peroxidase activity was blocked by incubating the slides in 3% H<sub>2</sub>O<sub>2</sub> for 15 min at room temperature. DNA was then denatured by immersing the slides in 2 N HCl for 90 min, followed by neutralization in 0.1 M borate buffer, pH 8.5, for 10 min at room temperature. Serum block using 5% horse serum was then applied to the slides for 20 min at room temperature. Specimens were then incubated for 2 h with anti-BrdU antibody. Specimens were incubated with Vectastain anti-mouse HRP for 30 min at room temperature, followed by color

development in DAB for 5 min. Specimens were then dehydrated in a graded ethanol series and coverslipped.

### **Immunofluorescence and immunohistochemistry of intestinal**

**sections:** Jejunal segments were fixed in 3% paraformaldehyde and embedded in paraffin. Sections were processed for tubulin and IC immunofluorescence.

Slides were heated in 10 mM citrate buffer, pH 6.0, for 10 min to perform antigen retrieval. Slides were then incubated in anti-tubulin or anti-IC (74.1) for 2 h at room temperature. Slides were then washed in PBST, 3 times for 5 min each and incubated with AlexaFluor 568 conjugated goat anti-mouse secondary antibody (Molecular Probes) for 1 h. Slides were washed and stained with Hoechst dye and mounted in ProLong Gold Anti-fade.

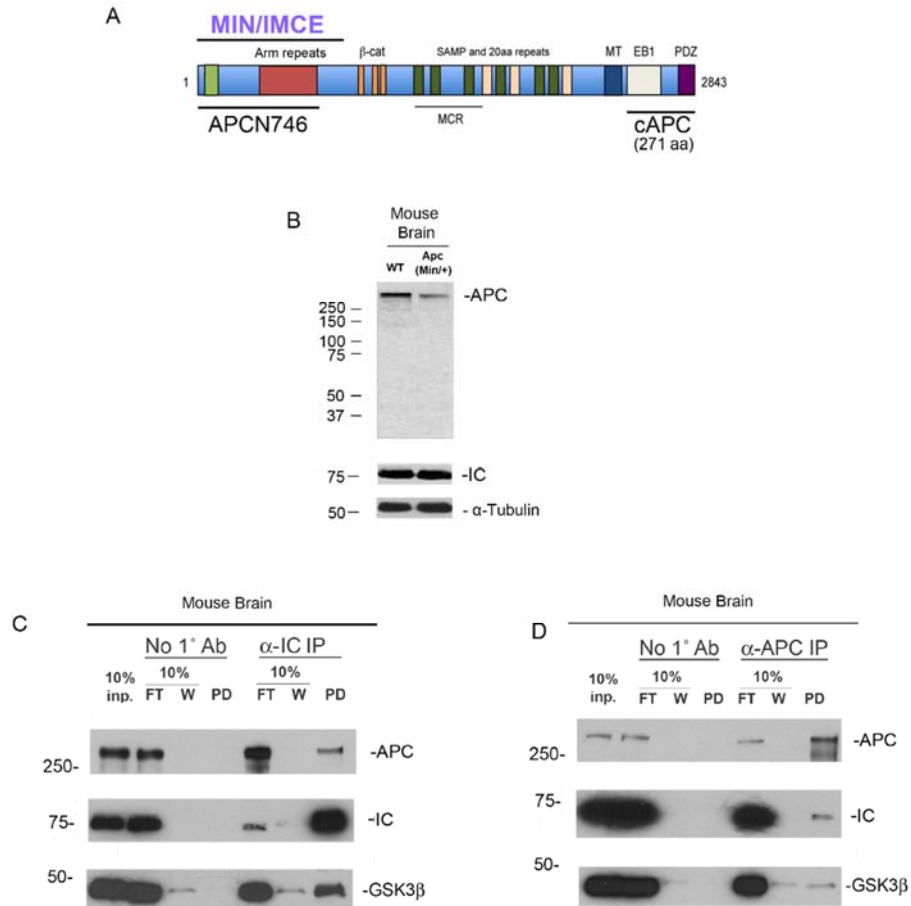


**Figure 2.1 Dynein, APC and GSK-3 $\beta$  physically interact with each other in mouse brain**

**A)** Schematic of APC protein showing domains, functions and truncated isoforms used in this study. MIN: An 850 aa N-terminal fragment present in *Apc* (*min/+*) mice and IMCE cells; APCN746: A 746 aa N-terminal fragment used in HCT116 cell transfections; cAPC: A 271 aa C-terminal fragment used in immunoprecipitation. **B)** APC-M2 antibody test in WT and *Apc* (*min/+*) mice brain by western blot. APC-M2 is able to recognize FL-APC in the brain extract of both mouse types, but *Min/+* mice has about two times less FL-APC than WT. There is no noticeable change in the IC expression. **C)** IC-IP from mouse brain extract showed that both FL-APC and GSK-3 $\beta$  were pulled down. **D)** APC-M2-IP from mouse brain extract showed that both dynein and GSK-3 $\beta$  were pulled down.

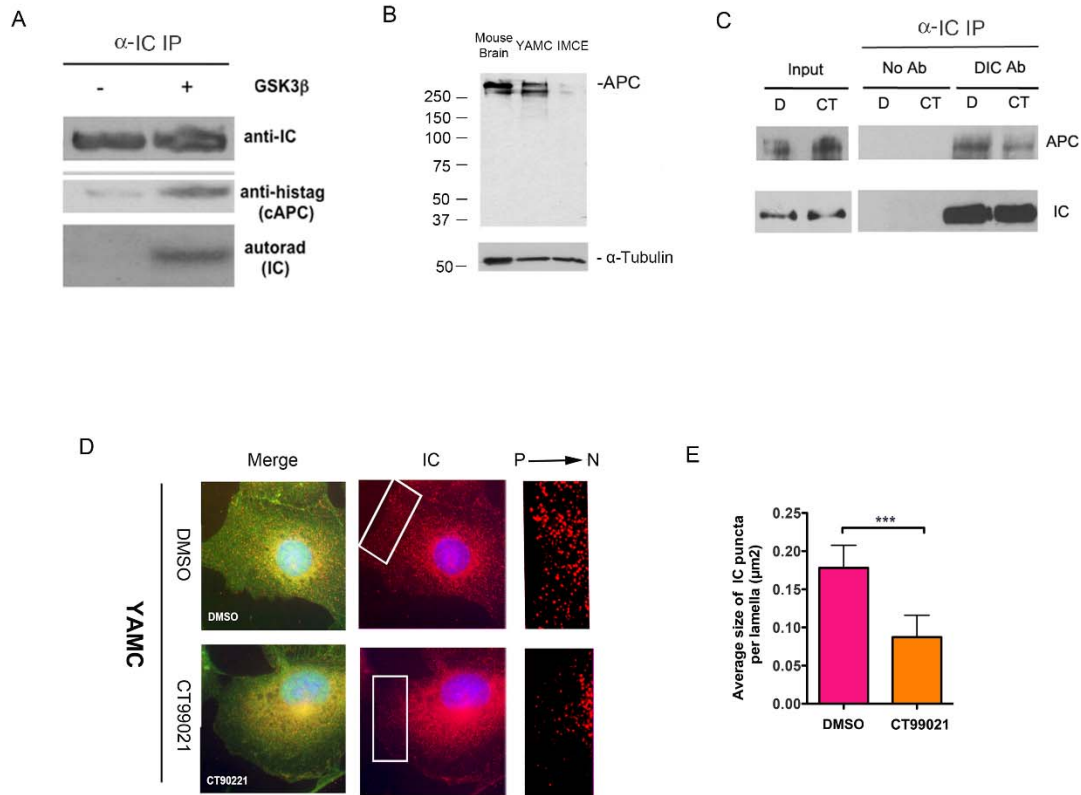


**Figure 2.2 GSK-3β positively regulates the interaction between dynein and APC.**

**A)** GSK-3β increased the interaction between dynein and cAPC *in vitro*. Purified bovine dynein was immunoprecipitated first and treated with or without GSK-3β in a kinase assay, followed by pull-down assay with recombinant cAPC (271 aa). **B)** Both YAMC and IMCE cells expressed FL-APC, but IMCE cells had significant less FL-APC expression than YAMC. **C)** YAMC cells were treated with or without CT99021 for 12 hr after serum starvation. Inhibition of GSK-3β by CT99021 (CT) reduced the dynein-FL-APC interaction compared to the DMSO (D). **(D, E).** YAMC cells were treated with or without CT99021 for 12 hr after serum starvation. Cells were fixed and immunostained with IC antibodies (red), APC-M2 antibody (green), and Hoechst dye to label nuclei. Inhibition of GSK-3β significantly decreased the colocalization of dynein and APC at the cell periphery. The representative figures were shown in (D), while quantification of dynein puncta size at the cell periphery was shown in (E) (P: periphery, N: nucleus; Mean +/- 95% CI; \*\*\*, P<0.0001, t-test).

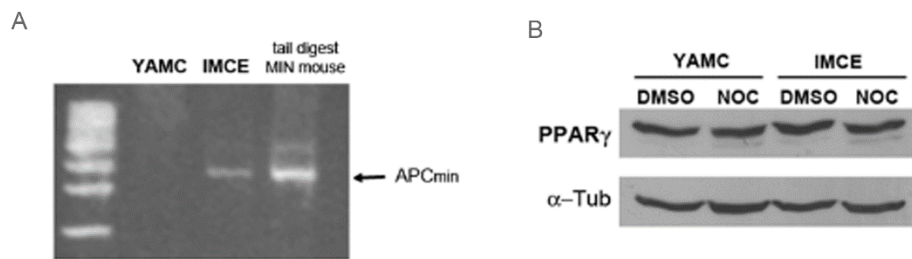


**Figure 2.3 Characterize APC status and PPAR- $\gamma$  expression in YAMC and IMCE**

**A)** Genomic DNA was extracted from YAMC cells, IMCE cells and Apc (min/+) mice. PCR was performed to detect the ApcMin mutation, which was present only in Apc (min/+) mice and IMCE cells but not YAMC cells. **B)** Western blots of YAMC and IMCE cell extracts show they express PPAR- $\gamma$  when randomly cycling (DMSO) and when arrested in prometaphase by nocodazole (NOC) exposure. (Sachin Hebbar performed the experiments in figure 2.3 for the manuscript.)

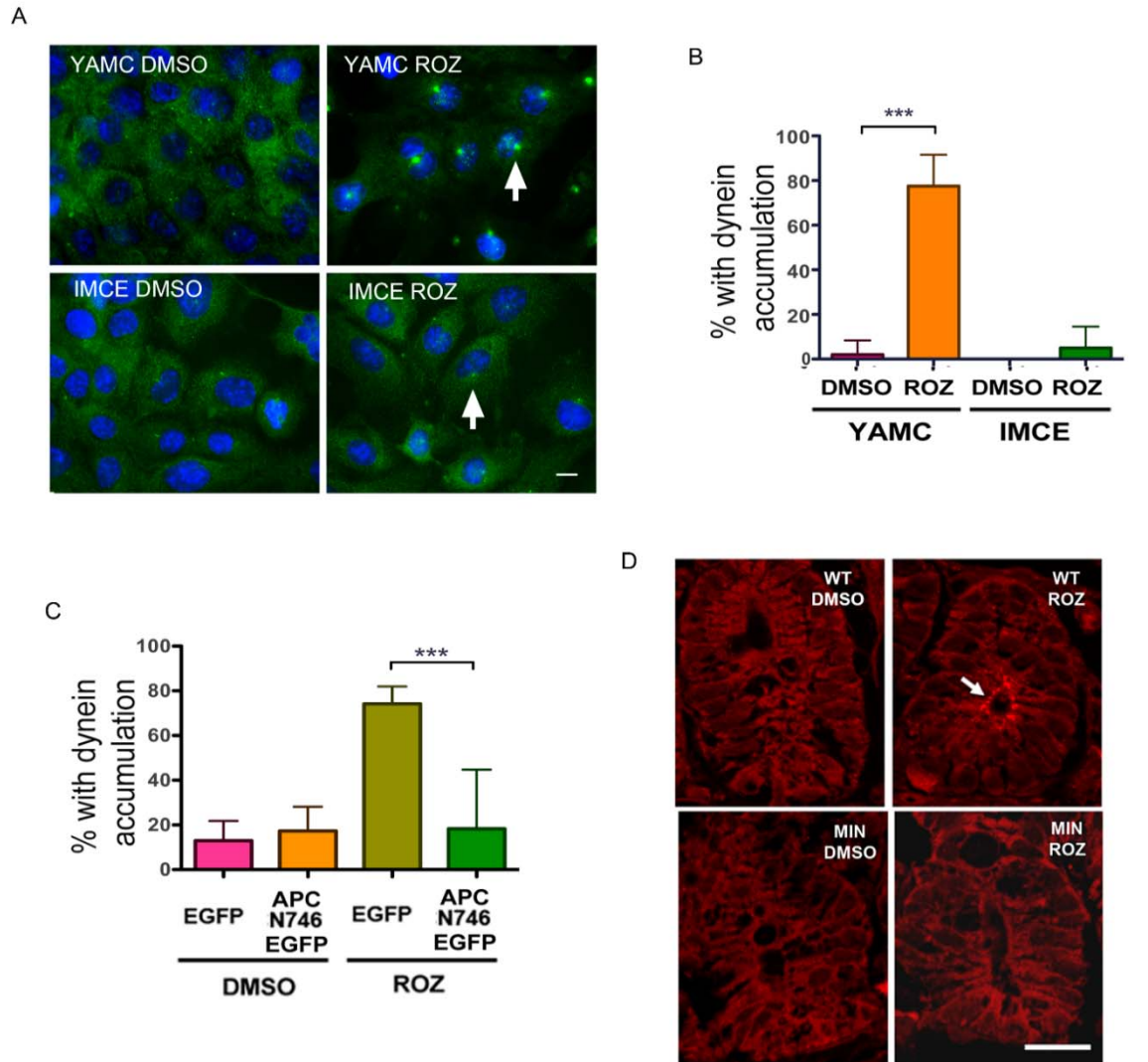


**Figure 2.4 The ApcMin mutation prevents dynein activation in response to rosiglitazone**

**A)** YAMC and IMCE cells were incubated with rosiglitazone (ROZ) for 12h after serum starvation and stained for IC (green). Nuclei were stained with Hoechst dye (blue). (Scale Bar is 10 $\mu$ M.) **B)** Percentage of dynein accumulation at the centrosome was measured. Cells with IC intensity equal to or greater than 60 arbitrary fluorescence units (afu) were considered to have dynein accumulation (three independent experiments, *Mean* +/- 95% *CI*; \*\*\*,  $p < 0.0001$ , *t*-test). **C)** Transient expression of a truncated APC isoform (APCN746) prior to drug exposure also completely blocked the dynein response to ROZ in HCT116 cells. **D)** Sections of intestinal crypts were processed and stained for dynein (red). Treatment with ROZ induced dynein accumulation at the apical surface (arrow) in WT mice (Top Panels), but not in MIN mice (bottom Panels). (Sachin Hebbar performed the experiments in figure 2.4 for the manuscript.)

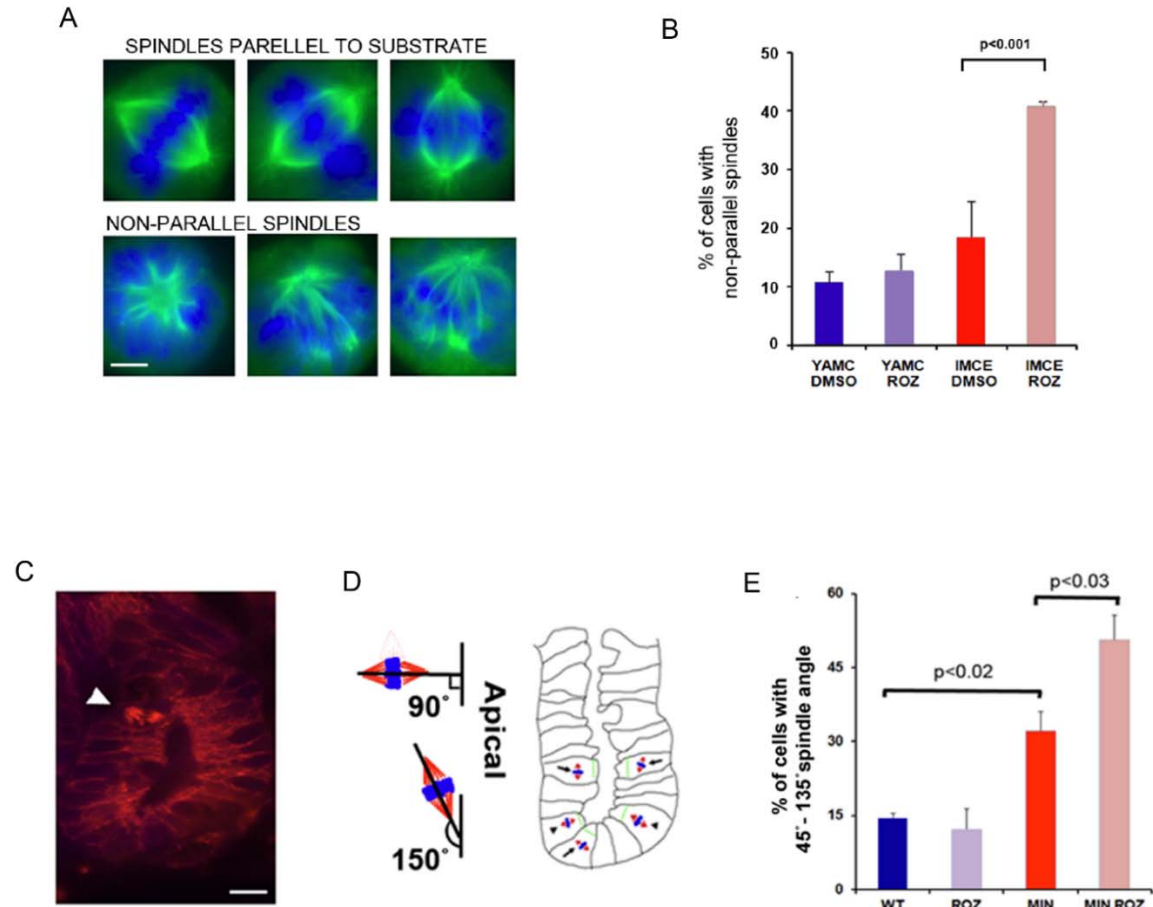


### Figure 2.5 The ApcMin mutation alters spindle orientation in response to rosiglitazone

**A)** Representative images of spindles to define parallel (in the top panels) and non-parallel (in the bottom panels) orientations in cultured cells. Spindles were visualized with an  $\alpha$ -tubulin antibody (green). Chromosomes were labeled with Hoechst (blue). **B)** The percentage of YAMC and IMCE cells with non-parallel spindles was analyzed. YAMC and IMCE cells were exposed to 10 $\mu$ M ROZ or DMSO for 12 hr after serum starvation. **C)** Representative image of Intestinal sections from WT and Apc (min/+) mice orally gavaged with ROZ or the DMSO control for six days. Sections were stained with an  $\alpha$ -tubulin antibody (red) to visualize spindles (arrowhead). **D)** Schematic Spindle angles are determined from a line drawn through the spindle poles and a line drawn parallel the apical surface (left). Schematic showing various orientations of spindles with respect to the apical surface (right): Arrows pointed spindles were categorized as near parallel (0-45° or 135-180°); arrowheads pointed spindles categorized as near perpendicular or non-parallel (45-135°). **E)** Percent of spindles with near perpendicular orientation was scored from three animals per group. (Sachin Hebbar performed the experiments in figure 2.5 for the manuscript.)

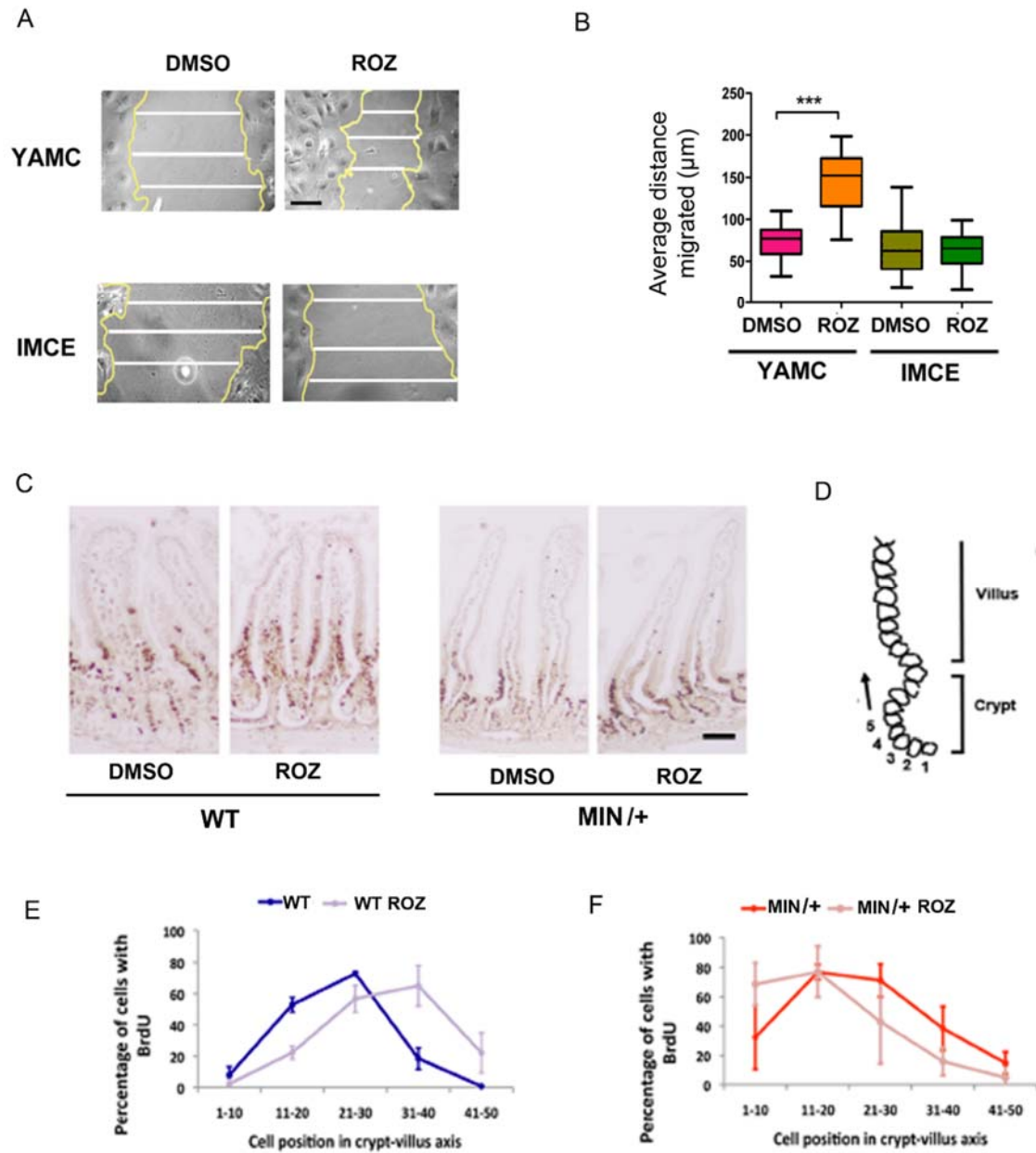


**Figure 2.6 The ApcMin mutation prevents rosiglitazone-induced cell migration by both wound healing assay and enterocyte motility assay**  
**A)** Representative images of wound healing response to ROZ in YAMC or IMCE cells. After a 12h exposure to ROZ or DMSO, a scratch wound was applied to confluent YAMC and IMCE cells. Wound edges (yellow lines) and typical gap widths (white lines) are shown 24 hr after wounding. **B)** Quantification of YAMC and IMCE wound healing assay. Average gap widths (AGW) at 0 and 24 hr after wounding were used to calculate mean distance migrated:  $(AGW (0hr) - AGW (24hr)) / 2$ . **C)** Representative images of enterocyte motility in response to ROZ in WT or Apc (min/+) mice. Mice were fed with ROZ or DMSO for 6 days and then

i.p injected with BrdU. After 12 hr. intestines were processed for BrdU immunoperoxidase activity. ROZ altered the distribution of labeled cells in WT mice (left panel), but not in Apc (min/+) mice (right panel). **D)** Schematic of epithelial cells lining the crypt and villus were numbered from the base of the crypt. **(E, F)**. Quantification of BrdU positive cells at different positions of the crypt-villus axis. ROZ induced a significant shift of BrdU positive cells from crypt towards villus in WT animals (E) but not in Apc (min/+) animals (F). 25 crypt-villus units were analyzed in each treatment. (*Sachin Hebbar performed the experiments in figure 2.6 for the manuscript.*)

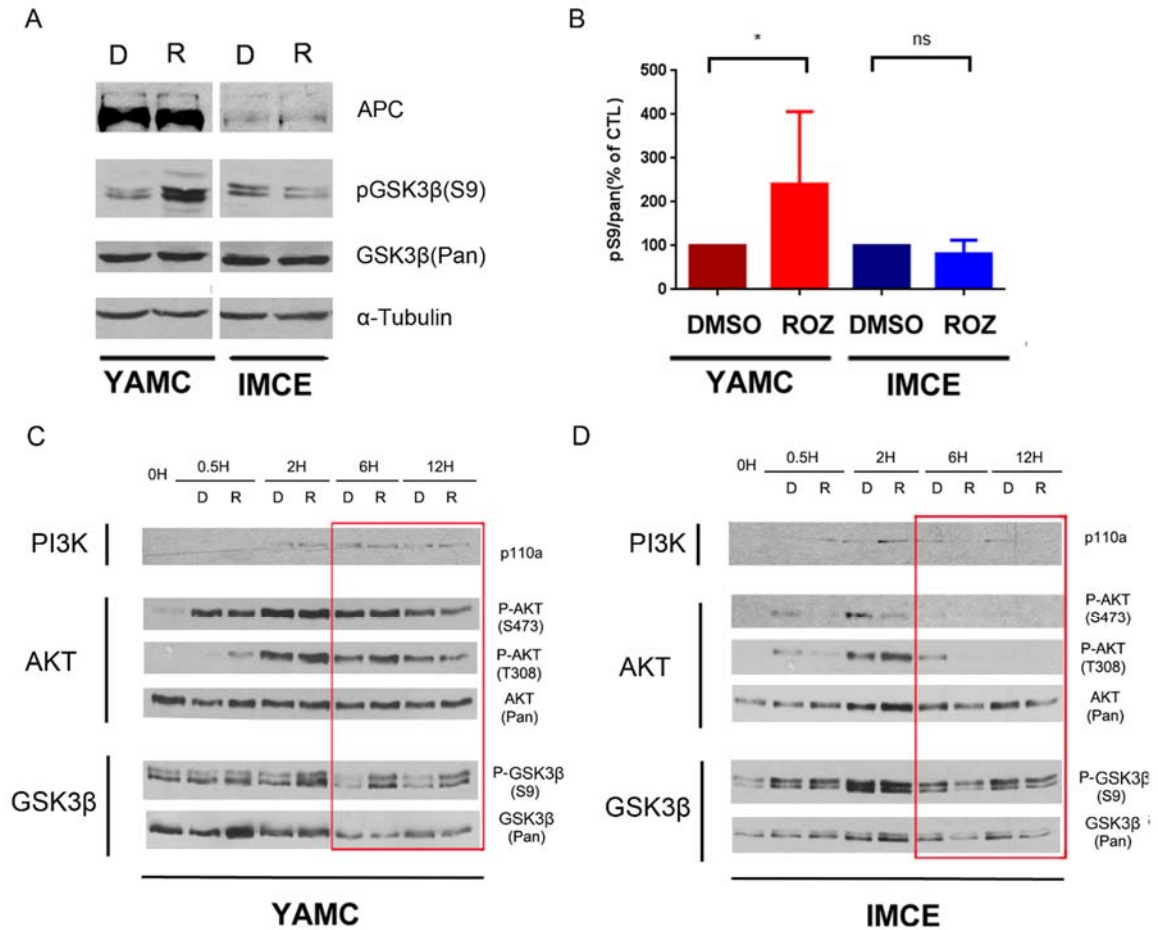


**Figure 2.7 The ApcMin mutation alters PI3K/AKT/GSK-3β signaling, which is essential for rosiglitazone response**

**A)** Western blot of YAMC and IMCE cells after exposure to rosiglitazone (R) for 12 hr were probed with pGSK-3β (S9) and pan-GSK-3β antibodies. Rosiglitazone significantly increased S9 phosphorylation compared to DMSO (D) in YAMC but not in IMCE cells. **B)** Quantification of ratio of pGSK-3β (S9) to pan-GSK-3β in response to rosiglitazone in both YAMC and IMCE cells (N=4, Mean +/- 95% CI; p=0.03, *t-test*). **(C, D).** YAMC and IMCE cells were exposed to rosiglitazone for 0, 0.5, 2, 6 or 12 hr and probed with related antibodies in PI3K/AKT/GSK-3β signaling as shown.

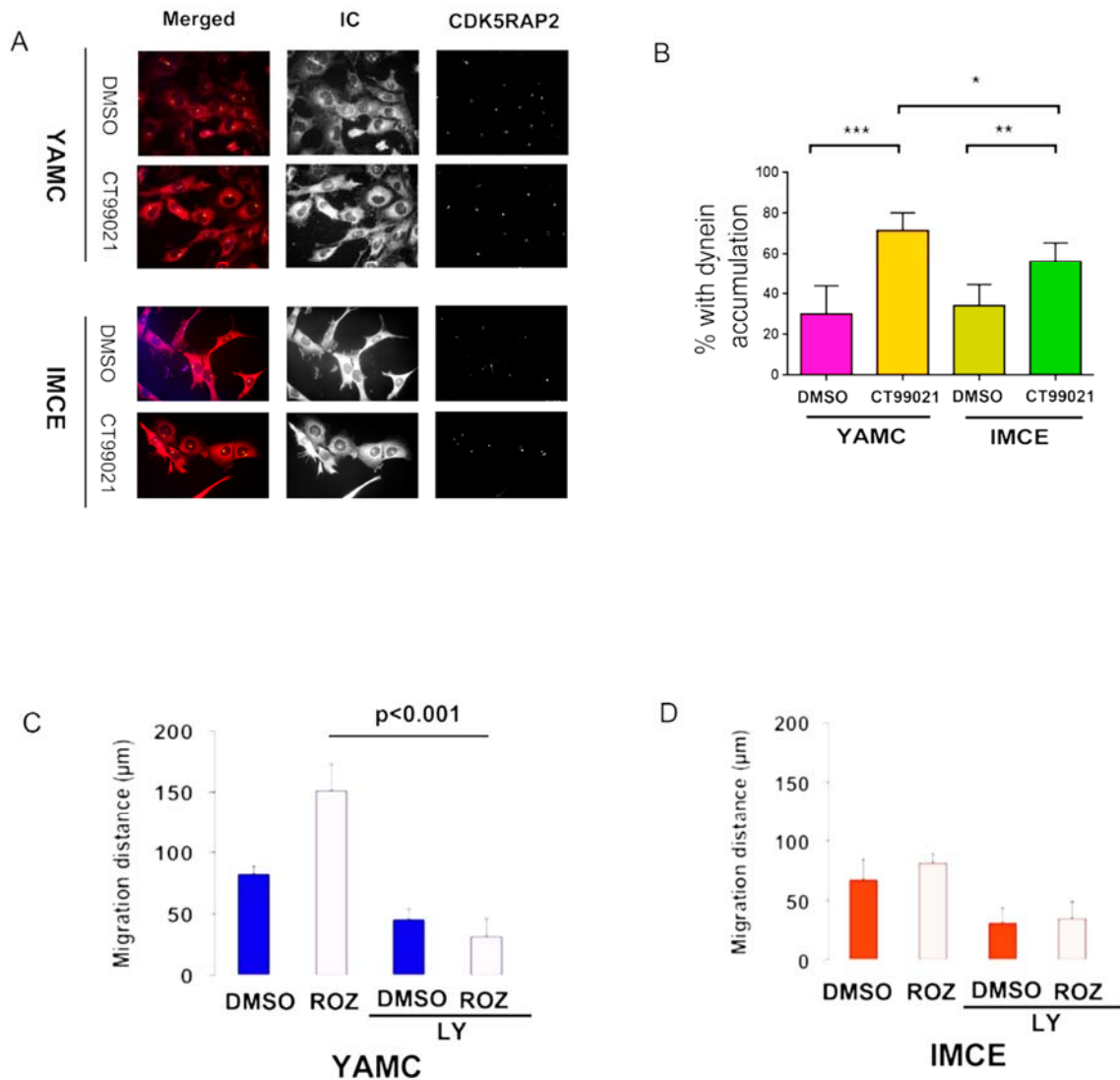


**Figure 2.8 GSK-3 $\beta$  inhibition significantly rescued dynein activation in Apc (min/+) cells, and PI3K inhibition prevent rosiglitazone-induced cell migration.**

**A)** YAMC and IMCE cells were exposed to CT99021 for 12 hr after serum starvation. Dynein distribution was visualized by IC immunofluorescence (red, and middle panels). Centrosomes were labeled by a CDK5RAP2 antibody (green, and right panels). Nuclei are stained with Hoechst dye (blue). Unlike ROZ, CT99021 also significantly increased dynein accumulation at the centrosomes in IMCE cells. **B)** Percentage of dynein accumulation at the centrosome was analyzed (N=400 cells, Mean  $\pm$  95% CI; N.S.,  $P > 0.05$ , \*  $P < 0.05$ , \*\*  $P < 0.01$ , \*\*\*  $P < 0.001$ , one-way ANOVA). **(C, D)** YAMC and IMCE cells were exposed to both ROZ and a PI3K inhibitor, LY294002(LY). Cell migration was analyzed by wound healing assay. (Sachin Hebbar performed the experiments in figure 2.8 C, D for the manuscript.)

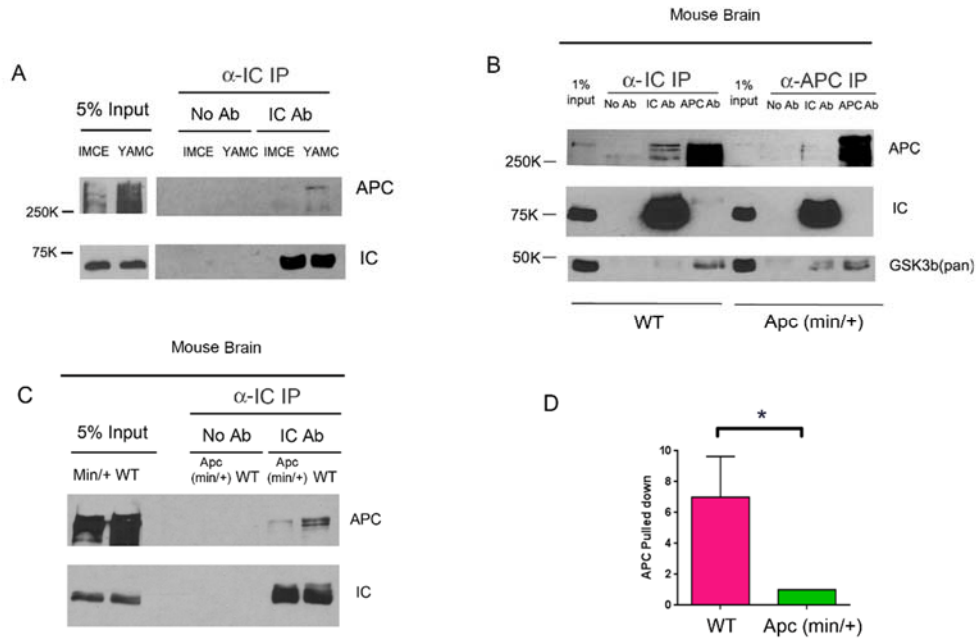


**Figure 2.9 The ApcMin mutation disrupts the interaction between dynein and WT APC**

**A)** IC-IP from YAMC and IMCE cell extract. Much more FL-APC was pulled down with IC in YAMC than IMCE. **B)** IC-IP and APC-IP from WT and Apc (min/+) mouse brain extract. More APC was pulled down by IC-IP in WT mice than Apc (min/+) mice, and more dynein was pulled down by APC-IP in WT mice than Apc (min/+) mice. **(C, D)** FL-APC pulled down ratio of WT mice to Apc (Min/+) was estimated ((N=4, Mean +/- 95% CI; p=0.017, t-test). Mean of the ratio was 7.000 ± 1.528, which was more than 3 times higher than the FL-APC expression ratio of WT mice to Apc (min/+).

## CHAPTER 3

A mass spectrometry-based systematic method to map GSK-3 $\beta$  phosphorylation sites on dynein intermediate chain

### ABSTRACT

Dynein intermediate chain (IC) is essential for dynein complex assembly and mediates the interactions of dynein with other regulators including dynactin, Ndel1/ Nde1, ZW10. However, the mechanism of how IC regulates these interactions is largely unknown. We previously demonstrated that GSK-3 $\beta$  regulates many dynein-dependent cellular functions and is able to directly phosphorylate IC *in vitro*. To dissect how GSK-3 regulates dynein, we develop a systematic method to map phosphorylation sites on IC, which integrates recombinant protein purification, *in vitro* kinase assay, tandem mass spectrometry (MS), mutagenesis, sequence conservation analysis and immunopurification. We identify T154, S88 and T89 on IC-2C are targeted by GSK-3 $\beta$  using MS and mutagenesis. We find that T154 is conserved in all mouse IC-2 isoforms but not in IC-1, and it exists in bovine and horse IC-2 but not in rat or human IC-2. However, S88 and T89 are conserved in all mouse IC isoforms as well as in ICs from all other mammalian species examined. Furthermore, we demonstrate that S87 or T88 on IC-1B from both mouse and rat (corresponding to <sup>3</sup>S88 or T89 on IC-2C) is targeted by GSK-3 $\beta$  using mass spectrometry.

---

Feng J. Gao<sup>1</sup>, Deanna S. Smith<sup>1\*</sup>. To be submitted to J of Biological Chemistry

Together, the method has been tested to map authentic GSK-3 $\beta$ -dependent phosphorylation sites on ICs, and has the potential to be applied to identify other *bona fide* substrates of GSK-3 $\beta$  or other kinases.

## **INTRODUCTION**

Cytoplasmic dynein is a microtubule-based retrograde molecular motor. It is a multisubunit complex with molecular weight of over 1.5 MDa, consisting of heavy chains (HCs), intermediate chains(ICs), light intermediate chains(LICs), and light chains(LCs) (Pfister et al., 2006). Dynein participates in a broad range of cellular functions, such as mitosis, cell migration, and organelle trafficking (Kardon and Vale, 2009). Dynein regulators such as dynactin, Ndel1/Nde1 and Lis1 appear to regulate the motor's functions by recruiting it to the appropriate sites or by modulating its mechanochemical properties (Kardon and Vale, 2009). Dynactin is a large multisubunit complex of ~1 MDa (Schroer, 2004), which plays many roles in dynein regulation, such as linking dynein to cargo, targeting dynein to specific subcellular locations , and increasing dynein's processivity (Culver-Hanlon et al., 2006). Ndel1/Nde1 function to recruit dynein to cargo as well as to recruit Lis1 to dynein (McKenney et al., 2010). Lis1 and Ndel1/Nde1 are crucial for many dynein functions including spindle orientation, cell migration, axon transport and more (Hebbar et al., 2008b; McKenney et al., 2010; Mesngon et al., 2006; Pandey and Smith, 2011; Wang et al., 2013). However, the mechanism of dynein regulation is still largely unknown.

The ICs are encoded by two genes, and both of them have several splicing isoforms (Allan, 2011; Kuta et al., 2010; Pfister et al., 2006; Wickstead

and Gull, 2007). ICs form a dimer during dynein complex assembly, and can dimerize with all combinations of isoforms (Lo et al., 2006). ICs act as a dynein regulatory center, because they directly interact with other dynein subunits as well as many dynein regulators and cargo. The C-terminus of ICs binds directly to HCs, and the N-terminus has three LC-binding domains (King et al., 2003; McKenney et al., 2011). Dynactin binds to the N-terminus of ICs via its subunit p150<sup>Glued</sup> (Karki and Holzbaaur, 1995; Vaughan and Vallee, 1995), and Ndel1/Nde1 also interact with ICs directly (Stehman et al., 2007). Ndel1/Nde1 have the same binding sites on IC as p150<sup>Glued</sup>, which causes a clear competition between them for binding to dynein (McKenney et al., 2011). ICs interact with zw10, which is a kinetochore protein playing a role in mitotic checkpoint signaling (Kardon and Vale, 2009). ICs are essential for dynein cargo selection (Kardon and Vale, 2009; Kuta et al., 2010): ICs interact with dynactin to modulate cargo and microtubule interactions (Schroer, 2004; Vaughan and Vallee, 1995); ICs directly interact with cargo, including  $\beta$ -catenin, casein kinase, neurofilaments, kinesin light chains, and huntingtin, adenovirus particles and lysosomes (Allan, 2011; Kuta et al., 2010). Therefore, precise regulation of ICs is needed by the cell.

The IC obviously is essential for dynein activity in response to various signaling, but there are few studies out there that is able to form a link between kinases, phosphorylation sites on IC and relevant functions. The phosphorylation of T89 on IC-2C acts as a switch of regulating the interaction of dynein with zw10 and p150<sup>Glued</sup> during mitosis (Whyte et al., 2008): phosphorylation of T89

increases the interaction of dynein and zw10 and recruits dynein to kinetochores, while the dephosphorylation of T89 increases the dynein-dynactin interaction and leads to poleward movement of kinetochore components (Vaughan et al., 2001; Whyte et al., 2008). Later, it was shown that Polo-like Kinase1 (PLK1) may phosphorylate T89 on the N-terminus of IC-2C (1-284 AA) *in vitro* (Bader et al., 2011). Recently, two groups have shown that the activation of extracellular-signal regulated kinase (ERK) signaling increases S80 phosphorylation on IC-2C, which helps dynein bind to certain signaling endosomes and subsequent axon transport (Mitchell et al., 2012; Pullikuth et al., 2013). Another kinase, casein kinase 1 (CK1) stimulates dynein motor activity by phosphorylation of ICs, but the target sites are not known (Ikeda et al., 2011).

Glycogen Synthase kinase (GSK-3), a serine/threonine protein kinase, was described to phosphorylate glycogen synthase in rabbit skeletal muscle (Embi et al., 1980). Later, it was found that GSK-3 plays a major role in phosphorylation of tau and regulating its association with microtubules (Ishiguro et al., 1993). To date, GSK-3 turns out to be a fundamental enzyme involved in almost all cellular processes, including embryonic development, cell differentiation, apoptosis, and insulin signaling (Sutherland, 2011). In mammals there are two GSK-3 genes, GSK-3 $\alpha$  and GSK-3 $\beta$  (Woodgett, 1991), but the catalytic domain is highly conserved (Castano et al., 2010; Mukai et al., 2002; Soutar et al., 2010; Wood-Kaczmar et al., 2009). Unlike most other kinases, GSK-3 $\beta$  is highly active in resting cells because of an activating auto-phosphorylation at Tyr 216. However, multiple kinases including AKT/PKB,

protein kinase A, and protein kinase C phosphorylate GSK-3 $\beta$  at Serine 9 (S9) to inhibit its activity (Cross et al., 1995; Fang et al., 2002; Fang et al., 2000). GSK-3 $\beta$  usually phosphorylates and inhibits its substrates (Sutherland, 2011). Many substrates have consensus sequences of S/TXXXpS/T (Fiol et al., 1987). In this case, priming phosphorylation at the residue, 4 or 5 amino acids C-terminal to the target site, is often required for the subsequent phosphorylation by GSK-3 $\beta$  (ter Haar et al., 2001). However, GSK-3 $\beta$  is also well-known as a proline-directed kinase (Mandelkow et al., 1992), and many GSK-3 $\beta$  substrates do not require priming phosphorylation (Doble and Woodgett, 2003; Eldar-Finkelman, 2002). So putative target site is not limited to the consensus sequences. There are about 100 proteins reported as GSK-3 $\beta$  substrates, but most of them have not been proved as *bona fide* substrates (Sutherland, 2011). In chapter 1, we provided evidence that GSK-3 $\beta$  can phosphorylate ICs *in vitro*.

Mapping of GSK-3 $\beta$  phosphorylation sites on IC is a necessary step to study the mechanism of how GSK-3 regulates dynein. We develop a systematic method with sequential steps for identifying authentic phosphorylation sites on IC by GSK-3 $\beta$  (Figure 3.1). We found S88 or T89 (corresponding to S87 or T88 on IC-1B), and T154 on IC-2C are targeted by GSK-3 $\beta$ . This method could also be applied to identify other *bona fide* substrates of GSK-3 $\beta$  or other kinases.

## RESULTS

### **GSK-3 $\beta$ phosphorylates N-terminal IC-2C without priming**

**phosphorylation:** Our previous study provides evidence that GSK-3 $\beta$  is able to phosphorylate IC-1 and IC-2, and that priming phosphorylation is required for

some but not all target sites. Here, we map GSK-3 $\beta$  phosphorylation sites on ICs, which do not require priming phosphorylation. There is high homology between IC isoforms, and IC-2C is regarded as the only ubiquitously expressed isoform (Brill and Pfister, 2000; Ha et al., 2008; King et al., 2003; Vaughan and Vallee, 1995).

IC-2C has 612 amino acids (aa). N-terminal coiled-coil and nearby regions of IC-2C are responsible for interacting with Ndel1/Nde1 and p150<sup>Glued</sup>, followed by three domains for binding to different types of LCs. The dimerization domain and 7 WD-40 repeats are essential for the assembly of dynein complex (Figure 3.2A). IC-2C sequences contain nine consensus sites and nine proline-directed serine/threonine sites (Figure 3.2B). Several of them are located at the N-terminus of IC-2C. To get reliable mass spectrometry analysis of IC-2C, we characterized and optimized N-terminal 237aa of IC-2C (N237) phosphorylation by GSK-3 $\beta$  using purified N237 protein (Figure 3.2C, D). It showed that the intensity of N237 phosphorylation was positively correlated with the amount of GSK-3 $\beta$  (Figure 3.2C), and that there was more N237 phosphorylation with longer incubation in a GSK-3 $\beta$  kinase assay (Figure 3.2D). We tested phosphorylation of the N-terminal 106 aa of IC-2C (N106) by GSK-3 $\beta$  and found that N106 was less phosphorylated compared to N237. It indicates that certain sites in N106 as well as in the region between positions 106 and 237 on IC-2C are phosphorylated by GSK-3 $\beta$ .

**Identification of phosphorylation sites on IC-2C by mass spectrometry:** To determine the functional significance of the specific sites

phosphorylated by GSK-3 $\beta$ , we used mass spectrometry (MS) to identify the phosphorylated sites on N237. There was no phosphorylated peptide detected by MS if the N237 protein was not incubated with GSK-3 $\beta$ . After incubation with the kinase, a tryptic peptide, EDEEEEDDVATPKPPVEPEEEK, was found to be phosphorylated in N237 (Figure 3.3A). MS/MS spectra analysis of the phosphorylated peptide showed that T154 was a site of phosphorylation. The table summarized MS information of the phosphorylated and un-phosphorylated peptides (Figure 3.3A). When N237 was digested with endoproteinase Asp-N, We found T154 phosphorylation was also detected by mass spectrometry after GSK-3 $\beta$  kinase assay (Figure 3.3B).

We detected another phosphorylated tryptic peptide, SVSTPSEAGSQDSGDGAVGSR, in MS of N237 after kinase assay. MS/MS spectra analysis of the phosphorylated peptide indicated that S86, S88 or T89 on IC-2C could be the target. The table showed the comparison of MS information about the phosphorylated and un-phosphorylated peptides (Figure 3.4A). To confirm if they were the real sites, we performed MS with in-gel Asp-N digestion of N237. A phosphorylated peptide (DSPIVPPPMSPSSKSVSTPSEAGSQ, M9-Ox) containing S86, S88 and T89 was detected and MS/MS spectra analysis excluded the possibility of S86 phosphorylation (Figure 3.4B). Many repeats have been done, but none of them excludes the S88 or T89. So we think that both could be targeted by GSK-3 $\beta$ . Interestingly, both T89 and T154 are followed by the proline residue.

**Quantification of phosphorylation of T154, S88 or T89 on IC-2C by mass spectrometry:** Sequence coverage of N237 in mass spectrometry was 79.3%, which contained 32 out of 35 S/T sites on N237 (Figure 3.5A). In order to estimate the phosphorylation of the individual site, the precursor intensity of the tryptic phosphorylated and unphosphorylated peptides were measured (Figure 3.5B, C). For the T154-containing peptide, the precursor intensity of unphospho-peptide is 341933 counts and the phospho-peptide is 98802 counts (Figure 3.5B). For the S88- and T89-containing peptide, the precursor intensity of unphospho-peptide is 1144776 counts, and the phospho-peptide is 20552 counts (Figure 3.5C). Another way to quantify the phosphorylation level of a given site is by comparing the precursor area of the phosphorylated peptide to that of the total area of the peptide (combining areas from both phosphorylated and unphosphorylated peptides). We applied this method and estimated that 12.5% of the peptides containing T154 were phosphorylated, and 4.81% of the peptides containing S88 and T89 were phosphorylated (Figure 3.5D).

**Confirmation of T154, S88 and T89 phosphorylation sites on IC-2C by mutagenesis:** To confirm that T154 was targeted by GSK-3 $\beta$ , we generated three N237 mutants, T154V, S91A/T154 and S84A/S91A/T154. Both S84 and S91 are in consensus sites on the N-terminus of IC-2C (Figure 3.2B). WT N237 and its mutants were expressed and purified from bacteria. All mutants had significantly less phosphorylation than WT in GSK-3 $\beta$  kinase assay (Figure 3.6A), suggesting that T154 but not the two consensus sites is the target on N237. Next, we confirmed that S88 or T89 was the target by showing the S88A/T89V

mutant of N106 was significantly less phosphorylated by GSK-3 $\beta$  comparing to WT N106 (Figure 3.6B). In order to test if S88, T89 and T154 were also targeted by GSK-3 $\beta$  in FL-IC-2C, we generated two EGFP-IC-2C mutants: T154V and S88A/T89V/T154V. WT and the mutants of EGFP-IC-2C were expressed in Cos-7 cells and immunopurified by GFP antibody, followed by a GSK-3 $\beta$  kinase assay. The T154V mutant was less phosphorylated than WT, and the S88A/T89V/T154V mutant had even less phosphorylation (Figure 3.6C). We found endogenous ICs were also in pulldown and phosphorylated by GSK-3 $\beta$  as shown in the red rectangle. Although the amount of endogenous ICs were a lot less than EGFP-IC-2C in pull-down as shown in Coomassie brilliant blue staining, their phosphorylation levels are about the same (Figure 3.6C). This indicates that the priming phosphorylation of endogenous ICs may make them better GSK-3 $\beta$  substrates.

**Location and conservation of T154, S88 and T89:** Our previous study demonstrates that GSK-3 $\beta$  negatively regulates dynein functions including intracellular transport, axon transport and cell migration. We also find that phosphorylation of GSK-3 $\beta$  reduces the interaction between dynein and Ndel1 and increases the interaction of dynein and APC. We need to create a link between the phosphorylation sites on IC and their related functions. S88 and T89 are located at the serine/threonine-rich region of IC-2C (Figure 3.7A), which may be important for regulation of Ndel1/Nde1 and P150<sup>Glued</sup> (Nyarko et al., 2012). S88 and T89 are conserved in all mouse IC isoforms and in other mammalian ICs including rat, human, bovine and horse (Figure 3.7B). T154-containing

phospho-peptide is near the dimerization domain and LC7 binding domain (Figure 3.7A), which may affect dynein assembly. In figure 3.6C, the phosphorylation of endogenous ICs pulled down by WT EGFP-IC-2C was higher than that from the mutants, which suggests that T154 may regulate the dimerization of ICs. T154 exists in all mouse IC-2 isoforms but not in IC-1, and T154 is conserved in bovine and horse IC-2 but not in rat or human IC-2 (Figure 3.7B).

**Confirmation of GSK-3 $\beta$ -dependent phosphorylation of S87 and T88 on rat IC-1B by MS:** IC-1B is a neuron specific isoform of ICs (Ha et al., 2008), which has S87 and T88 sites corresponding to S88 and T89 on mouse IC-2C. It does not have a corresponding site for T154. Previously, we found that rat EGFP-IC-1B was significantly phosphorylated by GSK-3 $\beta$ . EGFP-IC-1B were expressed in Cos-7 cells and immunopurified by GFP antibody, and GSK-3 $\beta$  kinase assay was performed for 1hr. We analyzed the GSK-3 $\beta$  dependent phosphorylation of EGFP-IC-1B by mass spectrometry with tryptic digestion. The sequence coverage of IC-1B is 69.65%, and a phospho-peptide (SVSTPSEAGSQDDLGPLTR) containing S87 and T88 was detected (Figure 3.8A). MS/MS spectra analysis of the peptide showed that S87 or T88 was the site of phosphorylation (Figure 3.8B, C). The precursor intensity (ion counts) of unphospho-peptide is 121891, and 57484 for the phospho-peptide (Figure 3.8D). When we used the precursor area to quantify phosphorylation of the peptide, there was ~ 4.91% of the peptides were phosphorylated (Figure 3.8E).

### **Confirmation of GSK-3 $\beta$ -dependent phosphorylation of S87 and T88**

**on mouse IC-1B by MS:** ICs were immunopurified by IC antibody-conjugated beads from mouse brain extract, and GSK-3 $\beta$  kinase assay was performed for 1hr. Mouse IC-1B was analyzed by mass spectrometry with tryptic digestion. The sequence coverage of mouse IC-1B was 64.17%, and a phospho-peptide (SVSTPSDAGSQDSGDLGPLTR) containing S87 and T88 was detected (Figure 3.9A). MS/MS spectrum showed S87 or T88 was the site of phosphorylation, which did not exist before GSK-3 $\beta$  kinase assay (Figure 3.9B, C). The precursor intensity (ion counts) of unphospho-peptide is 254328, and 124687 for the phospho-peptide (Figure 3.9D). We estimated that ~ 6.69% of the peptides were phosphorylated by GSK-3 $\beta$  using MS precursor area quantification (Figure 3.9E).

Together, these results show that GSK-3 $\beta$  is able to target S87 or T88 on IC-1B from both mouse and rat, which is consistent with the prediction by the sequence conservation analysis. We feel more confident to predict that GSK-3 $\beta$  phosphorylation of ICs is a real cellular event, which is happening in many species.

## DISCUSSION

**The efficiency of GSK-3 $\beta$  phosphorylation of IC *in vitro* is biological significance?** In GSK-3 $\beta$  kinase assay, we found that more kinase increased phosphorylation of N237, and longer incubation also increased phosphorylation. After optimizing the conditions of the kinase assay, we consistently detect that GSK-3 $\beta$  is able to phosphorylate ~5% of S88 or T89 and ~15% of T154 on IC-2C using MS precursor area quantification (Figure 5). In IC-1B phosphorylation experiments, GSK-3 $\beta$  is able to phosphorylate 5-7% of S87 or T88 on IC-1B after 1 hr (Figure 3.8 and Figure 3.9). People may think that if you incubate the kinase and substrate together for enough time, the percentage of phosphorylation could be close to 100%. However, this is not the case for GSK-3 $\beta$ . Besides activating auto-phosphorylation of Y216, purified GSK-3 $\beta$  also auto-phosphorylates at S9 and inhibits itself during *in vitro* kinase assay (Ilouz et al., 2008; Wang et al., 1994). We detect ~50% of GSK-3 $\beta$  with Y216 phosphorylation and ~50% of GSK-3 $\beta$  with S9 phosphorylation after kinase assay by mass spectrometry. Therefore, auto-inhibition property may prevent GSK-3 $\beta$  achieving higher phosphorylation efficacy of ICs *in vitro*, and the phosphorylation level of T154, S88 or T89 we get is reasonable to believe they are real target sites.

**Biological functions of T154, S88 or T89:** We show that GSK-3 $\beta$  is able to phosphorylate S88 or T89 on IC-2C (S87 or T88 on IC-1B). S88 and T89 are on S/T rich region of IC where is thought to be important for Ndel1 and dynactin regulation (Nyarko et al., 2012). Moreover, phosphorylation of T89 has been reported to reduce the dynein-dynactin interaction but increase the dynein-zw10

interaction (Whyte et al., 2008). Previously, we showed that dynein or IC-2C phosphorylation by GSK-3 $\beta$  reduces its interaction with Ndel1. Therefore, we think that S88 or T89 phosphorylation may have an important role in regulating the interaction of dynein to Ndel1, dynactin, and ZW10. These interactions are important for mitosis, and intracellular transport. Consistent with this, our previous study demonstrates that GSK-3 $\beta$  negatively regulates dynein functions including axon transport and cell migration.

We also provide evidence that GSK-3 $\beta$  phosphorylates T154 on IC-2C and that the site may be important for dynein assembly. There are two reasons for us to come to the hypothesis: first, T154 is located near the dimerization and LC-7 binding domain; second, when we transfected T154V IC-2C and S88A/T89V/T154V mutants into Cos-7 cells, it seemed that less endogenous IC was pulled down by the mutants than WT. The site does not exist in IC-1 or human IC-2, but the relevant function of the site should not be underestimated because of this.

In future, we will generate phospho-specific antibodies to detect whether GSK-3 $\beta$  phosphorylate ICs *in vitro* and *in vivo*. With the antibodies, we will explore how GSK-3 $\beta$  regulates ICs phosphorylation, dynein activity and the interaction of dynein to other regulators.

**Applications of the method:** The method is designed to quickly and accurately detect a novel kinase-substrate link, especially useful for detecting the site that does not require priming phosphorylation as demonstrated here. However, if a kinase targeting its substrate requires priming phosphorylation, the

method could be applied to screen priming kinases. For example, GSK-3 $\beta$  targets some sites on ICs requiring priming phosphorylation. First, we will determine the priming kinase candidates, which could be reached by combining information from literature and mass spectrometry of kinases pulldown by IC-immunoprecipitation from mouse brain extract. Second, we will apply the method to determine if it is the priming kinase, which is based on three criteria: 1, whether it phosphorylates purified IC; 2, whether the target site is at the priming site of consensus sites; 3, whether the phosphorylation of IC by this kinase significantly increases GSK-3 $\beta$  dependent phosphorylation.

## **MATERIALS AND METHODS**

**Constructs:** EGFP-IC2C, PRSET-A IC2C, PRSET-A N237 and PRSET-A N106 expression vectors were described previously (King et al., 2003). The EGFP-IC1B vector was provided by K. Pfister (Univ. VA). PRSET-A point mutants (T154V IC-2C, S88A/T89V/T154V IC-2C; T154V N237, S91A/T154V N237, S84A/S91/T154V N237; S88A/T89V N106) were generated from their related WT vector using the QuickChange site-directed mutagenesis kit. T154V EGFP-IC2C and S88A/T89V/T154V EGFP-IC2C were subcloned from PRSET-A IC-2C mutants.

**Expression and purification of proteins:** PRSET-A N106 and N237 constructs were expressed in BL-21 cells. Cells were grown at 37°C to an OD600 of 0.4, and 0.1 mM isopropyl-d-thiogalactoside (IPTG) was added to induce protein expression for 3 hr at 37 °C. Cells were lysed in his-tag protein purification binding buffer (Invitrogen) with protease inhibitors. Ni-NTA beads

(Invitrogen) were added into the cell supernatant and incubating at RT for 1 hr. The beads were washed 3 times and then the protein was eluted.

EGFP-IC2C and EGFP-IC1B constructs were transfected into Cos7 cells using Lipofectamine 2000 reagent (Invitrogen). Cells were collected after 30 hr. For immuno-purification of EGFP-ICs from cell extract, 1 $\mu$ g EGFP antibody was first incubated with 30  $\mu$ l Protein-A dynabeads (Invitrogen) for 2 hr at room temperature and washed with lysis buffer twice. The antibody conjugated dynabeads were incubated with 1 mg extracts at 4°C overnight. For immunopurification of ICs from mouse brain extract, 15  $\mu$ l 74.1 mouse monoclonal IC antibody conjugated agarose beads (IC-beads) were incubated with 1mg extract at 4°C overnight (Santa Cruz Biotechnology, Inc.). Dynabeads or IC-beads were subject to three washes with lysis buffer and then two washes with PBS-T at 4 °C. Beads were collected for kinase assay.

**Cell and brain extract preparation:** For preparation of cell extract, cells at 90% confluency were lysed in buffer containing 50 mM Tris (pH 7.5), 0.1% NP-40, 100mM NaCl, 1 mM MgCl<sub>2</sub>, 5 mM EDTA, protease inhibitor cocktail (Fisher) and Halt phosphatase inhibitor cocktail (Fisher) on ice for 30 minutes. Cell lysates were sonicated for 10 pulses at level 1 with 10% output 3 times. The lysates were incubated on ice for another 10 min and then centrifuged at 17,000 g for 20 minutes at 4 °C. For preparation of mouse brain extract, brains were dissected with clean tools as quickly as possible to prevent degradation. Tissues were dounce-homogenized in lysis buffer as above. The lysate would be

incubated on ice for 30 min and then centrifuged at 17,000 g for 30 minutes at 4 °C. Concentration of extracts were determined by BCA protein assay (Pierce).

**Protein kinase assay:** The GSK-3 $\beta$  Kinase Enzyme System which consists of GSK-3 $\beta$  Kinase, the substrate, reaction buffer and DTT was purchased from Promega. Purified proteins (IC-2C, N237 or N106) or immunopurified ICs (EGFP-IC2C or EGFP-IC1B or mouse brain ICs) were incubated with GSK-3 $\beta$  and 0.03  $\mu$ Ci/ $\mu$ l  $\gamma$  <sup>32</sup>P-ATP at 37°C for a specific amount of time. The reaction was stopped by the addition of sample buffer. Proteins were separated by SDS-PAGE, followed by Coomassie brilliant blue staining. The wet min-gel was sealed in saran wrap and exposed to X-ray film overnight at -80 °C.

**Mass spectrometry analysis of IC:** Gel bands were excised and subjected to in-gel digestion (Trypsin/Lys-c Mix or Asp-N from Promega) according to UCSF Protocol (2002.04.08 version). Sample introduction is via a Dionex Ultimate 3000 RSLC nano liquid chromatograph (nanospray ionization), and the Orbitrap Velos Pro (Thermo Fisher Scientific), a hybrid ion trap-orbitrap mass spectrometer, was used. This spectrometer is used for high resolution LC-MS/MS, which has complementary fragmentation modes including CID, HCD, and optional ETD. The raw data were searched by SEQUEST in Thermo Scientific Proteome Discoverer software (1.4). Cytoplasmic dynein 1 intermediate chains database was used, which was generated from uniprot database. Search parameters were set: variable modifications of oxidation (at methionine residues) and phosphorylation (at serine, threonine, and tyrosine); static Modification: Carbamidomethyl; proper enzyme selected; the number of allowed missed

cleavage sites at 2; fragment match tolerance at 0.8 Da; precursor Mass  
Tolerance: 10 ppm.

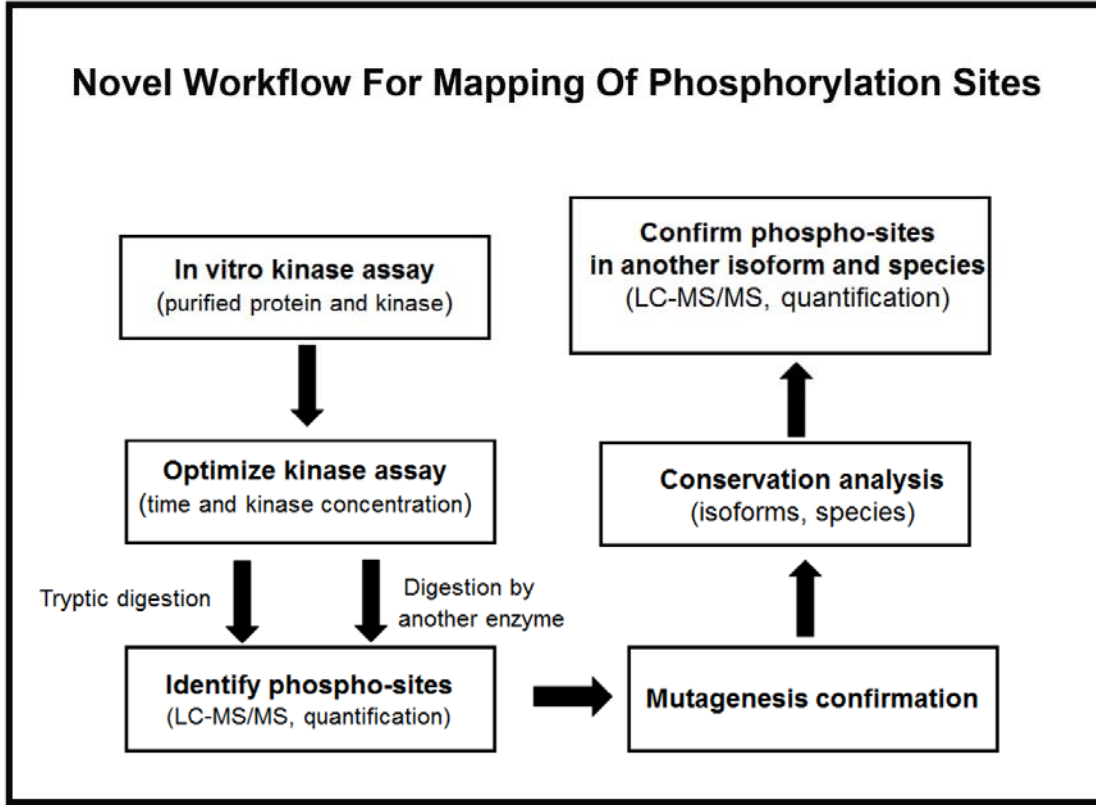


**Figure 3.1** A systematic workflow of identifying and confirming kinase-specific phosphorylation sites based on tandem mass spectrometry and mutagenesis.

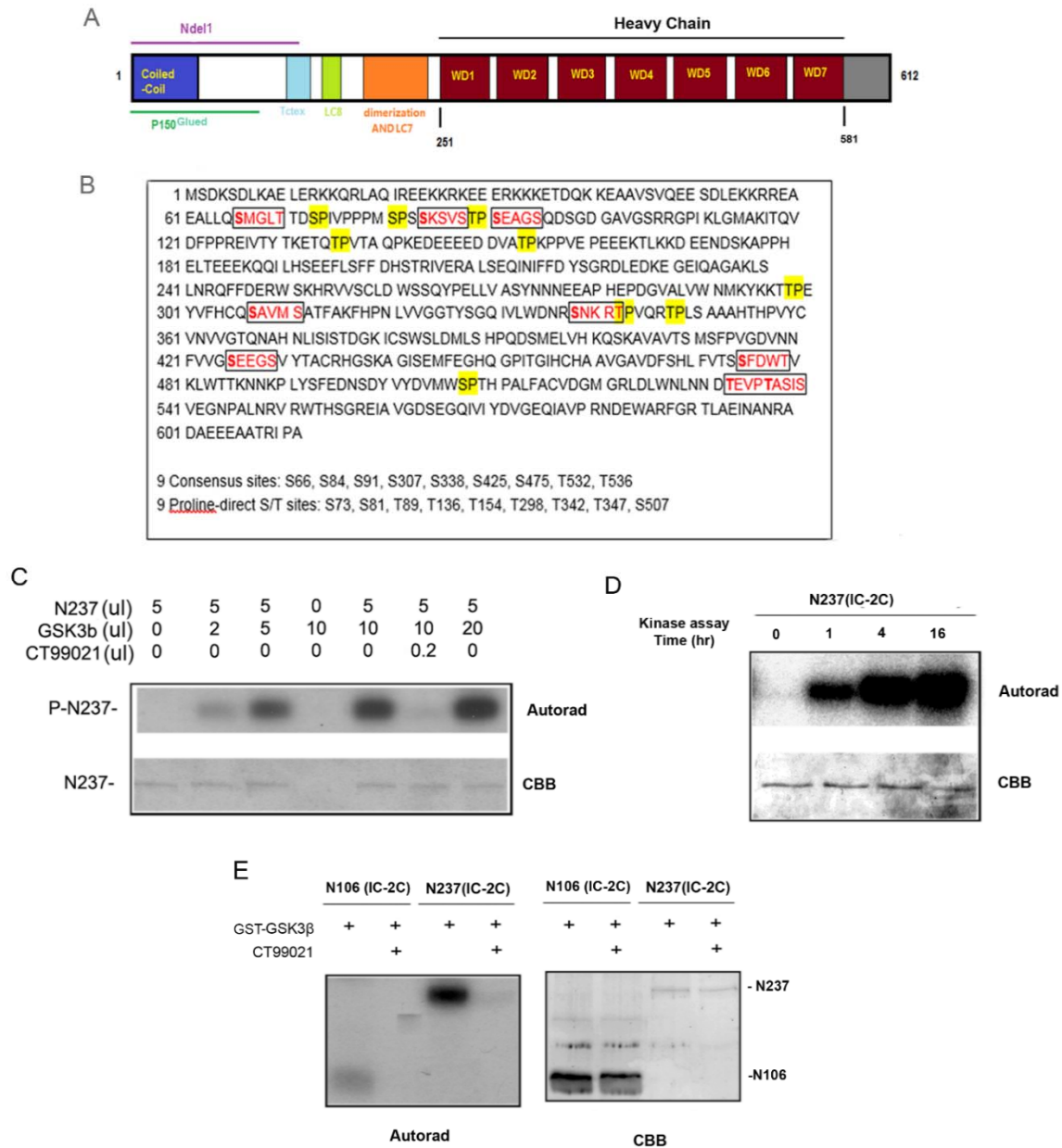


### Figure 3.2 GSK-3β phosphorylates the N-terminus of IC-2C without priming phosphorylation

**A)** Schematic of a mouse dynein intermediate chain protein (IC-2C). The protein has 612aa. Different domains and functions are labeled: N-terminal coiled-coil and nearby regions are responsible for Ndel1 and the p150<sup>Glued</sup> subunit of dynactin; Tctex, LC8 and LC7 domains are responsible for binding different dynein light chain as named; the dimerization domain is for dynein intermediate chain dimerization; 7 WD-40 repeats are known for dynein heavy chain interactions. **B)** GSK-3β consensus (S/TXXXS/T) sites and proline-direct sites on IC-2C. 9 consensus sites are colored in red and circled, and 9 proline-direct sites are highlighted with yellow. **C)** Characterized N237 phosphorylation with various

amount of GSK-3 $\beta$  in kinase assay. 5  $\mu$ l purified protein was incubated with 0, 2, 5, 10, or 20  $\mu$ l of purified GST-GSK-3 $\beta$  for 1hr, and autoradiograph (Autorad) showed that the N237 phosphorylation was positively correlated with the amount of the kinase added. If there was no N237 or added with CT99021, the phosphorylation signal was gone. Coomassie brilliant blue staining (CBB) showed the level of N237 protein in the kinase assay. **D)** Characterized N237 phosphorylation with various incubation times in kinase assay. The same amount of purified N237 protein and GSK-3 $\beta$  were incubated for 0, 1, 4 and 16 hr. It showed that the longer of the incubation time the more of the N237 phosphorylation. **E)** Compared the GSK-3 $\beta$  phosphorylation of two N-terminal fragments of IC-2C, N106 and N237. The same amount of the kinase was incubated with purified N106 and N237 protein for 1 hr. N106 was less phosphorylated by GSK-3 $\beta$  comparing to N237.

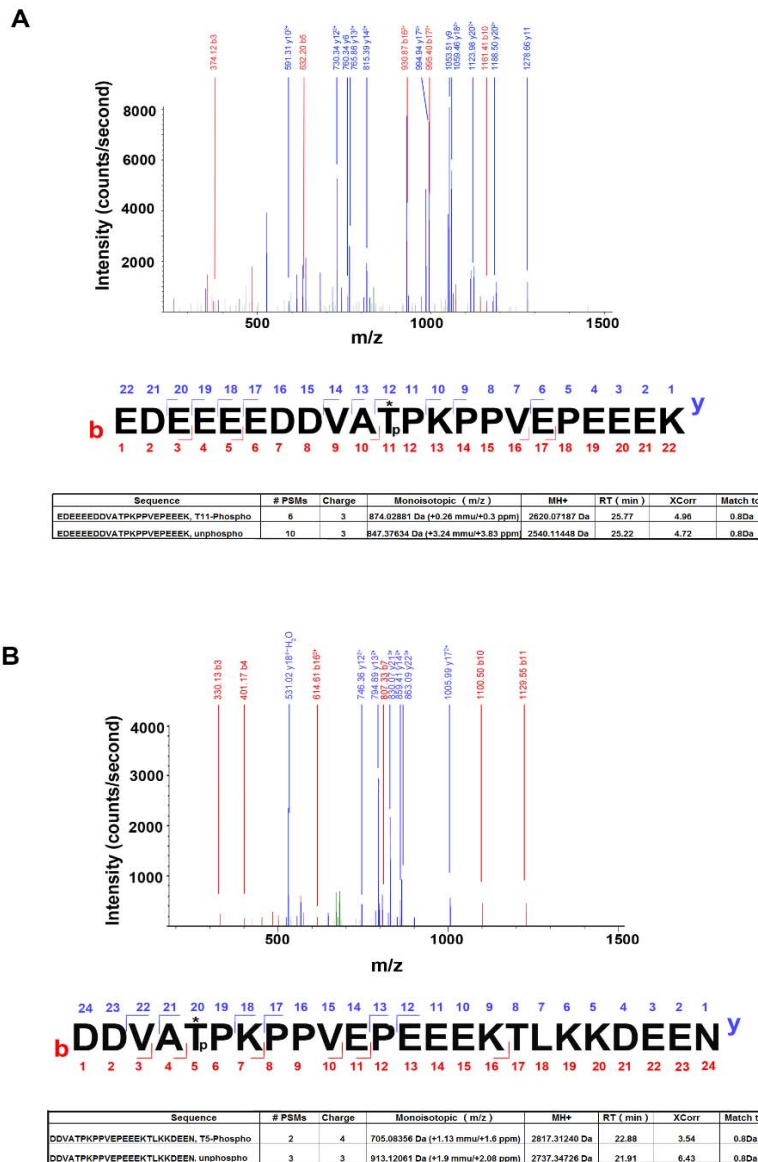


### Figure 3.3 Identification of GSK-3 $\beta$ -dependent phosphorylation of T154 on IC-2C by mass spectrometry

**A)** Detection of T154 phosphorylation in N237 after *in vitro* GSK-3 $\beta$  kinase assay followed by in-gel tryptic digest and mass spectrometry. MS/MS spectra analysis for the phosphorylated peptide (EDEEEEDDVATPKPPVEPEEEK, T11-Phospho) is shown, which was +3 charged and had 874.02881 Da (m/z). The MH<sup>+</sup> of the phospho-peptide (2620.07Da) was about 80 Da higher than related unphospho-peptide (2540.11Da), indicating a phosphorylated site on the peptide. There was only one potential site for phosphorylation on the peptide, and the spectrum confirmed T154 phosphorylation by showing nice b and y fragments: b3, b5, and b10 (did not contain T11) had no phosphorylation, while b16 and b17 (containing

T11) had phosphorylation; y6, y9 and y10 (did not contain T11) had no phosphorylation, while y13, y14, y17, y18, y19 and y20 (containing T11) had phosphorylation.

The table showed the comparison of MS information of the phosphorylated and un-phosphorylated peptides (EDEEEEDDVATPKPPVEPEEEK).

**B)** T154 phosphorylation was confirmed by in-gel Asp-N digest. MS/MS spectra analysis for the phosphorylated peptide (DDVATPKPPVEPEEEKTLKKDEEN, T5-Phospho) is shown, which was +4 charged and had m/z at 705.08356 Da. The MH<sup>+</sup> of the phospho-peptide (2817.31Da) was about 80 Da higher than related unphospho-peptide (2737.34Da). Although there were two possible phosphorylated sites in the peptide, the spectrum indicated T5 (corresponds to T154 in IC2C) was the only phosphorylated site: y12, y13, y17 and y18 fragments (containing T17) had no phosphorylation, which excluded T17 as the site of phosphorylation; b3, b4 (did not contain T5) had no phosphorylation, while b8, b10, b11, b16 fragments (only containing T5) had phosphorylation. Therefore, T154 (IC-2C) is the site of phosphorylation, and phosphorylated site is indicated with an asterisk.

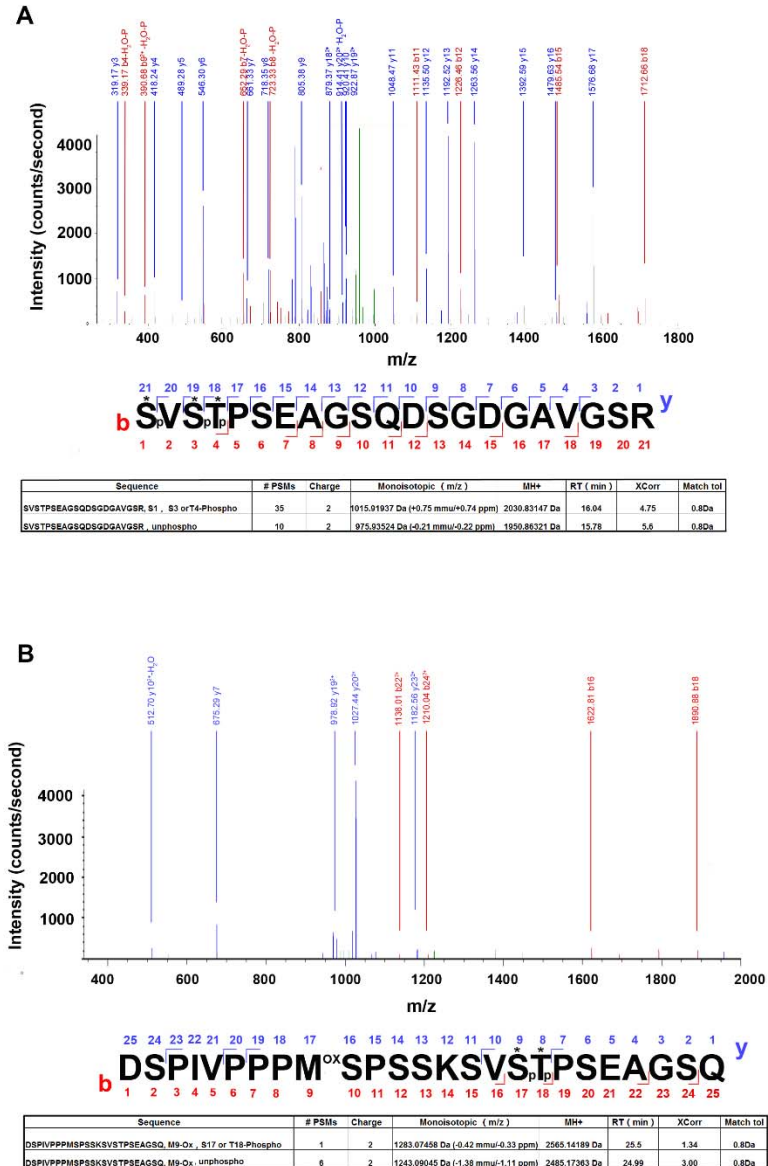


### Figure 3.4 Identification of GSK-3 $\beta$ -dependent phosphorylation of S88 and T89 on IC-2C by mass spectrometry

**A)** Detection of S88 or T89 phosphorylation on N237 after *in vitro* GSK-3 $\beta$  kinase assay followed by in-gel tryptic digest and mass spectrometry. MS/MS spectra analysis for the phosphorylated peptide (SVSTPSEAGSQDSGDGAVGSR, S1, S3 or T4-Phospho) is shown, which was +2 charged and had 1015.91937 Da (m/z). The MH<sup>+</sup> of the phospho-peptide (2030.83) was about 80 Da higher than related unphospho-peptide (1950.86Da), indicating a phosphorylated site in the peptide. Although there was 7 possible phosphorylation sites on the peptide, the spectra excluded 4 C-terminal amino acids as the site of modification at by showing y4, y5, y6, y7, y8, y9, y10, y11, y12, y13, y14, y15, y16, y17 fragments had no phosphorylation. The b4 fragment indicated there was a phosphorylation

in S1, S3 and T4 (corresponds to S86, S88 and T89 in IC2C, respectively), and y18 and y19 and y20 further confirmed there was a phosphorylation in S3 and T4. Therefore, although we couldn't exclude the possibility of S86 phosphorylation, S88 and T89 are more promising sites for phosphorylation on the peptide.

The table showed the comparison of MS information of the phosphorylated and un-phosphorylated peptides (SVSTPSEAGSQDSGDGAVGSR).

**B)** S88 and T89 phosphorylation was confirmed by in-gel Asp-N digest followed by mass spectrometry. MS/MS spectra analysis for the phosphorylated peptide (DSPIVPPPMSPSSKSVSTPSEAGSQ, M9-Ox, S17 or T18-Phospho) is shown, which was +2 charged and had m/z at 1283.07458 Da. The MH<sup>+</sup> of the phosphopeptide (2565.14 Da) was about 80 Da higher than related unphospho-peptide (2485.17Da), indicating a phosphorylated site on the peptide. There were 9 possible phosphorylated sites, but the spectra indicated S17 and T18 (corresponds to S88 and T89 in IC2C) were the only 2 possible phosphorylated sites: the b16 fragment had no phosphorylation which excluded 5 N-terminal amino acids as the site of modification; the y7 fragment had no phosphorylation which exclude another 2 C-terminal amino acids as the site of modification. The b18 and y10 fragments (containing S17 and T18) had phosphorylation indicating that there was phosphorylation of S17 or T18. Therefore, S88 or T89 on IC-2C is targeted by GSK-3 $\beta$  and phosphorylated site is indicated with an asterisk.

**A N237 sequence coverage: AA coverage(188/237) S/T coverage(32/35)**

MSDKSDLKAE LERKKQLAQ IREEKKRKEE ERKKKETDQK KEAAVSVQEE  
 SDLEKKRREA EALLQSMGLT TDSPIVPPPM SPSSKSVSTP SEAGSQDSGD  
 GAVGSRGPI KLGMAKITQV DFPPREIVTY TKETQTPVTA QPKEDDEEED  
 DVATPKPPVE PEEKTLKGD EENDSKAPPH ELTEEEKQOI LHSEEFLSFF  
 DHSTRIVERA LSEQINIFFD YSGRDLEDKE GEIQAGA

**B**



**C**



**D**

Peptide	Precursor area (ion counts), phosphorylated	Precursor area (ion counts), unphosphorylated	Total area	Percentage of phosphorylation
EDEEEEDVATPKPPVEPEEEK	1.395E+07	9.754E+07	1.115E+08	12.5%
SVSTPSEAGSQDSGDGAVGSR	5.751E+06	1.138E+08	1.196E+08	4.81%

**Figure 3.5 Quantification of T154, S88 and T89 phosphorylation on IC-2C by mass spectrometry**

**A)** Sequence coverage of N237 in mass spectrometry. N237 was phosphorylated by GSK-3 $\beta$  *in vitro*. Phosphorylated N237 was subjected to in-gel digestion with trypsin or Asp-N, and then analyzed by mass spectrometry. The sequence identified are shown in red. The analysis covered 79.3% aa and 91.4% of serine/threonine. **B)** The precursor intensity (ion counts) of the unphospho- and phospho- peptide containing T154 (EDEEEEDVATPKPPVEPEEEK). The precursor intensity of unphospho-peptide is 341933 (the peak of 847.37653 m/z), and the phospho-peptide is 98802 (the peak of 874.02881 m/z). **C)** The precursor intensity (ion counts) of the unphospho- and phospho- peptide

containing S88 or T89 (SVSTPSEAGSQDSGDGAVGSR). The precursor intensity of unphospho-peptide is 1144776 (the peak of 975.93524 m/z), and the phospho-peptide is 20552 (the peak of 1015.91937 m/z). **D)** Quantification of phosphorylation of T154, S88 or T89 by precursor area. The precursor area of phosphorylated and un-phosphorylated peptides were calculated, and the total area were calculated by adding them together. Percentage of phosphorylation = area of phosphorylated peptide/ total area. Estimated phosphorylation efficiency of T154 is 12.5%, while S88 and T89 is 4.81%.

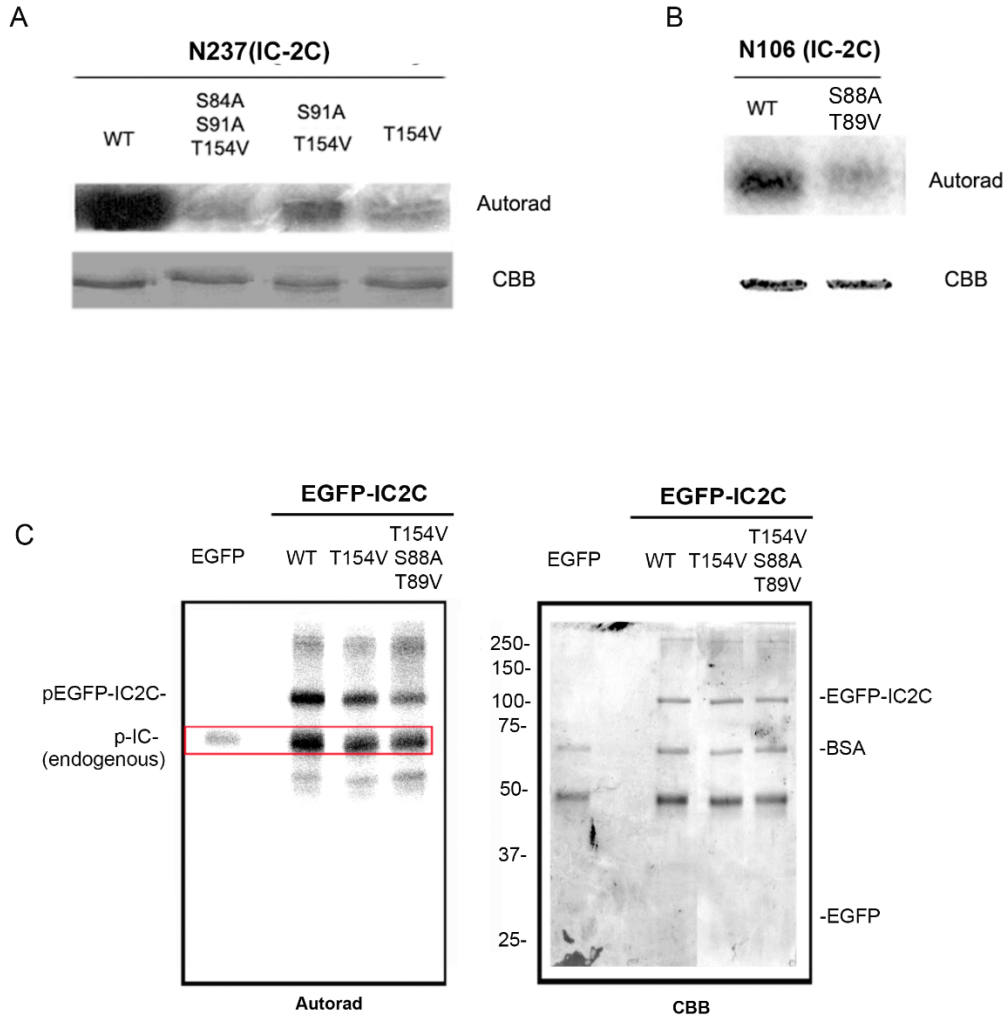


### Figure 3.6 Confirmation of GSK-3 $\beta$ -dependent phosphorylation of T154, S88 and T89 on IC-2C by mutagenesis

**A)** Confirming that T154 was targeted by GSK-3 $\beta$ . Three N237 mutants were generated: T154V, the mutant with a single mutation on T154; S91A/T154, the mutant with double mutations on S91 and T154; S84A/S91A/T154, the mutant with triple mutations on S84, S91 and T154. WT N237 and its mutants were expressed and purified from bacteria, followed by GSK-3 $\beta$  kinase assay. All mutants were significantly less phosphorylated GSK-3 $\beta$  than WT. **B)** confirming that S88 or T89 was targeted by GSK-3 $\beta$ . S88A/T89V N106 was a mutant with double mutations on S88 and T89. Comparing to WT N106, the mutant was significantly less phosphorylated by GSK-3 $\beta$ . **C)** Demonstrating that the S88, T89 and T154 were targeted GSK-3 $\beta$  in EGFP-IC-2C. Two EGFP-IC-2C mutants were generated: T154V and S88A/T89V/T154V. Phosphorylation of the T154V mutant was less than WT, but S88A/T89V/T154V mutant had even less

phosphorylation by GSK-3 $\beta$ . The phosphorylation signal in red rectangle was probably mainly from endogenous ICs pulled down by EGFP-IC-2C. Endogenous ICs were much less than EGFP-IC-2C in pulldown, but their phosphorylation signals are about the same.

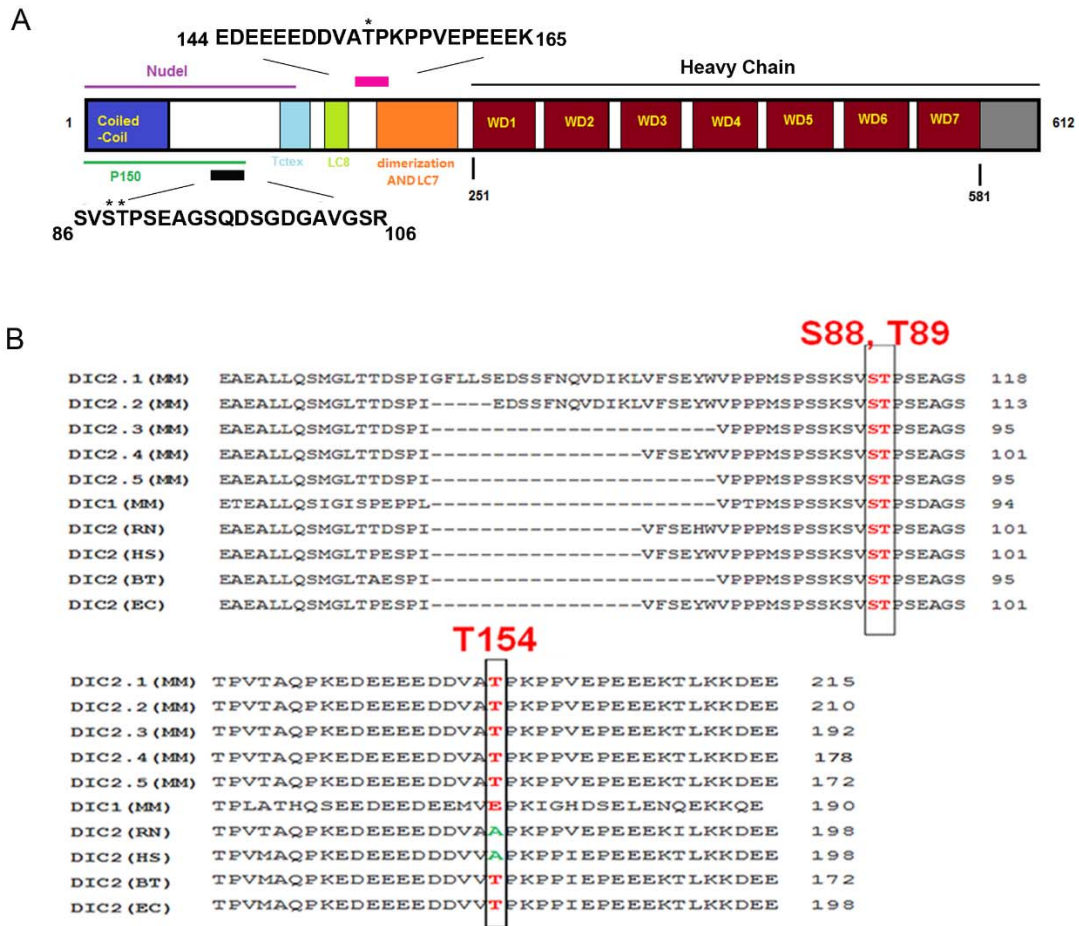


**Figure 3.7 Location of and conservation of T154, S88 and T89 on IC**

**A)** Location of the phosphorylation sites on mouse IC-2C. The black and pink bars indicates the position of phospho-peptides and their sequences. The GSK-3 $\beta$  targeted serine and threonine are indicated with asterisks. The N terminal phospho-peptide (containing S88 and T89) has part of region binds to Ndel1 and P150<sup>Glued</sup>. T154 contained phospho-peptide is near the dimerization domain and LC7 binding domain.

**B)** The conservation of the phosphorylation sites on ICs from different species. Both S88 and T89 are conserved in all mouse (MM) IC isoforms or other mammalian species including Rat (RN), human (HS), bovine (BT) and horse (EC). T154 is conserved in all mouse IC-2 but not in IC-1, and it also exists in bovine and horse ICs but not in rat or human IC

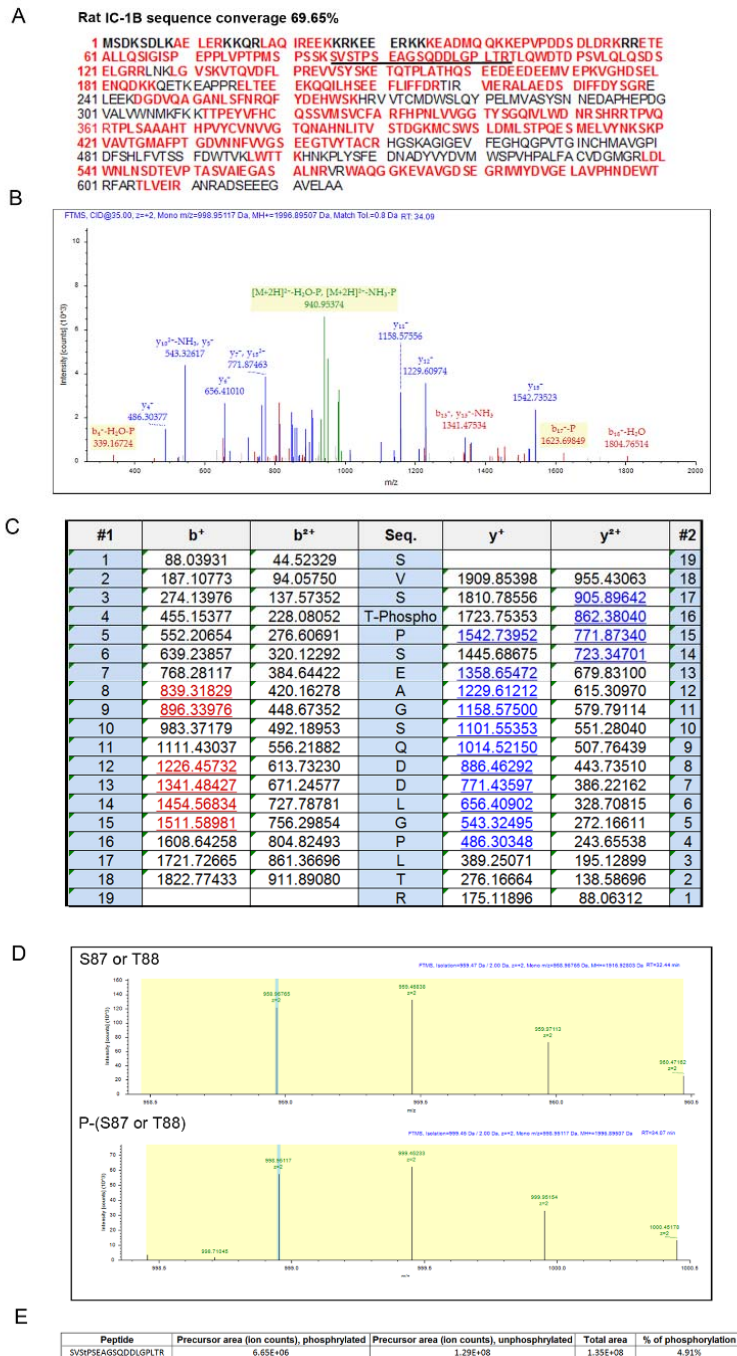


**Figure 3.8 Identification of GSK-3 $\beta$ -dependent phosphorylation of S87 and T88 on Rat IC-1B by MS**

**A)** The sequence coverage of rat IC-1B (the amino acids detected are in red). A phosphorylated peptide containing S87 or T88 was detected by mass spectrometry after GSK-3 $\beta$  kinase assay (the sequence was underlined) **B)** MS/MS spectrum of the phosphorylated peptide (SVSTPSEAGSQDDLGLPLTR, S3 or T4-Phospho) was shown. The analysis of the spectrum showed that S3 or

T4 (corresponding to S87 or T88 on IC-1B) was phosphorylated. **C)** The theoretical  $m/z$  values for MS/MS fragment ions of the phospho-peptide containing S87 or T88 was shown, and detected fragment ions were in red and underlined. Only the fragment ions without any losses were shown. **D)** The precursor intensity of the unphospho- and phospho- peptide containing S87 and T88. **E)** Quantification of phosphorylation efficiency of S87 or T88 on IC-1B by precursor area.

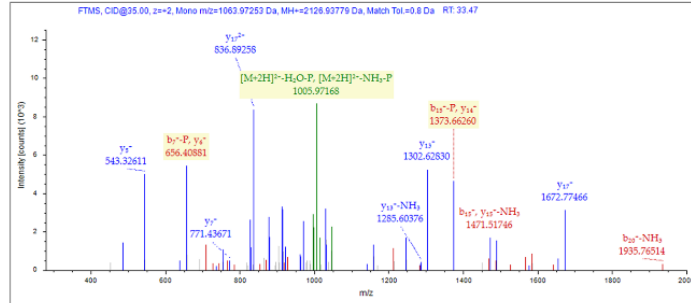
A

Mouse IC-1B sequence coverage 64.17%

```

1 MSDKSDLKAE LERKKQLRAQ IREEKKRKEE ERKKKEADMQ QKKEPVQDD S DLRKRKRETE
61 ALLQSIGISP EPLVPTPMS PSSKSVSTPS DAGSQDSDGL GPLTRTLQWD TDPVSLQLQS
121 DSELGRRRLHK LGVSKVTQVD FLPREWVSY KETQTPLATH QSEEDDEEE MVEPKIGHDS
181 ELENQEKQDV TKEAPPRELT EEEKQQLHS EEFUFDRT IRVIERALAE DSDIFFDYSG
241 RELEEKGDV QAGANLSFNR QFYDEHWSKH RVVTCMDWSL QYPELMVASY SNNEPAPHEP
301 DGVALWVNMK FKKTPTPEYVF HCQSSVMVVC FARFHPNLVV GGTYSQQVIL WDNRSRRTPT
361 VORTPLSAAA HTHPVYCVNV VGTQNAHNL TVSTDGKMC S WSLDMLSTPQ ESMELYNKS
421 KPVAVTGMAF PTGDVNVFV GSEEGVYTA CRHGSKAGIG EVFEGHQGPV TGINCHMAVG
481 PIDFSLFVIT SSFDWTVKLW TTKHNKPLYS FEDNADYYVD VMWSPHPAL FACVDGMGR L
541 DLWNLNSDTE VPTASVAIEG ASALNRVRWA QGGKEVAVGD SEGRIVWYDV GELAVPHNDE
601 WTRFARTLVE IRANRADSEE EGAVELAA
  
```

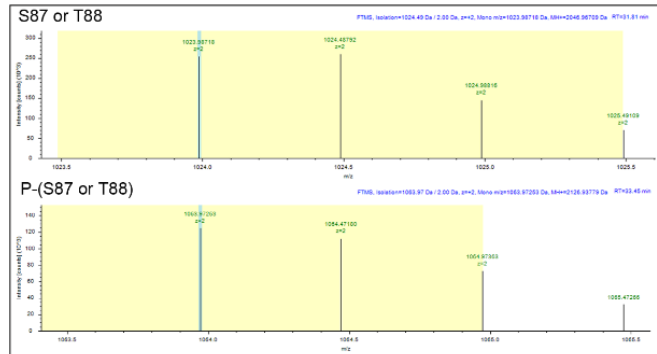
B



C

#1	b <sup>+</sup>	b <sup>+</sup> *	Seq.	y <sup>+</sup>	y <sup>+</sup> *	#2
1	88.03931	44.52329	S			21
2	187.10773	94.05750	V	2039.89183	1020.44955	20
3	354.10609	177.55668	S-Phospho	1940.82341	970.91534	19
4	455.15377	228.08052	T	1773.82505	887.41616	18
5	552.20654	276.60691	P	1672.77737	836.89232	17
6	639.23857	320.12292	S	1575.72460	788.36594	16
7	754.26552	377.63640	D	1488.69257	744.84992	15
8	825.30264	413.15496	A	1373.66562	687.33645	14
9	882.32411	441.66569	G	1302.62850	651.81789	13
10	969.35614	485.18171	S	1245.60703	623.30715	12
11	1097.41472	549.21100	Q	1158.57500	579.79114	11
12	1212.44167	606.72447	D	1030.51642	515.76185	10
13	1299.47370	650.24049	S	915.48947	458.24837	9
14	1356.49517	678.75122	G	828.45744	414.73236	8
15	1471.52212	736.26470	D	771.43597	386.22162	7
16	1584.60619	792.80673	L	656.40902	328.70815	6
17	1641.62766	821.31747	G	543.32495	272.16611	5
18	1738.68043	869.84385	P	486.30348	243.65538	4
19	1851.76450	926.38589	L	389.25071	195.12899	3
20	1952.81218	976.90973	T	276.16664	138.58696	2
21			R	175.11896	88.06312	1

D



E

Peptide	Precursor area (ion counts), phosphorylated	Precursor area (ion counts), unphosphorylated	Total area	% of phosphorylation
SVSTPSDAGSQDSDGLPLTR	6.21E+06	8.66E+07	9.28E+07	6.69%

**Figure 3.9 Identification of GSK-3β-dependent phosphorylation of S87 and T88 on mouse IC-1B by MS**

A) The sequence coverage of mouse rat IC-1B. A phosphorylated peptide containing S87 or T88 was detected by mass spectrometry after GSK-3β kinase

assay (the sequence was underlined) **B)** MS/MS spectrum of the phospho-peptide (SVSTPSDAGSQDSGDLGPLTR) containing S87 and T88 was detected. **C)** The theoretical m/z values for MS/MS fragment ions of the phospho-peptide containing S87 or T88 was shown, and detected fragment ions were in red and underlined. Only the fragment ions without any losses were shown. **D)** The precursor intensity of the unphospho- and phospho- peptide (SVSTPSDAGSQDSGDLGPLTR). **E)** Quantification of phosphorylation efficiency of S87 or T88 on IC-1B by precursor area.

## CONCLUSIONS

In this study, we have provided evidence that GSK-3 $\beta$  directly regulates dynein in both neurons and non-neuronal cells. GSK-3 $\beta$  interacts and phosphorylates dynein *in vitro*. Dynein phosphorylation by GSK-3 $\beta$  reduces its interaction with Ndel1, a regulator contributing to dynein force generation. Dynein motility is stimulated both by pharmacological GSK-3 $\beta$  inhibitors and by enhanced insulin signaling that leads to GSK-3 $\beta$  inactivation. Thus our study connects a well-characterized insulin-signaling pathway, PI3K/AKT/GSK-3, directly to dynein stimulation.

We find that dynein and APC physically interact with each other, which is positively regulated by GSK-3 $\beta$ . In both cell lines and mouse models, we demonstrate that rosiglitazone increases dynein activity and cell migration in WT cells but not in Apc (min/+) cells, and rosiglitazone induces spindle misorientation in Apc (min/+) cells but not in WT cells. We provide evidence that this involves different PI3K/AKT/GSK-3 $\beta$  signaling responses to rosiglitazone between WT and Apc (min/+) cells, and that ApcMin mutation negatively regulates the interaction of dynein with WT APC. Our discovery of the interplay of APC and dynein provides a new insight into how PPAR- $\gamma$  signaling regulates cancer development and other cellular events.

To dissect how GSK-3 $\beta$  and APC regulate dynein, we have demonstrated a mass spectrometry (MS)-based systematic method to map phosphorylation

sites on IC. We identified that T154, S88 and T89 on IC-2C are targeted by GSK-3 $\beta$  by using both MS and mutagenesis. S88 and T89 are conserved in all mouse IC isoforms as well as in ICs from all other mammalian species examined. Furthermore, we demonstrate that S87 or T88 on IC-1B (corresponding to S88 or T89 on IC-2C) from both mouse and rat are targeted by GSK-3 $\beta$  using MS analysis. The method has the potential to be applied to identify other *bona fide* substrates of GSK-3 $\beta$  or other kinases.

## REFERENCES

- Acevedo, N., X. Wang, R.L. Dunn, and G.D. Smith. 2007. Glycogen synthase kinase-3 regulation of chromatin segregation and cytokinesis in mouse preimplantation embryos. *Molecular reproduction and development*. 74:178-188.
- Allan, V.J. 2011. Cytoplasmic dynein. *Biochemical Society transactions*. 39:1169-1178.
- Ayala, R., T. Shu, and L.H. Tsai. 2007. Trekking across the brain: the journey of neuronal migration. *Cell*. 128:29-43.
- Baas, P.W., and S. Lin. 2011. Hooks and comets: The story of microtubule polarity orientation in the neuron. *Dev Neurobiol*. 71:403-418.
- Bader, J.R., J.M. Kasuboski, M. Winding, P.S. Vaughan, E.H. Hinchcliffe, and K.T. Vaughan. 2011. Polo-like kinase1 is required for recruitment of dynein to kinetochores during mitosis. *J Biol Chem*. 286:20769-20777.
- Baptista, F.I., M.J. Pinto, F. Elvas, T. Martins, R.D. Almeida, and A.F. Ambrosio. 2014. Diabetes induces changes in KIF1A, KIF5B and dynein distribution in the rat retina: Implications for axonal transport. *Experimental eye research*. 127:91-103.
- Barton, N.R., and L.S. Goldstein. 1996. Going mobile: microtubule motors and chromosome segregation. *Proceedings of the National Academy of Sciences of the United States of America*. 93:1735-1742.
- Bingham, J.B., S.J. King, and T.A. Schroer. 1998. Purification of dynactin and dynein from brain tissue. *Methods in enzymology*. 298:171-184.
- Blokhuis, A.M., E.J. Groen, M. Koppers, L.H. van den Berg, and R.J. Pasterkamp. 2013. Protein aggregation in amyotrophic lateral sclerosis. *Acta neuropathologica*. 125:777-794.
- Bobinnec, Y., X. Morin, and A. Debec. 2006. Shaggy/GSK-3beta kinase localizes to the centrosome and to specialized cytoskeletal structures in Drosophila. *Cell motility and the cytoskeleton*. 63:313-320.
- Bradshaw, N.J., W. Hennah, and D.C. Soares. 2013. NDE1 and NDEL1: twin neurodevelopmental proteins with similar 'nature' but different 'nurture'. *Biomolecular concepts*. 4:447-464.
- Brill, L.B., 2nd, and K.K. Pfister. 2000. Biochemical and molecular analysis of the mammalian cytoplasmic dynein intermediate chain. *Methods*. 22:307-316.
- Brinkley, B.R. 1985. Microtubule organizing centers. *Annual review of cell biology*. 1:145-172.
- Burgermeister, E., L. Tencer, and M. Liscovitch. 2003. Peroxisome proliferator-activated receptor-gamma upregulates caveolin-1 and caveolin-2 expression in human carcinoma cells. *Oncogene*. 22:3888-3900.

- Carnero, A., and J.M. Paramio. 2014. The PTEN/PI3K/AKT Pathway in vivo, Cancer Mouse Models. *Frontiers in oncology*. 4:252.
- Castano, Z., P.R. Gordon-Weeks, and R.M. Kypta. 2010. The neuron-specific isoform of glycogen synthase kinase-3beta is required for axon growth. *J Neurochem*. 113:117-130.
- Chang, C.H., J.W. Lin, L.C. Wu, M.S. Lai, L.M. Chuang, and K.A. Chan. 2012. Association of thiazolidinediones with liver cancer and colorectal cancer in type 2 diabetes mellitus. *Hepatology*. 55:1462-1472.
- Cole, A., S. Frame, and P. Cohen. 2004. Further evidence that the tyrosine phosphorylation of glycogen synthase kinase-3 (GSK3) in mammalian cells is an autophosphorylation event. *The Biochemical journal*. 377:249-255.
- Cross, D.A., D.R. Alessi, P. Cohen, M. Andjelkovich, and B.A. Hemmings. 1995. Inhibition of glycogen synthase kinase-3 by insulin mediated by protein kinase B. *Nature*. 378:785-789.
- Culver-Hanlon, T.L., S.A. Lex, A.D. Stephens, N.J. Quintyne, and S.J. King. 2006. A microtubule-binding domain in dynactin increases dynein processivity by skating along microtubules. *Nat Cell Biol*. 8:264-270.
- Doble, B.W., and J.R. Woodgett. 2003. GSK-3: tricks of the trade for a multi-tasking kinase. *Journal of cell science*. 116:1175-1186.
- Dobrowolski, R., and E.M. De Robertis. 2012. Endocytic control of growth factor signalling: multivesicular bodies as signalling organelles. *Nature reviews. Molecular cell biology*. 13:53-60.
- Dolma, K., G.J. Iacobucci, K. Hong Zheng, J. Shandilya, E. Toska, J.A. White, 2nd, E. Spina, and S. Gunawardena. 2014. Presenilin influences glycogen synthase kinase-3 beta (GSK-3beta) for kinesin-1 and dynein function during axonal transport. *Human molecular genetics*. 23:1121-1133.
- Dujardin, D.L., and R.B. Vallee. 2002. Dynein at the cortex. *Current opinion in cell biology*. 14:44-49.
- Eldar-Finkelman, H. 2002. Glycogen synthase kinase 3: an emerging therapeutic target. *Trends Mol Med*. 8:126-132.
- Eldar-Finkelman, H., and A. Martinez. 2011. GSK-3 Inhibitors: Preclinical and Clinical Focus on CNS. *Frontiers in molecular neuroscience*. 4:32.
- Embi, N., D.B. Rylatt, and P. Cohen. 1980. Glycogen synthase kinase-3 from rabbit skeletal muscle. Separation from cyclic-AMP-dependent protein kinase and phosphorylase kinase. *Eur J Biochem*. 107:519-527.
- Eschbach, J., and L. Dupuis. 2011. Cytoplasmic dynein in neurodegeneration. *Pharmacology & therapeutics*. 130:348-363.
- Espada, J., M.B. Calvo, S. Diaz-Prado, and V. Medina. 2009. Wnt signalling and cancer stem cells. *Clinical & translational oncology : official publication of the Federation of Spanish Oncology Societies and of the National Cancer Institute of Mexico*. 11:411-427.
- Etienne-Manneville, S. 2009. APC in cell migration. *Advances in experimental medicine and biology*. 656:30-40.
- Etienne-Manneville, S. 2010. From signaling pathways to microtubule dynamics: the key players. *Current opinion in cell biology*. 22:104-111.

- Fang, X., S. Yu, J.L. Tanyi, Y. Lu, J.R. Woodgett, and G.B. Mills. 2002. Convergence of multiple signaling cascades at glycogen synthase kinase 3: Edg receptor-mediated phosphorylation and inactivation by lysophosphatidic acid through a protein kinase C-dependent intracellular pathway. *Mol Cell Biol.* 22:2099-2110.
- Fang, X., S.X. Yu, Y. Lu, R.C. Bast, Jr., J.R. Woodgett, and G.B. Mills. 2000. Phosphorylation and inactivation of glycogen synthase kinase 3 by protein kinase A. *Proc Natl Acad Sci U S A.* 97:11960-11965.
- Ferrarese, A., O. Marin, V.H. Bustos, A. Venerando, M. Antonelli, J.E. Allende, and L.A. Pinna. 2007. Chemical dissection of the APC Repeat 3 multistep phosphorylation by the concerted action of protein kinases CK1 and GSK3. *Biochemistry.* 46:11902-11910.
- Fiol, C.J., A.M. Mahrenholz, Y. Wang, R.W. Roeske, and P.J. Roach. 1987. Formation of protein kinase recognition sites by covalent modification of the substrate. Molecular mechanism for the synergistic action of casein kinase II and glycogen synthase kinase 3. *J Biol Chem.* 262:14042-14048.
- Fleming, E.S., M. Temchin, Q. Wu, L. Maggio-Price, and J.S. Tirnauer. 2009. Spindle misorientation in tumors from APC(min/+) mice. *Molecular carcinogenesis.* 48:592-598.
- Franker, M.A., and C.C. Hoogenraad. 2013. Microtubule-based transport - basic mechanisms, traffic rules and role in neurological pathogenesis. *Journal of cell science.* 126:2319-2329.
- Friedrich, T., B. Richter, T. Gaiser, C. Weiss, K.P. Janssen, H. Einwachter, R.M. Schmid, M.P. Ebert, and E. Burgermeister. 2013. Deficiency of caveolin-1 in Apc(min/+) mice promotes colorectal tumorigenesis. *Carcinogenesis.* 34:2109-2118.
- Fu, M.M., and E.L. Holzbaur. 2014. Integrated regulation of motor-driven organelle transport by scaffolding proteins. *Trends in cell biology.* 24:564-574.
- Fumoto, K., P.C. Lee, H. Saya, and A. Kikuchi. 2008. AIP regulates stability of Aurora-A at early mitotic phase coordinately with GSK-3beta. *Oncogene.* 27:4478-4487.
- Gennerich, A., and R.D. Vale. 2009. Walking the walk: how kinesin and dynein coordinate their steps. *Current opinion in cell biology.* 21:59-67.
- Gibbons, I.R. 1988. Dynein ATPases as microtubule motors. *The Journal of biological chemistry.* 263:15837-15840.
- Gurnell, M., J.M. Wentworth, M. Agostini, M. Adams, T.N. Collingwood, C. Provenzano, P.O. Browne, O. Rajanayagam, T.P. Burris, J.W. Schwabe, M.A. Lazar, and V.K. Chatterjee. 2000. A dominant-negative peroxisome proliferator-activated receptor gamma (PPARgamma) mutant is a constitutive repressor and inhibits PPARgamma-mediated adipogenesis. *The Journal of biological chemistry.* 275:5754-5759.
- Ha, J., K.W. Lo, K.R. Myers, T.M. Carr, M.K. Humsi, B.A. Rasoul, R.A. Segal, and K.K. Pfister. 2008. A neuron-specific cytoplasmic dynein isoform preferentially transports TrkB signaling endosomes. *J Cell Biol.* 181:1027-1039.

- Hanson, C.A., and J.R. Miller. 2005. Non-traditional roles for the Adenomatous Polyposis Coli (APC) tumor suppressor protein. *Gene*. 361:1-12.
- Harada, A., Y. Takei, Y. Kanai, Y. Tanaka, S. Nonaka, and N. Hirokawa. 1998. Golgi vesiculation and lysosome dispersion in cells lacking cytoplasmic dynein. *The Journal of cell biology*. 141:51-59.
- Harwood, A.J., J.E. Forde-Thomas, H. Williams, M. Samereier, and A. Muller-Taubenberger. 2013. Aberrant spindle dynamics and cytokinesis in *Dictyostelium discoideum* cells that lack glycogen synthase kinase 3. *European journal of cell biology*. 92:222-228.
- Hebbar, S., A.M. Guillotte, M.T. Mesngon, Q. Zhou, A. Wynshaw-Boris, and D.S. Smith. 2008a. Genetic enhancement of the Lis1<sup>+/-</sup> phenotype by a heterozygous mutation in the adenomatous polyposis coli gene. *Developmental neuroscience*. 30:157-170.
- Hebbar, S., M.T. Mesngon, A.M. Guillotte, B. Desai, R. Ayala, and D.S. Smith. 2008b. Lis1 and Ndel1 influence the timing of nuclear envelope breakdown in neural stem cells. *J Cell Biol*. 182:1063-1071.
- Heerssen, H.M., M.F. Pazyra, and R.A. Segal. 2004. Dynein motors transport activated Trks to promote survival of target-dependent neurons. *Nature neuroscience*. 7:596-604.
- Hernandez, R., T. Teruel, and M. Lorenzo. 2003. Rosiglitazone produces insulin sensitisation by increasing expression of the insulin receptor and its tyrosine kinase activity in brown adipocytes. *Diabetologia*. 46:1618-1628.
- Hirokawa, N., S. Niwa, and Y. Tanaka. 2010. Molecular motors in neurons: transport mechanisms and roles in brain function, development, and disease. *Neuron*. 68:610-638.
- Huang, J., T. Imamura, and J.M. Olefsky. 2001. Insulin can regulate GLUT4 internalization by signaling to Rab5 and the motor protein dynein. *Proceedings of the National Academy of Sciences of the United States of America*. 98:13084-13089.
- Huang, J., A.J. Roberts, A.E. Leschziner, and S.L. Reck-Peterson. 2012. Lis1 acts as a "clutch" between the ATPase and microtubule-binding domains of the dynein motor. *Cell*. 150:975-986.
- Ikeda, K., O. Zhapparova, I. Brodsky, I. Semenova, J.S. Tirnauer, I. Zaliapin, and V. Rodionov. 2011. CK1 activates minus-end-directed transport of membrane organelles along microtubules. *Mol Biol Cell*. 22:1321-1329.
- Ikeda, S., M. Kishida, Y. Matsuura, H. Usui, and A. Kikuchi. 2000. GSK-3 $\beta$ -dependent phosphorylation of adenomatous polyposis coli gene product can be modulated by beta-catenin and protein phosphatase 2A complexed with Axin. *Oncogene*. 19:537-545.
- Ilouz, R., S. Pietrokovski, M. Eisenstein, and H. Eldar-Finkelman. 2008. New insights into the autoinhibition mechanism of glycogen synthase kinase-3 $\beta$ . *J Mol Biol*. 383:999-1007.
- Ishiguro, K., A. Shiratsuchi, S. Sato, A. Omori, M. Arioka, S. Kobayashi, T. Uchida, and K. Imahori. 1993. Glycogen synthase kinase 3 beta is identical to tau protein kinase I generating several epitopes of paired helical filaments. *FEBS Lett*. 325:167-172.

- Izumi, N., K. Fumoto, S. Izumi, and A. Kikuchi. 2008. GSK-3beta regulates proper mitotic spindle formation in cooperation with a component of the gamma-tubulin ring complex, GCP5. *The Journal of biological chemistry*. 283:12981-12991.
- Jimbo, T., Y. Kawasaki, R. Koyama, R. Sato, S. Takada, K. Haraguchi, and T. Akiyama. 2002. Identification of a link between the tumour suppressor APC and the kinesin superfamily. *Nature cell biology*. 4:323-327.
- Kardon, J.R., and R.D. Vale. 2009. Regulators of the cytoplasmic dynein motor. *Nature reviews. Molecular cell biology*. 10:854-865.
- Karki, S., and E.L. Holzbaur. 1995. Affinity chromatography demonstrates a direct binding between cytoplasmic dynein and the dynactin complex. *J Biol Chem*. 270:28806-28811.
- Kim, D., S. Kim, H. Koh, S.O. Yoon, A.S. Chung, K.S. Cho, and J. Chung. 2001. Akt/PKB promotes cancer cell invasion via increased motility and metalloproteinase production. *FASEB journal : official publication of the Federation of American Societies for Experimental Biology*. 15:1953-1962.
- King, S.J., C.L. Brown, K.C. Maier, N.J. Quintyne, and T.A. Schroer. 2003. Analysis of the dynein-dynactin interaction in vitro and in vivo. *Mol Biol Cell*. 14:5089-5097.
- Kongkanuntn, R., V.J. Bubb, O.J. Sansom, A.H. Wyllie, D.J. Harrison, and A.R. Clarke. 1999. Dysregulated expression of beta-catenin marks early neoplastic change in Apc mutant mice, but not all lesions arising in Msh2 deficient mice. *Oncogene*. 18:7219-7225.
- Kotak, S., and P. Gonczy. 2013. Mechanisms of spindle positioning: cortical force generators in the limelight. *Current opinion in cell biology*. 25:741-748.
- Kuta, A., W. Deng, A. Morsi El-Kadi, G.T. Banks, M. Hafezparast, K.K. Pfister, and E.M. Fisher. 2010. Mouse cytoplasmic dynein intermediate chains: identification of new isoforms, alternative splicing and tissue distribution of transcripts. *PLoS One*. 5:e11682.
- Lam, C., M.A. Vergnolle, L. Thorpe, P.G. Woodman, and V.J. Allan. 2010. Functional interplay between LIS1, NDE1 and NDEL1 in dynein-dependent organelle positioning. *Journal of cell science*. 123:202-212.
- Landberg, G., M. Erlanson, G. Roos, E.M. Tan, and C.A. Casiano. 1996. Nuclear autoantigen p330d/CENP-F: a marker for cell proliferation in human malignancies. *Cytometry*. 25:90-98.
- Landreth, G., Q. Jiang, S. Mandrekar, and M. Heneka. 2008. PPARgamma agonists as therapeutics for the treatment of Alzheimer's disease. *Neurotherapeutics*. 5:481-489.
- Lansbergen, G., I. Grigoriev, Y. Mimori-Kiyosue, T. Ohtsuka, S. Higa, I. Kitajima, J. Demmers, N. Galjart, A.B. Houtsmuller, F. Grosveld, and A. Akhmanova. 2006. CLASPs attach microtubule plus ends to the cell cortex through a complex with LL5beta. *Dev Cell*. 11:21-32.
- Larsson, S.C., N. Orsini, and A. Wolk. 2005. Diabetes mellitus and risk of colorectal cancer: a meta-analysis. *J Natl Cancer Inst*. 97:1679-1687.
- Lauffenburger, D.A., and A.F. Horwitz. 1996. Cell migration: a physically integrated molecular process. *Cell*. 84:359-369.

- Lefebvre, A.M., I. Chen, P. Desreumaux, J. Najib, J.C. Fruchart, K. Geboes, M. Briggs, R. Heyman, and J. Auwerx. 1998. Activation of the peroxisome proliferator-activated receptor gamma promotes the development of colon tumors in C57BL/6J-APCMin/+ mice. *Nature medicine*. 4:1053-1057.
- Li, J., W.L. Lee, and J.A. Cooper. 2005. NudEL targets dynein to microtubule ends through LIS1. *Nat Cell Biol*. 7:686-690.
- Liao, H., R.J. Winkfein, G. Mack, J.B. Rattner, and T.J. Yen. 1995. CENP-F is a protein of the nuclear matrix that assembles onto kinetochores at late G2 and is rapidly degraded after mitosis. *The Journal of cell biology*. 130:507-518.
- Liu, X., H. Gong, and K. Huang. 2013. Oncogenic role of kinesin proteins and targeting kinesin therapy. *Cancer science*. 104:651-656.
- Lo, K.W., H.M. Kan, and K.K. Pfister. 2006. Identification of a novel region of the cytoplasmic Dynein intermediate chain important for dimerization in the absence of the light chains. *J Biol Chem*. 281:9552-9559.
- Mallik, R., A.K. Rai, P. Barak, A. Rai, and A. Kunwar. 2013. Teamwork in microtubule motors. *Trends in cell biology*. 23:575-582.
- Mandelkow, E.M., G. Drewes, J. Biernat, N. Gustke, J. Van Lint, J.R. Vandenheede, and E. Mandelkow. 1992. Glycogen synthase kinase-3 and the Alzheimer-like state of microtubule-associated protein tau. *FEBS Lett*. 314:315-321.
- Marin, H.E., M.A. Peraza, A.N. Billin, T.M. Willson, J.M. Ward, M.J. Kennett, F.J. Gonzalez, and J.M. Peters. 2006. Ligand activation of peroxisome proliferator-activated receptor beta inhibits colon carcinogenesis. *Cancer research*. 66:4394-4401.
- Markus, S.M., J.J. Punch, and W.L. Lee. 2009. Motor- and tail-dependent targeting of dynein to microtubule plus ends and the cell cortex. *Current biology : CB*. 19:196-205.
- Marmol, F. 2008. Lithium: bipolar disorder and neurodegenerative diseases Possible cellular mechanisms of the therapeutic effects of lithium. *Prog Neuropsychopharmacol Biol Psychiatry*. 32:1761-1771.
- Marsh, M., and H.T. McMahon. 1999. The structural era of endocytosis. *Science*. 285:215-220.
- McKenney, R.J., W. Huynh, M.E. Tanenbaum, G. Bhabha, and R.D. Vale. 2014. Activation of cytoplasmic dynein motility by dynactin-cargo adapter complexes. *Science*. 345:337-341.
- McKenney, R.J., M. Vershinin, A. Kunwar, R.B. Vallee, and S.P. Gross. 2010. LIS1 and NudE induce a persistent dynein force-producing state. *Cell*. 141:304-314.
- McKenney, R.J., S.J. Weil, J. Scherer, and R.B. Vallee. 2011. Mutually Exclusive Cytoplasmic Dynein Regulation by NudE-Lis1 and Dynactin. *J Biol Chem*. 286:39615-39622.
- Meijer, L., M. Flajolet, and P. Greengard. 2004. Pharmacological inhibitors of glycogen synthase kinase 3. *Trends Pharmacol Sci*. 25:471-480.
- Mesngon, M.T., C. Tarricone, S. Hebbar, A.M. Guillotte, E.W. Schmitt, L. Lanier, A. Musacchio, S.J. King, and D.S. Smith. 2006. Regulation of cytoplasmic

- dynein ATPase by Lis1. *The Journal of neuroscience : the official journal of the Society for Neuroscience*. 26:2132-2139.
- Mimori-Kiyosue, Y., N. Shiina, and S. Tsukita. 2000. Adenomatous polyposis coli (APC) protein moves along microtubules and concentrates at their growing ends in epithelial cells. *The Journal of cell biology*. 148:505-518.
- Mimori-Kiyosue, Y., and S. Tsukita. 2003. "Search-and-capture" of microtubules through plus-end-binding proteins (+TIPs). *Journal of biochemistry*. 134:321-326.
- Minde, D.P., Z. Anvarian, S.G.D. Rudiger, and M.M. Maurice. 2011. Messing up disorder: how do missense mutations in the tumor suppressor protein APC lead to cancer? *Mol Cancer*. 10.
- Mitchell, D.J., K.R. Blasier, E.D. Jeffery, M.W. Ross, A.K. Pullikuth, D. Suo, J. Park, W.R. Smiley, K.W. Lo, J. Shabanowitz, C.D. Deppmann, J.C. Trinidad, D.F. Hunt, A.D. Catling, and K.K. Pfister. 2012. Trk activation of the ERK1/2 kinase pathway stimulates intermediate chain phosphorylation and recruits cytoplasmic dynein to signaling endosomes for retrograde axonal transport. *J Neurosci*. 32:15495-15510.
- Mogensen, M.M., J.B. Tucker, J.B. Mackie, A.R. Prescott, and I.S. Nathke. 2002. The adenomatous polyposis coli protein unambiguously localizes to microtubule plus ends and is involved in establishing parallel arrays of microtubule bundles in highly polarized epithelial cells. *The Journal of cell biology*. 157:1041-1048.
- Moon, H.M., Y.H. Youn, H. Pemble, J. Yingling, T. Wittmann, and A. Wynshaw-Boris. 2014. LIS1 controls mitosis and mitotic spindle organization via the LIS1-NDEL1-dynein complex. *Human molecular genetics*. 23:449-466.
- Morfini, G., G. Szebenyi, R. Elluru, N. Ratner, and S.T. Brady. 2002. Glycogen synthase kinase 3 phosphorylates kinesin light chains and negatively regulates kinesin-based motility. *EMBO J*. 21:281-293.
- Moughamian, A.J., G.E. Osborn, J.E. Lazarus, S. Maday, and E.L. Holzbaur. 2013. Ordered recruitment of dynactin to the microtubule plus-end is required for efficient initiation of retrograde axonal transport. *J Neurosci*. 33:13190-13203.
- Mukai, F., K. Ishiguro, Y. Sano, and S.C. Fujita. 2002. Alternative splicing isoform of tau protein kinase I/glycogen synthase kinase 3beta. *J Neurochem*. 81:1073-1083.
- Murphy, J.T., J.M. Tucker, C. Davis, and F.G. Berger. 2004. Raltitrexed increases tumorigenesis as a single agent yet exhibits anti-tumor synergy with 5-fluorouracil in ApcMin/+ mice. *Cancer biology & therapy*. 3:1169-1176.
- Nathke, I.S. 2004. The adenomatous polyposis coli protein: the Achilles heel of the gut epithelium. *Annual review of cell and developmental biology*. 20:337-366.
- Nyarko, A., Y. Song, and E. Barbar. 2012. Intrinsic disorder in dynein intermediate chain modulates its interactions with NudE and dynactin. *J Biol Chem*. 287:24884-24893.

- Pal, I., and M. Mandal. 2012. PI3K and Akt as molecular targets for cancer therapy: current clinical outcomes. *Acta pharmacologica Sinica*. 33:1441-1458.
- Pandey, J.P., and D.S. Smith. 2011. A Cdk5-dependent switch regulates Lis1/Ndel1/dynein-driven organelle transport in adult axons. *J Neurosci*. 31:17207-17219.
- Pellman, D. 2001. Cancer. A CINtillating new job for the APC tumor suppressor. *Science*. 291:2555-2556.
- Peters, J.M., Y.M. Shah, and F.J. Gonzalez. 2012. The role of peroxisome proliferator-activated receptors in carcinogenesis and chemoprevention. *Nature reviews. Cancer*. 12:181-195.
- Pfister, K.K., P.R. Shah, H. Hummerich, A. Russ, J. Cotton, A.A. Annuar, S.M. King, and E.M. Fisher. 2006. Genetic analysis of the cytoplasmic dynein subunit families. *PLoS Genet*. 2:e1.
- Phelps, R.A., S. Chidester, S. Dehghanizadeh, J. Phelps, I.T. Sandoval, K. Rai, T. Broadbent, S. Sarkar, R.W. Burt, and D.A. Jones. 2009. A two-step model for colon adenoma initiation and progression caused by APC loss. *Cell*. 137:623-634.
- Polakis, P. 2002. Casein kinase 1: a Wnt'er of disconnect. *Current biology : CB*. 12:R499-R501.
- Pullikuth, A.K., A. Ozdemir, D. Cardenas, E. Bailey, N.E. Sherman, K.K. Pfister, and A.D. Catling. 2013. Epidermal growth factor stimulates extracellular-signal regulated kinase phosphorylation of a novel site on cytoplasmic Dynein intermediate chain 2. *International journal of molecular sciences*. 14:3595-3620.
- Quintyne, N.J., and T.A. Schroer. 2002. Distinct cell cycle-dependent roles for dynactin and dynein at centrosomes. *The Journal of cell biology*. 159:245-254.
- Quyn, A.J., P.L. Appleton, F.A. Carey, R.J. Steele, N. Barker, H. Clevers, R.A. Ridgway, O.J. Sansom, and I.S. Nathke. 2010. Spindle orientation bias in gut epithelial stem cell compartments is lost in precancerous tissue. *Cell stem cell*. 6:175-181.
- Raaijmakers, J.A., and R.H. Medema. 2014. Function and regulation of dynein in mitotic chromosome segregation. *Chromosoma*. 123:407-422.
- Raaijmakers, J.A., M.E. Tanenbaum, and R.H. Medema. 2013. Systematic dissection of dynein regulators in mitosis. *The Journal of cell biology*. 201:201-215.
- Rai, A.K., A. Rai, A.J. Ramaiya, R. Jha, and R. Mallik. 2013. Molecular adaptations allow dynein to generate large collective forces inside cells. *Cell*. 152:172-182.
- Reya, T., and H. Clevers. 2005. Wnt signalling in stem cells and cancer. *Nature*. 434:843-850.
- Ridley, A.J., M.A. Schwartz, K. Burridge, R.A. Firtel, M.H. Ginsberg, G. Borisy, J.T. Parsons, and A.R. Horwitz. 2003. Cell migration: integrating signals from front to back. *Science*. 302:1704-1709.

- Roberts, A.J., B.S. Goodman, and S.L. Reck-Peterson. 2014. Reconstitution of dynein transport to the microtubule plus end by kinesin. *eLife*. 3:e02641.
- Rodionov, V., E. Nadezhdina, and G. Borisy. 1999. Centrosomal control of microtubule dynamics. *Proceedings of the National Academy of Sciences of the United States of America*. 96:115-120.
- Rubinsztein, D.C. 2006. The roles of intracellular protein-degradation pathways in neurodegeneration. *Nature*. 443:780-786.
- Saez, E., P. Tontonoz, M.C. Nelson, J.G. Alvarez, U.T. Ming, S.M. Baird, V.A. Thomazy, and R.M. Evans. 1998. Activators of the nuclear receptor PPARgamma enhance colon polyp formation. *Nature medicine*. 4:1058-1061.
- Saltiel, A.R., and J.E. Pessin. 2002. Insulin signaling pathways in time and space. *Trends in cell biology*. 12:65-71.
- Sansom, O.J., K.R. Reed, A.J. Hayes, H. Ireland, H. Brinkmann, I.P. Newton, E. Battle, P. Simon-Assmann, H. Clevers, I.S. Nathke, A.R. Clarke, and D.J. Winton. 2004. Loss of Apc in vivo immediately perturbs Wnt signaling, differentiation, and migration. *Genes & development*. 18:1385-1390.
- Sato, N., and R. Morishita. 2014. Brain alterations and clinical symptoms of dementia in diabetes: abeta/tau-dependent and independent mechanisms. *Frontiers in endocrinology*. 5:143.
- Schenck, A., L. Goto-Silva, C. Collinet, M. Rhinn, A. Giner, B. Habermann, M. Brand, and M. Zerial. 2008. The endosomal protein Appl1 mediates Akt substrate specificity and cell survival in vertebrate development. *Cell*. 133:486-497.
- Schiavo, G., L. Greensmith, M. Hafezparast, and E.M. Fisher. 2013. Cytoplasmic dynein heavy chain: the servant of many masters. *Trends in neurosciences*. 36:641-651.
- Schlager, M.A., H.T. Hoang, L. Urnavicius, S.L. Bullock, and A.P. Carter. 2014. In vitro reconstitution of a highly processive recombinant human dynein complex. *The EMBO journal*. 33:1855-1868.
- Schmoranzner, J., J.P. Fawcett, M. Segura, S. Tan, R.B. Vallee, T. Pawson, and G.G. Gundersen. 2009. Par3 and dynein associate to regulate local microtubule dynamics and centrosome orientation during migration. *Current biology : CB*. 19:1065-1074.
- Schroer, T.A. 2004. Dynactin. *Annu Rev Cell Dev Biol*. 20:759-779.
- Seo, M., S. Lee, J.H. Kim, W.H. Lee, G. Hu, S.J. Elledge, and K. Suk. 2014. RNAi-based functional selection identifies novel cell migration determinants dependent on PI3K and AKT pathways. *Nature communications*. 5:5217.
- Smith, D.S., M. Niethammer, R. Ayala, Y. Zhou, M.J. Gambello, A. Wynshaw-Boris, and L.H. Tsai. 2000. Regulation of cytoplasmic dynein behaviour and microtubule organization by mammalian Lis1. *Nature cell biology*. 2:767-775.
- Soutar, M.P., W.Y. Kim, R. Williamson, M. Peggie, C.J. Hastie, H. McLauchlan, W.D. Snider, P.R. Gordon-Weeks, and C. Sutherland. 2010. Evidence that

- glycogen synthase kinase-3 isoforms have distinct substrate preference in the brain. *J Neurochem.* 115:974-983.
- Stamos, J.L., and W.I. Weis. 2013. The beta-catenin destruction complex. *Cold Spring Harbor perspectives in biology.* 5:a007898.
- Stehman, S.A., Y. Chen, R.J. McKenney, and R.B. Vallee. 2007. NudE and NudEL are required for mitotic progression and are involved in dynein recruitment to kinetochores. *J Cell Biol.* 178:583-594.
- Su, L.K., K.W. Kinzler, B. Vogelstein, A.C. Preisinger, A.R. Moser, C. Luongo, K.A. Gould, and W.F. Dove. 1992. Multiple intestinal neoplasia caused by a mutation in the murine homolog of the APC gene. *Science.* 256:668-670.
- Su, W., C.R. Bush, B.M. Necela, S.R. Calcagno, N.R. Murray, A.P. Fields, and E.A. Thompson. 2007. Differential expression, distribution, and function of PPAR-gamma in the proximal and distal colon. *Physiol Genomics.* 30:342-353.
- Sutherland, C. 2011. What Are the bona fide GSK3 Substrates? *Int J Alzheimers Dis.* 2011:505607.
- Taketo, M.M., and W. Edelmann. 2009. Mouse models of colon cancer. *Gastroenterology.* 136:780-798.
- Tanzi, R.E., and L. Bertram. 2005. Twenty years of the Alzheimer's disease amyloid hypothesis: a genetic perspective. *Cell.* 120:545-555.
- ter Haar, E., J.T. Coll, D.A. Austen, H.M. Hsiao, L. Swenson, and J. Jain. 2001. Structure of GSK3beta reveals a primed phosphorylation mechanism. *Nat Struct Biol.* 8:593-596.
- Tighe, A., A. Ray-Sinha, O.D. Staples, and S.S. Taylor. 2007. GSK-3 inhibitors induce chromosome instability. *BMC cell biology.* 8:34.
- Tsai, J.W., K.H. Bremner, and R.B. Vallee. 2007. Dual subcellular roles for LIS1 and dynein in radial neuronal migration in live brain tissue. *Nature neuroscience.* 10:970-979.
- Tsai, L.H., and J.G. Gleeson. 2005. Nucleokinesis in neuronal migration. *Neuron.* 46:383-388.
- Vale, R.D. 2003. The molecular motor toolbox for intracellular transport. *Cell.* 112:467-480.
- Vallee, R.B., G.E. Seale, and J.W. Tsai. 2009. Emerging roles for myosin II and cytoplasmic dynein in migrating neurons and growth cones. *Trends in cell biology.* 19:347-355.
- Vaughan, K.T., and R.B. Vallee. 1995. Cytoplasmic dynein binds dynactin through a direct interaction between the intermediate chains and p150Glued. *J Cell Biol.* 131:1507-1516.
- Vaughan, P.S., J.D. Leszyk, and K.T. Vaughan. 2001. Cytoplasmic dynein intermediate chain phosphorylation regulates binding to dynactin. *J Biol Chem.* 276:26171-26179.
- Velebit, J., H.H. Chowdhury, M. Kreft, and R. Zorec. 2011. Rosiglitazone balances insulin-induced exo- and endocytosis in single 3T3-L1 adipocytes. *Mol Cell Endocrinol.* 333:70-77.

- Wakefield, J.G., D.J. Stephens, and J.M. Tavare. 2003. A role for glycogen synthase kinase-3 in mitotic spindle dynamics and chromosome alignment. *Journal of cell science*. 116:637-646.
- Wang, Q.M., C.J. Fiol, A.A. DePaoli-Roach, and P.J. Roach. 1994. Glycogen synthase kinase-3 beta is a dual specificity kinase differentially regulated by tyrosine and serine/threonine phosphorylation. *J Biol Chem*. 269:14566-14574.
- Wang, S., S.A. Ketcham, A. Schon, B. Goodman, Y. Wang, J. Yates, 3rd, E. Freire, T.A. Schroer, and Y. Zheng. 2013. Nudel/NudE and Lis1 promote dynein and dynactin interaction in the context of spindle morphogenesis. *Mol Biol Cell*. 24:3522-3533.
- Wang, S., and Y. Zheng. 2011. Identification of a novel dynein binding domain in nudel essential for spindle pole organization in *Xenopus* egg extract. *The Journal of biological chemistry*. 286:587-593.
- Wang, Y., Y. Azuma, D.B. Friedman, R.J. Coffey, and K.L. Neufeld. 2009. Novel association of APC with intermediate filaments identified using a new versatile APC antibody. *BMC cell biology*. 10:75.
- Weaver, C., C. Leidel, L. Szpankowski, N.M. Farley, G.T. Shubeita, and L.S. Goldstein. 2013. Endogenous GSK-3/shaggy regulates bidirectional axonal transport of the amyloid precursor protein. *Traffic*. 14:295-308.
- Whitehead, R.H., and J.L. Joseph. 1994. Derivation of conditionally immortalized cell lines containing the Min mutation from the normal colonic mucosa and other tissues of an "Immortomouse"/Min hybrid. *Epithelial cell biology*. 3:119-125.
- Whitehead, R.H., P.E. VanEeden, M.D. Noble, P. Ataliotis, and P.S. Jat. 1993. Establishment of conditionally immortalized epithelial cell lines from both colon and small intestine of adult H-2Kb-tsA58 transgenic mice. *Proceedings of the National Academy of Sciences of the United States of America*. 90:587-591.
- Whyte, J., J.R. Bader, S.B. Tauhata, M. Raycroft, J. Hornick, K.K. Pfister, W.S. Lane, G.K. Chan, E.H. Hinchcliffe, P.S. Vaughan, and K.T. Vaughan. 2008. Phosphorylation regulates targeting of cytoplasmic dynein to kinetochores during mitosis. *J Cell Biol*. 183:819-834.
- Wickstead, B., and K. Gull. 2007. Dyneins across eukaryotes: a comparative genomic analysis. *Traffic*. 8:1708-1721.
- Wojcik, E.J. 2008. A mitotic role for GSK-3beta kinase in *Drosophila*. *Cell cycle*. 7:3699-3708.
- Wood-Kaczmar, A., M. Kraus, K. Ishiguro, K.L. Philpott, and P.R. Gordon-Weeks. 2009. An alternatively spliced form of glycogen synthase kinase-3beta is targeted to growing neurites and growth cones. *Mol Cell Neurosci*. 42:184-194.
- Woodgett, J.R. 1991. cDNA cloning and properties of glycogen synthase kinase-3. *Methods Enzymol*. 200:564-577.
- Wu, C., B. Cui, L. He, L. Chen, and W.C. Mobley. 2009. The coming of age of axonal neurotrophin signaling endosomes. *Journal of proteomics*. 72:46-55.

- Yamada, M., S. Toba, Y. Yoshida, K. Haratani, D. Mori, Y. Yano, Y. Mimori-Kiyosue, T. Nakamura, K. Itoh, S. Fushiki, M. Setou, A. Wynshaw-Boris, T. Torisawa, Y.Y. Toyoshima, and S. Hirotsune. 2008. LIS1 and NDEL1 coordinate the plus-end-directed transport of cytoplasmic dynein. *The EMBO journal*. 27:2471-2483.
- Yamada, Y., and H. Mori. 2007. Multistep carcinogenesis of the colon in Apc(Min/+) mouse. *Cancer science*. 98:6-10.
- Yano, H., F.S. Lee, H. Kong, J. Chuang, J. Arevalo, P. Perez, C. Sung, and M.V. Chao. 2001. Association of Trk neurotrophin receptors with components of the cytoplasmic dynein motor. *J Neurosci*. 21:RC125.
- Yingling, J., Y.H. Youn, D. Darling, K. Toyo-Oka, T. Pramparo, S. Hirotsune, and A. Wynshaw-Boris. 2008. Neuroepithelial stem cell proliferation requires LIS1 for precise spindle orientation and symmetric division. *Cell*. 132:474-486.
- Zhang, J., L. Zhuang, Y. Lee, J.F. Abenza, M.A. Penalva, and X. Xiang. The microtubule plus-end localization of Aspergillus dynein is important for dynein-early-endosome interaction but not for dynein ATPase activation. *Journal of cell science*. 123:3596-3604.
- Zweifel, L.S., R. Kuruvilla, and D.D. Ginty. 2005. Functions and mechanisms of retrograde neurotrophin signalling. *Nature reviews. Neuroscience*. 6:615-625.